UNIVERSIDADE FEDERAL DE GOIÁS
ESCOLA DE AGRONOMIA
PROGRAMA DE PÓS-GRADUAÇÃO EM AGRONOMIA

SENSOR MULTIESPECTRAL EMBARCADO EM SISTEMA DE AERONAVE REMOTAMENTE PILOTADA PARA MANEJO DE NITROGÊNIO EM MILHO E FEIJÃO-COMUM

DIOGO CASTILHO SILVA

Orientadora:
Drª. Beata Emoke Madari

Goiânia – GO – Brasil
Março – 2024

UNIVERSIDADE FEDERAL DE GOIÁS
ESCOLA DE AGRONOMIA

TERMO DE CIÊNCIA E DE AUTORIZAÇÃO (TECA) PARA DISPONIBILIZAR VERSÕES ELETRÔNICAS DE TESES

E DISSERTAÇÕES NA BIBLIOTECA DIGITAL DA UFG

Na qualidade de titular dos direitos de autor, autorizo a Universidade Federal de Goiás (UFG) a disponibilizar, gratuitamente, por meio da Biblioteca Digital de Teses e Dissertações (BDTD/UFG), regulamentada pela Resolução CEPEC nº 832/2007, sem ressarcimento dos direitos autorais, de acordo com a Lei 9.610/98, o documento conforme permissões assinaladas abaixo, para fins de leitura, impressão e/ou download, a título de divulgação da produção científica brasileira, a partir desta data.

O conteúdo das Teses e Dissertações disponibilizado na BDTD/UFG é de responsabilidade exclusiva do autor. Ao encaminhar o produto final, o autor(a) e o(a) orientador(a) firmam o compromisso de que o trabalho não contém nenhuma violação de quaisquer direitos autorais ou outro direito de terceiros.

1. Identificação do material bibliográfico

[ ] Dissertação [X] Tese [ ] Outro*:_____

*No caso de mestrado/doutorado profissional, indique o formato do Trabalho de Conclusão de Curso, permitido no documento de área, correspondente ao programa de pós-graduação, orientado pela legislação vigente da CAPES.

Exemplos: Estudo de caso ou Revisão sistemática ou outros formatos.

2. Nome completo do autor

Diogo Castilho Silva

3. Título do trabalho

SENSOR MULTIESPECTRAL EMBARCADO EM SISTEMA DE AERONAVE REMOTAMENTE PILOTADA PARA MANEJO DE NITROGÊNIO EM MILHO E FEIJÃO-COMUM

4. Informações de acesso ao documento (este campo deve ser preenchido pelo orientador)

Concorda com a liberação total do documento [ ] SIM [X] NÃO[1]

[1] Neste caso o documento será embargado por até um ano a partir da data de defesa. Após esse período, a possível disponibilização ocorrerá apenas mediante:
a) consulta ao(à) autor(a) e ao(à) orientador(a);
b) novo Termo de Ciência e de Autorização (TECA) assinado e inserido no arquivo da tese ou dissertação.
O documento não será disponibilizado durante o período de embargo.
Casos de embargo:
- Solicitação de registro de patente;
- Submissão de artigo em revista científica;
- Publicação como capítulo de livro;
- Publicação da dissertação/tese em livro.

Obs. Este termo deverá ser assinado no SEI pelo orientador e pelo autor.

Documento assinado eletronicamente por **Diogo Castilho Silva**, **Discente**, em 28/03/2024, às 14:44, conforme horário oficial de Brasília, com fundamento no § 3º do art. 4º do Decreto nº 10.543, de 13 de novembro de 2020.

Documento assinado eletronicamente por **Beata Emoke Madari**, **Usuário Externo**, em 28/03/2024, às 15:06, conforme horário oficial de Brasília, com fundamento no § 3º do art. 4º do Decreto nº 10.543, de 13 de novembro de 2020.

A autenticidade deste documento pode ser conferida no site https://sei.ufg.br/sei/controlador_externo.php?acao=documento_conferir&id_orgao_acesso_externo=0, informando o código verificador **4480136** e o código CRC **266D4350**.

Referência: Processo nº 23070.016007/2024-09 SEI nº 4480136

UNIVERSIDADE FEDERAL DE GOIÁS
ESCOLA DE AGRONOMIA

TERMO DE CIÊNCIA E DE AUTORIZAÇÃO (TECA) PARA DISPONIBILIZAR VERSÕES ELETRÔNICAS DE TESES

E DISSERTAÇÕES NA BIBLIOTECA DIGITAL DA UFG

Na qualidade de titular dos direitos de autor, autorizo a Universidade Federal de Goiás (UFG) a disponibilizar, gratuitamente, por meio da Biblioteca Digital de Teses e Dissertações (BDTD/UFG), regulamentada pela Resolução CEPEC nº 832/2007, sem ressarcimento dos direitos autorais, de acordo com a Lei 9.610/98, o documento conforme permissões assinaladas abaixo, para fins de leitura, impressão e/ou download, a título de divulgação da produção científica brasileira, a partir desta data.

O conteúdo das Teses e Dissertações disponibilizado na BDTD/UFG é de responsabilidade exclusiva do autor. Ao encaminhar o produto final, o autor(a) e o(a) orientador(a) firmam o compromisso de que o trabalho não contém nenhuma violação de quaisquer direitos autorais ou outro direito de terceiros.

1. Identificação do material bibliográfico

[ ] Dissertação [X] Tese [ ] Outro*:_____

*No caso de mestrado/doutorado profissional, indique o formato do Trabalho de Conclusão de Curso, permitido no documento de área, correspondente ao programa de pós-graduação, orientado pela legislação vigente da CAPES.

Exemplos: Estudo de caso ou Revisão sistemática ou outros formatos.

2. Nome completo do autor

Diogo Castilho Silva

3. Título do trabalho

SENSOR MULTIESPECTRAL EMBARCADO EM SISTEMA DE AERONAVE REMOTAMENTE PILOTADA PARA MANEJO DE NITROGÊNIO EM MILHO E FEIJÃO-COMUM

4. Informações de acesso ao documento (este campo deve ser preenchido pelo orientador)

Concorda com a liberação total do documento [X] SIM [ ] NÃO[1]

[1] Neste caso o documento será embargado por até um ano a partir da data de defesa. Após esse período, a possível disponibilização ocorrerá apenas mediante:
a) consulta ao(à) autor(a) e ao(à) orientador(a);
b) novo Termo de Ciência e de Autorização (TECA) assinado e inserido no arquivo da tese ou dissertação.
O documento não será disponibilizado durante o período de embargo.
Casos de embargo:
- Solicitação de registro de patente;
- Submissão de artigo em revista científica;
- Publicação como capítulo de livro;
- Publicação da dissertação/tese em livro.

Obs. Este termo deverá ser assinado no SEI pelo orientador e pelo autor.

Documento assinado eletronicamente por **Diogo Castilho Silva**, **Usuário Externo**, em 02/04/2025, às 08:54, conforme horário oficial de Brasília, com fundamento no § 3º do art. 4º do Decreto nº 10.543, de 13 de novembro de 2020.

Documento assinado eletronicamente por **Beata Emoke Madari**, **Usuário Externo**, em 02/04/2025, às 08:57, conforme horário oficial de Brasília, com fundamento no § 3º do art. 4º do Decreto nº 10.543, de 13 de novembro de 2020.

A autenticidade deste documento pode ser conferida no site https://sei.ufg.br/sei/controlador_externo.php?acao=documento_conferir&id_orgao_acesso_externo=0, informando o código verificador **5281667** e o código CRC **BC7C79FA**.

Referência: Processo nº 23070.016007/2024-09 SEI nº 5281667

DIOGO CASTILHO SILVA

SENSOR MULTIESPECTRAL EMBARCADO EM SISTEMA DE AERONAVE REMOTAMENTE PILOTADA PARA MANEJO DE NITROGÊNIO EM MILHO E FEIJÃO-COMUM

Tese apresentada ao Programa de Pós-Graduação em Agronomia , da Escola de Agronomia, da Universidade Federal de Goiás (UFG), como requisito para obtenção do título de Doutor em Agronomia.

Área de concentração: Solo e Água

Orientadora:
Drª. Beata Emoke Madari

Coorientadores:
Prof. Dr. Manuel Eduardo Ferreira
Drª. Maria da Conceição Santana Carvalho

Goiânia, GO – Brasil
2024

Ficha de identificação da obra elaborada pelo autor, através do
Programa de Geração Automática do Sistema de Bibliotecas da UFG.

Silva, Diogo Castilho
Sensor multiespectral embarcado em sistema de aeronave remotamente pilotada para manejo de nitrogênio em milho e feijão-comum [manuscrito] / Diogo Castilho Silva. - 2024.
105 f.

Orientador: Profa. Dra. Beata Emoke Madari; co-orientador Dr. Manuel Eduardo Ferreira; co-orientadora Dra. Maria da Conceição Santana Carvalho.
Tese (Doutorado) - Universidade Federal de Goiás, Escola de Agronomia (EA), Programa de Pós-Graduação em Agronomia, Goiânia, 2024.
Bibliografia.
Inclui mapas, fotografias, tabelas.

1. Sistema de aeronave pilotada remotamente (RPAS). 2. Imagem multiespectral. 3. Índice de vegetação. 4. Feijão. 5. Milho. I. Emoke Madari, Beata, orient. II. Título.

CDU 631/635

UNIVERSIDADE FEDERAL DE GOIÁS

ESCOLA DE AGRONOMIA

ATA DE DEFESA DE TESE

Ata Nº PPGA/020/2024 da sessão de Defesa de Tese de **Diogo Castilho Silva** que confere o título de Doutor em Agronomia, na área de concentração em Solo e Água.

Aos vinte e um dias do mês de março do ano de dois mil e vinte e quatro, a partir das catorze horas, por meio de videoconferência, realizou-se a sessão pública de Defesa de Tese intitulada "USO DE SENSORES ESPECTRAIS MONTADOS EM SISTEMA DE AERONAVE PILOTADA REMOTAMENTE (RPAS) PARA GERENCIAMENTO IDEAL DE NITROGÊNIO EM CULTURAS DE MILHO E FEIJÃO". Os trabalhos foram instalados pela Orientadora, Doutora Beata Emoke Madari (Embrapa Arroz e Feijão) com a participação dos demais membros da Banca Examinadora: Professor Manuel Eduardo Ferreira (IESA/UFG), coorientador; Doutora Maria da Conceição Santana Carvalho (Embrapa Arroz e Feijão), coorientadora; Professor Alisson Neves Harmyans Moreira (EA/UFG), membro titular externo; Doutor Luis Fernando Chimelo Ruiz (Salva Digital), membro titular externo, Professor Tavvs Micael Alves (IF Goiano), membro titular externo; Professor Diogo Silva Pena (EA/UFG), membro titular externo; Doutora Mellissa Ananias Soler da Silva (Embrapa Arroz e Feijão), membro titular externo. Durante a arguição os membros da banca fizeram sugestão de alteração do título do trabalho. A Banca Examinadora reuniu-se em sessão secreta a fim de concluir o julgamento da Tese tendo sido o candidato **aprovado** pelos seus membros. Proclamados os resultados pela Doutora Beata Emoke Madari, Presidente da Banca Examinadora, foram encerrados os trabalhos e, para constar, lavrou-se a presente ata que é assinada pelos Membros da Banca Examinadora, aos vinte e um dias do mês de março do ano de dois mil e vinte e quatro.

TÍTULO SUGERIDO PELA BANCA

SENSOR MULTIESPECTRAL EMBARCADO EM SISTEMA DE AERONAVE REMOTAMENTE PILOTADA PARA MANEJO DE NITROGÊNIO EM MILHO E FEIJÃO-COMUM

Documento assinado eletronicamente por **Beata Emoke Madari**, **Usuário Externo**, em 21/03/2024, às 17:34, conforme horário oficial de Brasília, com fundamento no § 3º do art. 4º do Decreto nº 10.543, de 13 de novembro de 2020.

Documento assinado eletronicamente por **Mellissa Ananias Soler da Silva**, **Usuário Externo**, em 21/03/2024, às 17:41, conforme horário oficial de Brasília, com fundamento no § 3º do art. 4º do Decreto nº 10.543, de 13 de novembro de 2020.

Documento assinado eletronicamente por **Luis Fernando Chimelo Ruiz**, **Usuário Externo**, em 22/03/2024, às 17:12, conforme horário oficial de Brasília, com fundamento no § 3º do art. 4º do Decreto nº 10.543, de 13 de novembro de 2020.

Documento assinado eletronicamente por **MARIA DA CONCEIÇÃO SANTANA CARVALHO**, **Usuário Externo**, em 22/03/2024, às 18:12, conforme horário oficial de Brasília, com fundamento no § 3º do art. 4º do Decreto nº 10.543, de 13 de novembro de 2020.

Documento assinado eletronicamente por **Alisson Neves Harmyans Moreira**, **Professor do Magistério Superior**, em 26/03/2024, às 06:57, conforme horário oficial de Brasília, com fundamento no § 3º do art. 4º do Decreto nº 10.543, de 13 de novembro de 2020.

Documento assinado eletronicamente por **Diogo Silva Pena**, **Professor do Magistério Superior**, em 26/03/2024, às 07:56, conforme horário oficial de Brasília, com fundamento no § 3º do art. 4º do Decreto nº 10.543, de 13 de novembro de 2020.

Documento assinado eletronicamente por **Manuel Eduardo Ferreira**, **Professor do Magistério Superior**, em 27/03/2024, às 12:28, conforme horário oficial de Brasília, com fundamento no § 3º do art. 4º do Decreto nº 10.543, de 13 de novembro de 2020.

Documento assinado eletronicamente por **Flavio Alves Da Silva**, **Coordenador de Pós-Graduação**, em 28/03/2024, às 09:12, conforme horário oficial de Brasília, com fundamento no § 3º do art. 4º do Decreto nº 10.543, de 13 de novembro de 2020.

A autenticidade deste documento pode ser conferida no site https://sei.ufg.br/sei/controlador_externo.php?acao=documento_conferir&id_orgao_acesso_externo=0, informando o código verificador **4467283** e o código CRC **C0E1C3E4**.

Referência: Processo nº 23070.016007/2024-09 SEI nº 4467283

AGRADECIMENTOS

Agradeço a Deus a grande presença em minha vida dando força e sabedoria para encarar os desafios acadêmicos;

Aos meus pais, Ivai Junior e Maria Divina ao apoio incondicional em dar sequência aos estudos da pós-graduação e em todos os passos de minha vida;

À Drª. Beata Emoke Madari a orientação, ensinamentos impagáveis, confiança e grande paciência que depositou em mim durante quatro anos juntos além de incentivar a uma viagem para fazer o Doutorado Sanduiche no exterior (Manhattan, Kansas – EUA) com o objetivo de aprimorar e publicar nosso primeiro capítulo desta tese;

Ao Prof. Dr. Manuel Eduardo Ferreira a coorientação prestada, ensinamentos e disponibilização em tempo hábil de drones e câmeras para avaliação dos experimentos à campo;

À Drª. Maria da Conceição Santana Carvalho a coorientação prestada desde o início da introdução do nosso experimento cedendo seu experimento que vinha conduzindo há anos para que pudéssemos encaixar meu projeto de tese ao dela;

Aos técnicos da Embrapa Arroz e Feijão a imensa amizade, ajuda e apoio na condução, colheita e avaliação dos experimentos feitos por dois anos consecutivos;

À Universidade Federal de Goiás, em especial à Escola de Agronomia, a oportunidade gratuita de cursar a graduação, mestrado e, por último, doutorado em Agronomia;

A todo corpo docente do Programa de Pós-graduação em Agronomia, área de concentração Solo e Água, aos ensinamentos transmitidos durante as disciplinas optativas;

À Coordenação de Aperfeiçoamento de Pessoal de Nível Superior (CAPES) a concessão da bolsa de estudos tanto no doutorado quanto no doutorado sanduíche feito durante 7 meses nos Estados Unidos, onde surgiu, com muito suor e dedicação, o primeiro capítulo desta tese.

Aos amigos e colegas da pós-graduação e integrantes do grupo de pesquisa LAPIG (Laboratório de Processamento de Imagens e Geoprocessamento) a grande ajuda nas avaliações à campo com drone.

Ainda, agradeço aos professores que aceitaram compor a banca para compartilhar a experiência de escrita e resultados desse trabalho.

Meu muito obrigado!

SUMÁRIO

RESUMO

CASTILHO SILVA, D. **Sensor multiespectral embarcado em sistema de aeronave remotamente pilotada para manejo de nitrogênio em milho e feijão-comum**. 2024. 105 f. Tese (Doutorado em Agronomia: Solo e Água) – Escola de Agronomia, Universidade Federal de Goiás, Goiânia, 2024.[1]

Este estudo abrangente visa avançar no campo da fenotipagem rápida, aproveitando sistema de aeronave pilotada remotamente (RPAS) e imagens multiespectrais para aprimorar a avaliação de características críticas das plantas, com foco particular no conteúdo de nitrogênio e na otimização do rendimento. Com base numa revisão sistemática de 41 artigos revisados por pares de 13 países, no primeiro capítulo, sintetizamos o conhecimento existente sobre a associação entre índices de vegetação (IVs) e características das plantas em diferentes estágios de crescimento de 11 principais espécies agrícolas. Extraindo insights de experimentos conduzidos ao longo de dois anos consecutivos, investigamos a correlação entre IVs, teor de nitrogênio foliar (LNC) e produtividade nos principais estágios de crescimento do milho e do feijão comum. O segundo capítulo examinou a eficácia dos IVs, como Green Normalized Difference Vegetation Index (GNDVI), Green to Near–Infrared Band Ratio (GN) e Transformed Chlorophyll Absorption in Reflectance Index (TCARI) na previsão de doses de nitrogênio e produtividade em milho nos estágios V6, V11 e R1. O terceiro capítulo focou no crescimento do feijão comum, integrando IVs selecionados com dados de textura (GLCM) derivados de imagens multiespectrais baseadas em RPAS para estimar com precisão o LNC em estágios críticos de crescimento (V4, R5 e R7). Notavelmente, o Green Normalized Difference Vegetation Index (GNDVI) e Modified Chlorophyll Absorption in Reflectance Index (MCARI) surgiram como preditores robustos do LNC, com a adição de métricas de textura (GLCM) aumentando a precisão, especialmente quando combinados com modelos de aprendizado de máquina como Random Forest (RF) e Support Vector Machine (SVM). Nossas descobertas ressaltam o potencial das imagens multiespectrais baseadas em RPAS, juntamente com técnicas avançadas para revolucionar os esforços de fenotipagem, facilitando o monitoramento mais preciso das principais variáveis das plantas e otimizando estratégias de manejo de culturas para melhor uso de insumos e manutenção de produtividade ao longo do tempo.

Palavras-chave: sistema de aeronave pilotada remotamente (RPAS), imagem multiespectral, índice de vegetação, feijão, milho.

---

[1] Orientadora: Drª. Beata Emoke Madari. Embrapa Arroz e Feijão.
Coorientadores: Dr. Manuel Eduardo Ferreira. LAPIG, IESA.
Drª. Maria da Conceição Santana Carvalho. Embrapa Arroz e Feijão.

ABSTRACT

CASTILHO SILVA, D. **Harnessing UAV-mounted spectral sensors for optimal nitrogen management in corn and bean crops**. 2024. 105 p. Thesis (Master in Agronomy: Soil and Water) - School of Agronomy, Federal University of Goiás, Goiânia – GO, 2024.[1]

This comprehensive study aims to advance the field of rapid phenotyping by leveraging unmanned aerial vehicles (UAVs) and multispectral imagery to enhance the assessment of critical plant traits, with a particular focus on nitrogen content and yield optimization. Building upon a systematic review of 41 peer-reviewed papers from 13 countries, on the first chapter, we synthesized existing knowledge on the association between vegetation indices (VIs) and plant traits across different growth stages of 11 major crop species. Drawing insights from experiments conducted over two consecutive years, we investigated the correlation between VIs, leaf nitrogen content (LNC), and yield at key growth stages of corn and common bean. The second chapter examined the efficacy of VIs such as Green Normalized Difference Vegetation Index (GNDVI), Green to Near–Infrared Band Ratio (GN) and Transformed Chlorophyll Absorption in Reflectance Index (TCARI) in predicting nitrogen rates and grain yield in corn at V6, V11, and R1 stages. The third chapter focused on common bean growth, integrating selected VIs with texture data derived from UAV-based multispectral images to accurately estimate LNC across critical growth stages (V4, R5, and R7). Notably, the Green Normalized Difference Vegetation Index (GNDVI) and Modified Chlorophyll Absorption in Reflectance Index (MCARI) emerged as robust predictors of LNC, with the addition of texture metrics enhancing accuracy, especially when combined with machine learning models like random forest (RF) and support vector machine (SVM). Our findings underscore the potential of UAV-based multispectral imagery coupled with advanced analytical techniques to revolutionize phenotyping efforts, facilitating more precise monitoring of key plant traits and optimizing crop management strategies for better use of inputs and maintenance of yield over time.

Key words: unmanned aerial vehicle (UAV), multispectral imagery, vegetation index, common bean, corn.

[1] Advisor: Drª. Beata Emoke Madari. Embrapa Arroz e Feijão.
Co-advisor: Dr. Manuel Eduardo Ferreira. LAPIG, IESA.
Drª. Maria da Conceição Santana Carvalho. Embrapa Arroz e Feijão.

1 INTRODUÇÃO

Nas práticas tradicionais de produção agrícola, a fertilidade das terras agrícolas é geralmente assumida como homogênea, sendo adotada uma estratégia uniforme de gerenciamento de nitrogênio (N), enquanto o estado real de N do solo e da cultura apresenta grande variabilidade espacial e temporal ao longo da área (Zhang et al., 2022). A aplicação adequada de fertilizantes nitrogenados é a estratégia chave para garantir a produtividade ideal das culturas (Han et al., 2022). A melhor indicação do estado nutricional da planta é o teor foliar de N, porém os meios tradicionais de medição do N foliar são demorados, trabalhosos e, portanto, não atendem às necessidades de monitoramento rápido e em tempo real (Blackmer & Schepers, 1996). A obtenção remota e eficaz do teor foliar de N sempre foi um problema urgente a ser resolvido para impulsionar zonas com maior potencial de rendimento e/ou reduzir insumos (Marang et al., 2021; Li et al., 2022).

O sistema de aeronave pilotada remotamente (RPAS) têm atraído considerável atenção científica e pública nos últimos anos, pois apresenta a vantagem de ser flexível de manipular, agindo como um método rápido, não destrutivo e eficiente (Jiang et al., 2020; Chen & Wang, 2022). A sua utilização oferece a possibilidade de obter dados de campo de forma fácil e rentável, resultando em imagens com alta resolução espacial e temporal (García-Martínez et al., 2020; Li et al., 2022). A principal vantagem do uso de RPAS é que grandes populações de plantas podem ser avaliadas rapidamente, ao mesmo tempo que reduzem imprecisões resultantes da amostragem de um subconjunto limitado de plantas (Costa et al., 2021). Os RPAS superaram as deficiências da deteção de aparelhos portáteis terrestres e de alta altitude (satélites), proporcionando um forte apoio à tecnologia de monitorização de informações sobre culturas na agricultura de precisão (Fu et al., 2020). Vários estudos mostraram o potencial de RPAS para estimar o conteúdo foliar de N em diversas culturas, como uva, algodão, milho, citrus, arroz e feijão (Osco et al., 2019; Wang et al., 2021; Xu et al., 2021; Peng et al., 2021; Peng et al., 2022).

Muitos esforços têm sido dedicados à identificação dos índices de vegetação (IVs) que melhor se correlacionam com as características das plantas (Almeida-Ñauñay et al., 2023). Os mais relevantes ligados ao status de N da cultura incluem o conteúdo de N foliar, a concentração de N na planta, o índice de nutrição de N (NNI) e a concentração de N (NC) para diferentes frações de plantas (Oliveira et al., 2020; Kou et al., 2022).

Um desafio crítico à medida que a tecnologia evolui e o número de estudos publicados sobre este tema cresce exponencialmente com o tempo é acompanhar o progresso atual e identificar lacunas no conhecimento da investigação. A maioria dos estudos que utilizam RPAS avaliam o conteúdo de nutrientes usando um modelo de regressão simples, tipicamente modelos lineares (Barbedo, 2019), e geralmente focados em algumas características das plantas. Até o momento, a literatura acadêmica existente sobre a fusão de estudos utilizando os mesmos IVs e características de plantas é limitada. O desenvolvimento de uma revisão mais organizada e estruturada pode ajudar a identificar IVs e características de plantas promissores, ao mesmo tempo que desenvolve um conjunto de dados aberto para auxiliar no progresso futuro neste tópico.

Embora muito trabalho tenha sido feito demonstrando que um RPAS com sensores multiespectrais passivos pode detectar estresse de N nas culturas, poucos estudos foram feitos para transformar essas leituras de sensores multiespectrais em um sistema prático de recomendação de N para ser aplicado em operações agrícolas. Além disso, estes estudos ignoraram mais informações armazenadas nas imagens de alta resolução adquiridas a baixa altura de voo, que contêm não apenas espectrais (IVs ou bandas únicas), mas também informações de textura relacionadas com as propriedades do N da cultura, como exemplo texturas baseadas em matriz de coocorrência de nível de cinza (GLCM).

Modelos como platô linear ou platô quadrático, podem ter vantagens sobre os outros, uma vez que utilizam IVs para correlacionar com conteúdo de N foliar, produtividade ou doses de N no milho. Estudos que utilizaram esses modelos conduziram os voos de RPAS em estágios mais avançados do milho (acima de V12), o que pode ser tarde demais para identificar e corrigir a deficiência de N, além disso, estimar a taxa de N nos estágios iniciais de crescimento do milho é de grande importância na produtividade final (Benincasa et al., 2017).

Nos últimos anos, aprendizado de máquina como Support Vector Machine (SVM), Random Forest (RF) e outros métodos têm sido cada vez mais aplicados na predição de N da cultura, superando os modelos tradicionais em termos de precisão. Pesquisas para a estimativa de conteúdo de N foliar para feijoeiro usando sensores baseados em RPAS são relativamente escassas. A maioria dos estudos existentes concentrou-se na estimativa da produtividade, índice

de área foliar e teor de matéria seca (Gutiérrez-Rodríguez et al., 2006; Köksal et al., 2008; Monteiro et al., 2013; Santana et al., 2016; Saravia et al., 2023). No entanto, a importância de estimar N foliar usando RF e SVM, em conjunto com IVs e métricas de textura GLCM, não pode ser subestimada no feijão.

Seguindo esse raciocínio, esse trabalho teve como objetivos produzir três capítulos mostrando no primeiro: um processo de revisão sistemática com foco na recuperação de conjuntos de dados sobre o estado da arte na avaliação de características de plantas baseadas em RPAS. Nosso conjunto de dados global concentra-se nas principais espécies de culturas agrícolas, 11 no total, recuperadas de estudos publicados durante as últimas duas décadas (2000 a 2023) em 13 países, com foco na relação entre IVs e características das plantas para caracterizar o status de N da cultura e identificar lacunas de conhecimento para orientar pesquisas futuras sobre avaliações de características de plantas baseadas em RPAS; no segundo capítulo: desenvolver um modelo para prever a dose de N necessária em cobertura para milho no estágio fenológico V6 usando dose de N e/ou conteúdo de N foliar; e no terceiro capítulo: determinar IVs e métricas de textura ideais de imagens multiespectrais de RPAS para estimar conteúdo de N foliar em feijão, explorando a capacidade de integração de informações espectrais e texturais na melhoria do monitoramento do status de N.

CAPÍTULO 1

A GLOBAL DATASET FOR ASSESSING NITROGEN-RELATED PLANT TRAITS USING DRONE IMAGERY IN MAJOR FIELD CROP SPECIES[1]

Diogo Castilho[2,3]; Danilo Tedesco[4]; Carlos Hernandez[4]; Beata Emoke Madari[2,3]; Ignacio Ciampitti[4]

[1] Capítulo submetido como artigo ao periódico científico Nature (Scientific Data). Submetido em 13 jun. 2023.

[2] Programa de Pós-graduação em Agronomia (PPGA), Universidade Federal de Goiás, Goiânia, Goiás, Brasil.
[3] Embrapa Arroz e Feijão, Santo Antônio de Goiás, Goiás, Brazil.
[4] Departamento de Agronomia, Kansas State University, 1712 Claflin Rd., Manhattan, KS, 66506, USA.

ABSTRACT

Enhancing rapid phenotyping for key plant traits, such as biomass and nitrogen content, is critical for effectively monitoring crop growth and maximizing yield. Studies have explored the relationship between vegetation indices (VIs) and plant traits using drone imagery. However, there is a gap in the literature regarding data availability, accessible datasets. Based on this context, we conducted a systematic review to retrieve relevant data worldwide on the state of the art in drone-based plant trait assessment. The final dataset consists of 41 peer-reviewed papers with 11,189 observations for 11 major crop species distributed across 13 countries. It focuses on the association of plant traits with VIs at different growth stages. This dataset provides foundational knowledge on the key VIs to focus for phenotyping key plant traits. In addition, future updates to this dataset may include new open datasets. Our goal is to continually update this dataset, encourage collaboration and data inclusion, and thereby facilitate a more rapid advance of phenotyping for critical plant traits to increase yield gains over time.

2.1 Background & Summary

Agriculture is an important industry, serving as the foundation of food security and of the global economy[1]. The complexity of biological systems is reflected in the spatial temporal variability of the soil and crop N status within a field[2]. To ensure optimal use of outputs, fertilizers should be provided at the right time, place, with an adequate source and at the right rate, only when necessary[3]. Therefore, a variable nitrogen (N) management strategy must be implemented to optimize fertilizer N rates, economic benefits, and maintaining or increasing both yield and quality[4].

N is a critical element for crop growth and one of the most important nutrients in agriculture to improve crop yield and for protein formation[5]. Furthermore, the utilization of the right fertilizer N rate is crucial not only to increase yields but to reduce the environmental footprint of this practice[3,6]. Traditional methods for detecting crop N status involve time-consuming field sampling and costly laboratory analysis[7]. Monitoring crop N status efficiently and effectively remains an urgent problem to be solved[8,9].

In recent years, technological innovations based on the utilization of multispectral and hyperspectral sensors mounted in different platforms help to provide critical imagery data for phenotyping and developing new tools for precision agriculture[10]. The emergence of unmanned aerial vehicles (UAV, or commonly known as drone) has advanced remote sensing applications at fine scales. UAV have gained significant scientific and public interest, due to their flexibility,

easiness to use, and affordability[11,12]. The aerial platform and sensor cost with a rapid image availability make this equipment valuable for assessing critical plant traits for advancing yield gains[13,14].

Characterization of key plant traits can vary depending on the crop and growth stage. Many efforts have been dedicated to identifying VIs that best correlates to plant traits[15–18]. The most relevant linked to crop N status include leaf N content (LNC), plant N concentration (PNC), N nutrition index (NNI), and N concentration (NC) for different plant fractions[19–24]. Several crops have been investigated using drone technology to assess plant traits, including but not limited to wheat (*Triticum aestivum* L.)[15], corn (*Zea mays* L.)[16], rice (*Oryza sativa* L.)[17], and barley *(Hordeum vulgare)*[18]. Different crops may require species-specific VIs to better characterize crop N status, as differences in leaf structure, canopy architecture, N allocation, and phenological stage should be taken into account when comparing across them[4,25,26]. In addition, other factors such as soil exposure, crop residues, and N application levels can also affect the stability of an index[27], provide restrictions to use a more universal index for accurately estimate similar plant traits across crop species[11]. For example, NDVI has been found to be a reliable index for N estimation in corn but less effective for rice[28–31]. Therefore, it is important to identify and evaluate the most effective VIs more directly targeting specific plant traits across major field crops.

A critical challenge as technology is evolving and the number of published studies on this topic grows exponentially with time is to keep up with the current progress and identify research knowledge gaps. Furthermore, as the analysis is based on a single experiment with N treatments and small plots, further research is needed to translate current findings to real-world scenarios[32]. Most studies using UAV assess nutrient content using a simple regression model, typically linear models[14], and usually focused on a few plant traits. To date, the existing academic literature on the merger of studies utilizing the same VIs and plant traits is limited. Therefore, developing a more organized and structured review can help identify promising VIs and plant traits while developing an open dataset to assist future progress on this topic.

Following this rationale, a systematic review process focusing on retrieving datasets on the state of the art in drone-based plant traits assessment was executed. Our global dataset focuses on major field crop species, 11 total, retrieved from studies published during the last two decades (2000 to 2023) in 13 countries. The final dataset contains 41 peer-reviewed scientific manuscripts focusing on the relationship between VIs and plant traits for characterizing crop

N status and identifying knowledge gaps to guide future research on drone-based plant traits assessments.

2.2 Methods

A literature search was conducted, involving identification, screening, eligibility, and inclusion of relevant records (Fig. 1a). The Scopus and Web of Science search engines were the main data sources. The keywords “multispectral airborne images” or “drone” or “UAV” or “UAS” or “unmanned aerial vehicle” or “remotely piloted aircraft system”, AND “nitrogen” AND “yield” were included in the search criteria, restricting the duration from 2000 to March 2023 to identify the most promising modern technologies.

After retrieving all relevant records (number of studies, n = 372), a first screening process was performed to remove duplicates (n = 264) for further processing. As a next step, an intensive analysis/full text reading was executed. Studies presenting the following criteria were excluded of the final database: 1) languages other than English, 2) unavailability of full-text publication, 3) lack of focus on field experiments (other setting greenhouse, growth chamber, pots, etc.), 4) articles that did not use drones to collect RGB, multi- or hyperspectral images, 5) used more than one crop/plant mixed (not focus on a single cropping specie), 6) study not focused on plant N/yield association, 7) lack of observed N determinations (excluding indirect N measurements such as chlorophyll meters, handheld sensors), and lastly, 8) those studies only benchmarking UAV derived imagery data with handheld sensors.

In the next step, full-text screening was performed to exclude studies that did not report data on VIs and plant trait, removing 222 papers. An additional 23 papers were identified and reviewed by examining citations from the remaining manuscripts, resulting in the inclusion of 22 additional studies. These studies were checked for duplicates. As a result, a final database comprises 41 articles published between 2010 to 2023 (Fig. 1b).

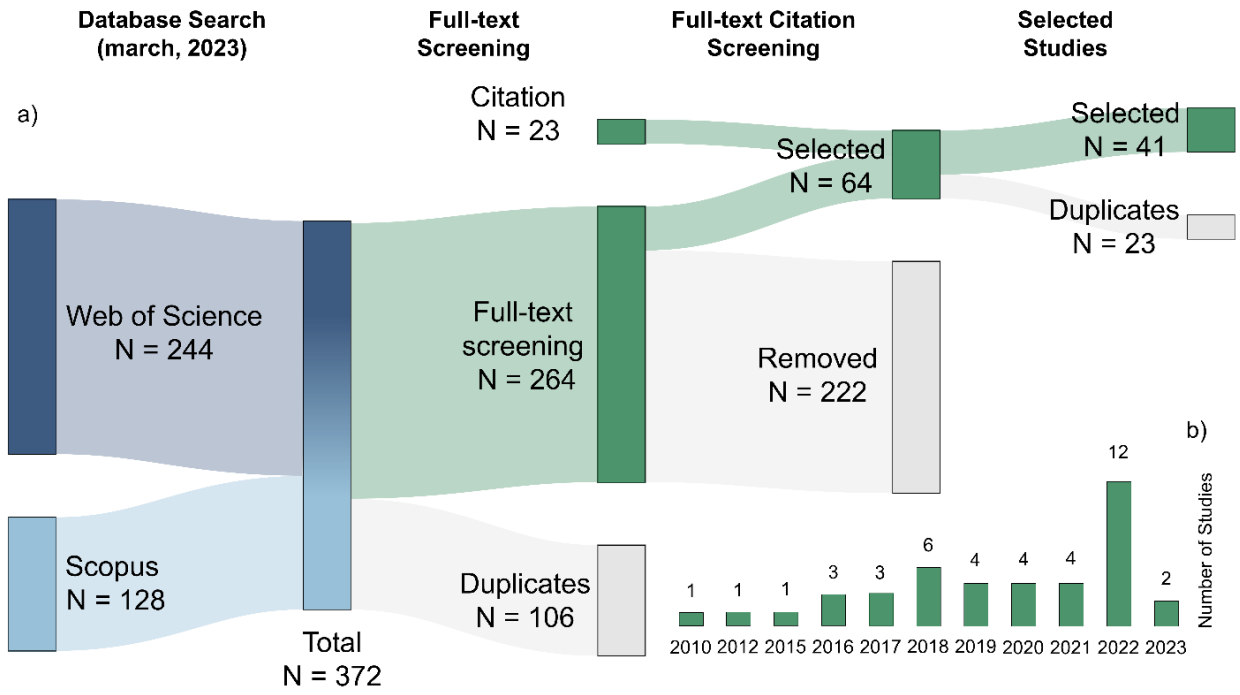

Fig. 1 a) Sankey diagram illustrating the studies search, collection, filtering, and selection. b) Number of studies selected per year.

A total of 41 records were identified fulfilling the main criterion of crop N estimation using different crops with RGB, multispectral, and hyperspectral data derived from the utilization of drones. The data retrieved from each paper included: i) geographic location of the experiments, ii) crop species, iii) plant traits (N content/concentration, N nutrition index (NNI), N uptake, leaf/plant N accumulation, canopy N content, N rate, and biomass), iv) VIs/bands, v) applied N rates, and vi) timing of UAV flights/phenological stages (further details presented in Table 1).

ID	Author	Year	Country	Crop	Phenological Stage / Time[1]	Plant Traits	Vegetation Index[2]	Ref
01	Almeida-Ñauñay et al.	2023	Spain	Wheat	Stem Elongation, Flowering	Yield (t ha^{-1})	NDVI	15
02	Argento et al.	2021	Switzerland	Winter Wheat	Tillering, Stem Elongation, Heading	Plant N Concentration (%), NNI, N uptake (kg ha^{-1})	MCARI/MTVI2, NDRE	33
03	Ballester et al.	2017	Australia	Cotton	First Flower, First Cracked Boll, Maturity	Plant N Concentration (%), N uptake (kg ha^{-1})	SCCCI, TCARI/OSAVI, TGI, VARI, NDRE, NDVI	34
04	Benincasa et al.	2017	Italy	Winter Wheat	Stem Elongation, Heading	Yield (t ha^{-1})	NDVI	3
05	Cai et al.	2019	USA	Corn	VT, R3, R4, R5, R6	Yield (t ha^{-1}), Leaf N Concentration (%)	CIg	16
06	Caturegli et al.	2019	Italy	Bermudagrass, Tall fescue	Mature	Leaf N Concentration (%)	DGCI	35
07	Chen et al.	2019	China	Winter Wheat	Stem Elongation	NNI, Relative Yield	-	36
08	De Andrade et al.	2022	Brazil	Soybean	R3	Leaf N Content (g m^{-2})	CVI, GRVI, RECI, SCCCI	37
09	Fassa et al.	2022	Italy	Corn	V7	Yield (t ha^{-1})	NDRE	38
10	Fu et al.	2020	China	Winter Wheat	Stem Elongation, Heading, Flowering	Plant N Concentration (%), Leaf N Concentration (%), Leaf N Density (g m^{-2}), Plant N Density (g m^{-2})	CIVE, ExR, GLI	39
11	Fu et al.	2021	China	Wheat	Stem Elongation - Heading - Flowering - Ripening	Leaf N Concentration (%)	NDRE	40
12	Geipel et al.	2016	Germany	Winter Wheat	Stem Elongation, Heading, Flowering, Ripening	Plant N Concentration (%), Yield (t ha^{-1})	REIP	32
13	Heinemann et al.	2022	Germany	Wheat	Stem Elongation, Heading, Flowering	N uptake (kg ha^{-1})	REIP	41
14	Jiang et al.	2022	China	Winter Wheat	Tillering, Heading	NNI, Yield (t ha^{-1})	-	42
15	Kefauver et al.	2017	Spain	Barley	150 DAP[3]	Yield (t ha^{-1})	NDVI, OSAVI, RDVI, SAVI, WBI	18
16	Lebourgeois et al.	2012	Reunion Island	Sugarcane	Grand Growth	Canopy N Content (g m^{-2}), Leaf N Content (g m^{-2})	NDVI, GNDVI, SRPI	12
18	Li et al.	2010	China	Winter Wheat	Tillering - Heading	Plant N Concentration (%)	NDI (365, 410), SR (787 / 765)	43
19	Li et al.	2015	China	Rice	Filling	Leaf N Concentration (%)	DGCI	17

ID	Author	Year	Country	Crop	Phenological Stage / Time[1]	Plant Traits	Vegetation Index[2]	Ref
17	Li et al.	2018	USA	Sorghum	120 DAP[3]	Biomass (t ha^{-1})	RDVI	44
20	Liu et al.	2018	China	Oilseed Rape	Vegetative	NNI	CIRE, VARI	45
21	Luo et al.	2022	China	Rice	Booting, Heading	Yield (t ha^{-1})	SAVI, WDRVI	46
22	Maresma et al.	2016	Spain	Corn	V12	N rate (kg ha^{-1})	NDVI, GRVI, WDRVI	47
23	Namoi et al.	2022	USA	*Miscanthus × giganteus*	Mid-summer growing season	Biomass (t ha^{-1})	NDRE	48
24	Osco et al.	2020	Brazil	Corn	V12	Leaf N Concentration (%)	GNDVI, NDRE, NDVI, NIR, Red, SAVI	49
25	Pipatsitee et al.	2022	Thailand	Corn	Vegetative, Reproductive	Yield (t ha^{-1}), Biomass (t ha^{-1})	NDRE, NDVI	50
26	Rodene et al.	2022	USA	Corn	R1	Leaf N Concentration (%)	VEG	51
27	Vergara-Diaz et al.	2016	Zimbabwe	Corn	R1	Leaf N Concentration (%)	NDVI	52
28	Viljanen et al.	2018	Finland	Grass Swards	06, 15, 19, 28 / June	Biomass (t ha^{-1})	MSAVI	53
29	Walsh et al.	2018	USA	Spring Wheat	Tillering, Heading	Plant N Concentration (%)	Clg, CIRE, EVI2, MTCI, NDRE, NDVI	54
30	Walsh et al.	2022	USA	Wheat	Stem Elongation, Heading	Yield (t ha^{-1})	NDVI	55
31	Walsh et al.	2023	USA	Wheat	Stem Elongation, Heading	Yield (t ha^{-1}), N uptake (kg ha^{-1})	NDVI	56
32	Wang et al.	2019	Denmark	Grass	GDD[4] 432 - 861	Plant N Concentration (%), Biomass (t ha^{-1})	-	57
33	Wang et al.	2021	China	Rice	Tillering, Jointing, Booting	Leaf N Concentration (%)	CIRE	58
34	Wang et al.	2022	China	Rice	Jointing, Booting, Heading	Leaf N Concentration (%)	CIRE, CIREg, SAVI	59
35	Xu et al.	2021	USA	Switchgrass (Panicum virgatum)	End of season	Plant N Concentration (%)	NDRE	60
36	Xu et al.	2022	China	Rice	Jointing, Heading, Filling	Biomass (t ha^{-1})	GOSAVI	61
37	Yang et al.	2020	China	Winter Wheat	Flowering - Ripening	NUE - Plant N Content (kg ha^{-1})	GNDVI, NDRE, RNDVI	62
38	Zhang et al.	2022	China	Wheat	Stem Elongation, Heading, Flowering	Yield (t ha^{-1}), N uptake (kg ha^{-1}), Biomass (t ha^{-1})	DATT, RESAVI	2
39	Zheng et al.	2018	China	Rice	Jointing, Booting, Heading, Filling	Plant N Concentration (%)	Clg, CIRE, NDVI, OSAVI, Viopt	7

ID	Author	Year	Country	Crop	Phenological Stage / Time[1]	Plant Traits	Vegetation Index[2]	Ref
40	Zheng et al.	2018	China	Rice	Tillering, Jointing, Booting	Leaf N Accumulation (g m^{-2}), Plant N Accumulation (g m^{-2})	CIRE, DATT, ENDVI, ExG, GNDVI, NGRDI	63
41	Zheng et al.	2020	China	Rice	Jointing - Booting - Heading - Filling	Plant N Concentration (%), Leaf N Concentration (%), Leaf N Accumulation (g m^{-2}), Plant N Accumulation (g m^{-2})	NDRE	64

Table 1. Study identification (ID), author, year, country, crop, phenological stage/time, plant traits and vegetation index. [1]Stages followed by a comma or dashes represent studies that assessed plant traits in each or across phenological stages, respectively. [2]A missing vegetation index value indicates that only plant traits were assessed. Information regarding the full VIs names is available on the figshare repository[65]. [3]DAP: Days After Planting. [4]GDD: Growing Degrees Days.

The overall distribution of the selected studies, main crop species, and number of observations of the data are presented in Fig 2. Among the 41 studies selected, 15 reported data on wheat, 8 for rice, 7 for corn, 4 for grasses, and 7 for other crops, such as barley, cotton (*Gossypium hirsutum* L.), *Miscanthus* x *giganteus*, oilseed rape (*Brassica napus* L.), sorghum (*Sorghum bicolor* L.), soybean (*Glycine max*), and sugarcane (Saccharum officinarum).

The total number of pairs of observed plant traits and VIs per crop were: barley (*Hordeum vulgare*) 251, corn (*Zea mays* L.) 1282, cotton (*Gossypium hirsutum* L.) 876, grass (bermudagrass hybrid, tall fescue, grass sward, perennial ryegrass, red fescue, and *Panicum virgatum*) 367, *Miscanthus* x *giganteus* 57, oilseed rape (*Brassica napus* L.) 94, rice (*Oryza sativa* L.) 3232, sorghum (*Sorghum bicolor* L.) 196, soybean (*Glycine max*) 78, sugarcane (Saccharum officinarum) 1026, and wheat (*Triticum aestivum* L.) 3730 observations in 13 countries (Fig. 2).

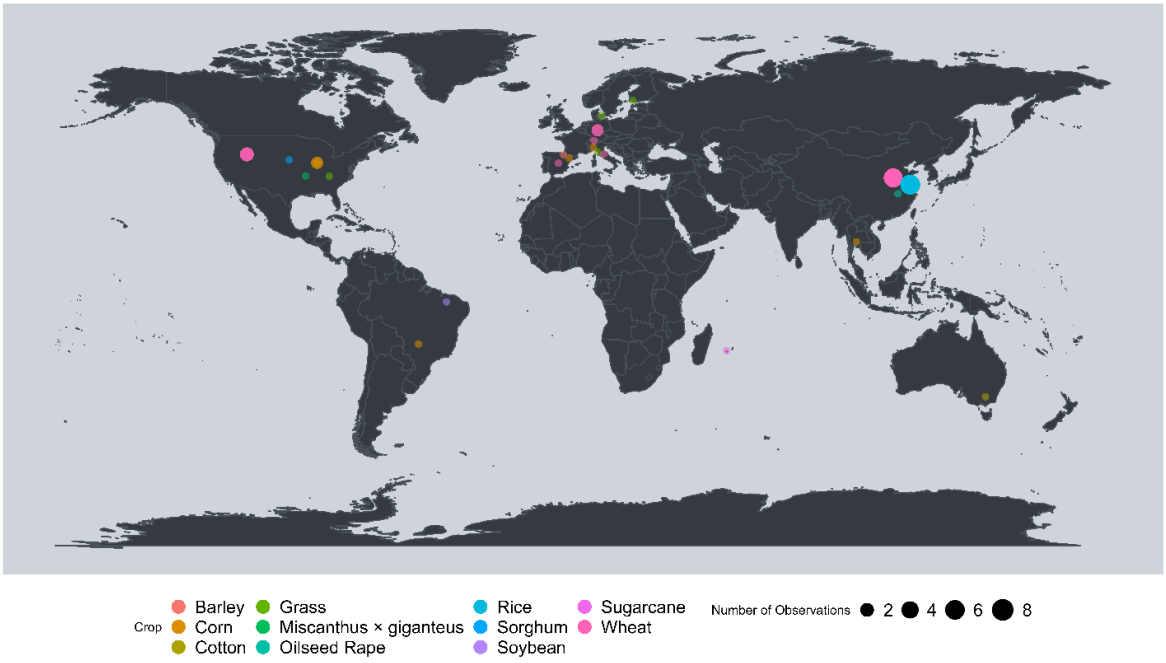

Fig. 2 Distribution of studies (number of observations) included in the final database according to their countries of origin and tested field crops.

For each article presented in Table 1, all available information on VIs and plant traits from figures, tables, text, and supplementary material was extracted using the 'juicr' R package[66]. Also, the data were visually inspected to ensure the information was associated with plant development stage.

Among the 14 plant traits identified during data extraction (Table 2a), only two plant traits (i.e., relative yield and N uptake) could be combined, considering crop type (i.e., wheat and cotton), VIs (i.e., NDVI and NDRE), and phenological stage (Table 2b).

a)

Plant Trait	Crop
Yield (Mg ha^{-1})	Barley, Corn, Rice, Wheat
Plant N Density (g m^{-2})	Wheat
Plant N Concentration (%)	Cotton, Grass, Rice, Wheat
Plant N Accumulation (g m^{-2})	Rice
NUE - Plant N Content (kg ha^{-1})	Wheat
NNI	Oilseed Rape, Wheat
N uptake (kg ha^{-1})	Cotton, Wheat
N rate (kg ha^{-1})	Corn
Leaf N Density (g m^{-2})	Wheat
Leaf N Content (g m^{-2})	Soybean, Sugarcane
Leaf N Concentration (%)	Corn, Grass, Rice, Wheat
Leaf N Accumulation (g m^{-2})	Rice
Canopy N Content (g m^{-2})	Sugarcane
Biomass (Mg ha^{-1})	Corn, Grass, *Miscanthus* x *giganteus*, Rice, Sorghum, Wheat

b)

Plant Trait	Crop	Time	Index	Study
Yield (Mg ha^{-1})	Wheat	Tillering, Stem Elongation, Heading	NDVI	3,15,55,56
N uptake (kg ha^{-1})	Wheat, Cotton	Stem Elongation, Heading (Wheat); First Cracked Boll, First Flower, Maturity (Cotton)	NDVI, NDRE	33,34,56

Table 2. Overview of the 11 crops with their respective plant traits performed. a) The table comprises all possible estimated plant traits based on the crop. b) The table comprises the information of articles that were possible to combine based on the same VI for the respective time used in each crop plant.

2.3 Data Records

The data are accessible on the figshare repository[65], available at https://doi.org/10.6084/m9.figshare.22938797, and includes the following files:

1. "UAV_database.xlsx" includes the data.

2. "Summary of the database.docx", includes a summary of the dataset, defining each column, data extracted from the studies, the units for each variable when pertinent, and a definition for each variable.

3. “List of references.docx”, presents all the references of the publications included in the dataset.

4. “List of vegetation indices.docx”, presents all the abbreviated VIs with their full names of the studies located in the dataset.

5. “Codes.zip”, includes all codes to make the figures of this study.

The “UAV_database” contains all the information collected on this systematic analysis. The “Summary of the database” presents a description for each column of the “UAV_database” file with the information separated into three categories:

Category I, general specification of the study, containing information for author and publication year, and paper identification for each study included in the dataset.

Category II, experiment information, describing species, VI used, VI value, coefficient of determination (R^2), root mean square error (RMSE), and phenological stage sampling moment or dates.

Category III, key for the dataset related to plant traits used. All plant traits information is reported with their units, as expressed in the data collected from those respective studies. This category shows the amount of N rate applied, plant/leaf N concentration/content, N nutrition index, yield, relative yield, N uptake, leaf/plant N density, leaf/plant N accumulation, canopy N content, and the aboveground biomass values.

Table 1 describes the main topics of the 41 selected studies, including species, country for the study location, author, and year of publication, phenological stage sampling moment, plant traits and VIs utilized for each study, and relevant keyword for the study.

2.4 Technical Validation

To demonstrate the value of the dataset, the relationship between VIs and plant traits was investigated. After constructing the database, we checked for potential outliers and carefully summarized the information to analyze the interaction of multiple studies with the goal of merging them.

Data of N uptake and two VIs (NDRE and NDVI) are presented in Fig. 3 for three studies across stages and crops (cotton and wheat). These three studies were conducted in Switzerland, Australia, and the United States for wheat crop at three stages (tillering, stem

elongation, and heading) and then for cotton crop at three stages (first flower, first cracked boll, and maturity). The N uptake (kg N ha^{-1}) was calculated by multiplying the dry matter biomass (kg ha^{-1}) with the corresponding N concentration (%) of the plant sample[33]. Although these two crops are managed differently with respect to crop management such as time of nutrient application, the overall trend was similar between VIs and the key plant N trait identified for these crop species.

In contrast to NDRE, NDVI saturated shortly after stem elongation before decreasing rapidly during the senescence phase1 when studies were combined (saturation point when NDVI ≥ 0.5). The NDVI seems to be a viable N status indicator for a first N application, when the crop leaf canopy has not closed yet. The NDRE progress was linear until the stage of spike emergence, which takes place after the fertilizer application in winter wheat. Thus, it is plausible that NDRE is a better VI for the creation of fertilizer prescription maps and N uptake assessment than NDVI. Moreover, the correlation value for NDRE (R^2 = 0.80 and 0.67 for wheat and cotton, respectively) confirmed the assumption that NDRE can be used to monitor the N status of the wheat and cotton crops. Lastly, these studies provide initial evidence of the potential superiority of red-edge-NIR based spectral indices over NDVI (R^2 between 0.11 – 0.65 across crops)[33,34]. In addition, this dataset helps to demonstrate the need of expanding the exploration of other spectral bands to target specific plant N traits more directly.

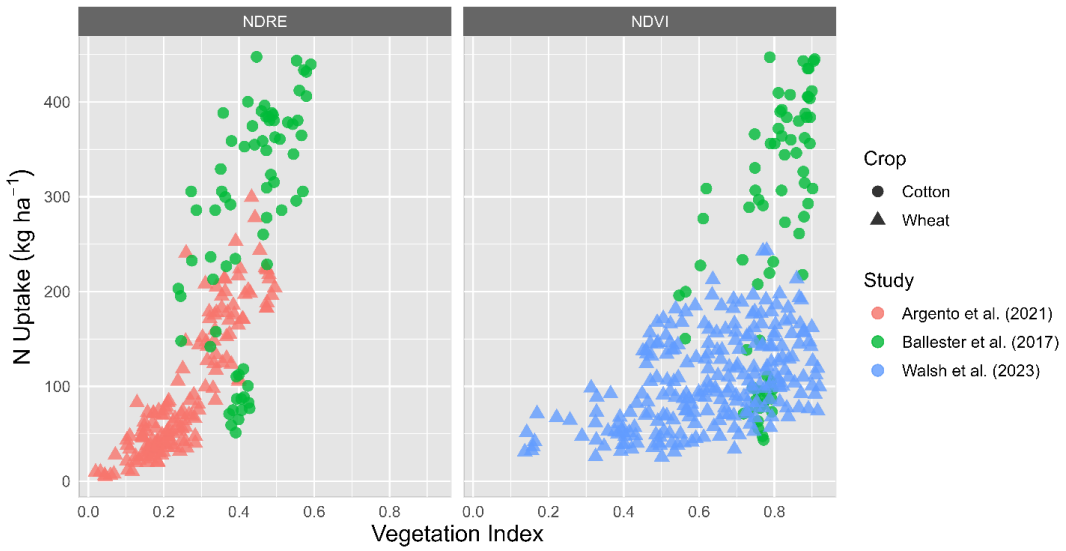

Fig. 3 Relationship between nitrogen (N) uptake (kg ha^{-1}) and two VIs (NDRE, NDVI) for cotton and wheat crops. Colors refer to different studies, and type of symbols represent the different field crop.

2.5 Usage Notes

This dataset can be used in studies to diagnose N status and various plant traits in different crop species using UAV imagery. For example, recent studies have used NDVI as a yield predictor for wheat[3,15,55,56]. However, when combining data from these studies conducted across different environments, it is not possible to gain insights about the relationship between relative yield and NDVI (Fig. 4). It is noteworthy to understand that different growth stages will present varying conditions, which indicates the need to properly report crop phenology (growth stage) and environmental conditions (rainfed vs. Irrigated) when correlating yield with any VI[67]. For instance, some studies have highlighted the importance of obtaining an estimation of crop biomass in reducing variability/noise when exploring crop N status[68]. This approach could lead to more reliable models and the development of more universal N management guidelines.

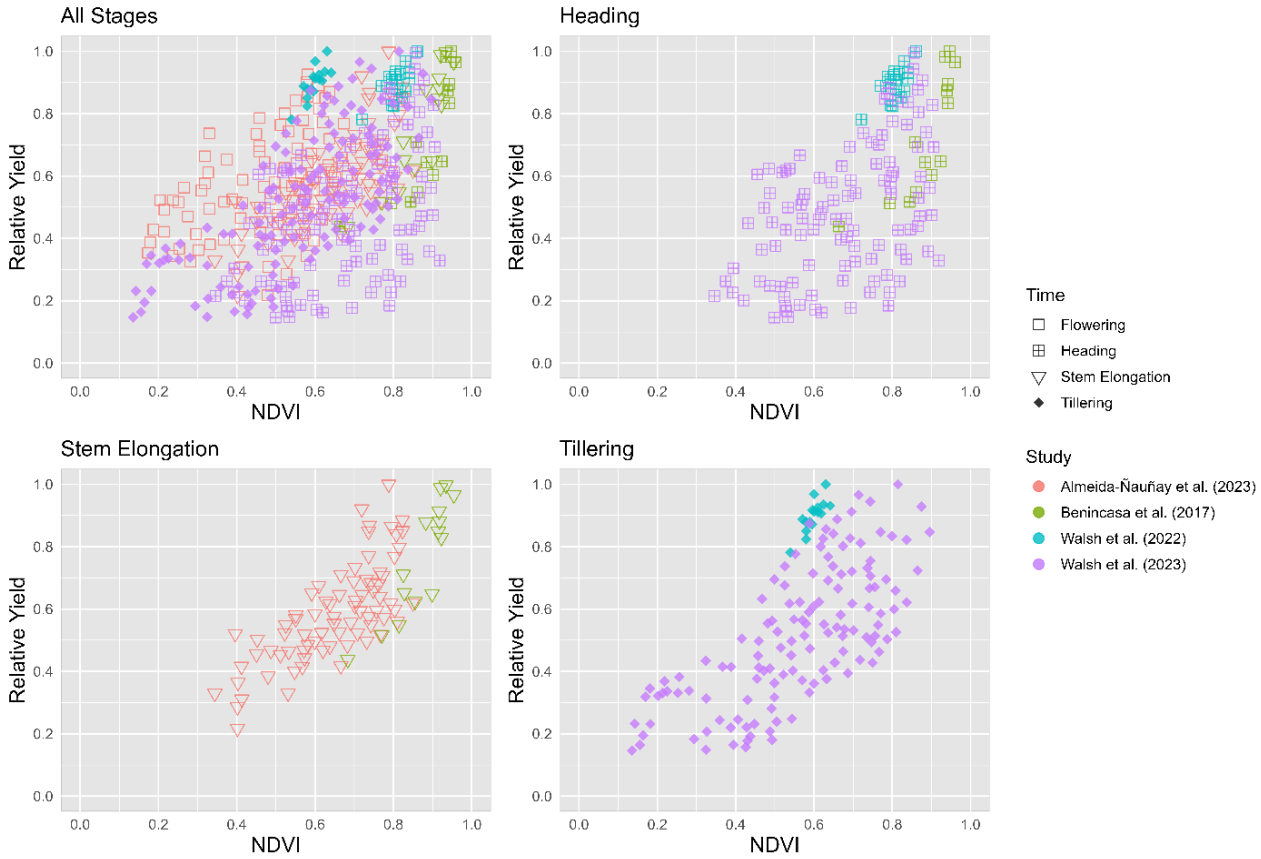

Fig. 4 Relationship between relative yield and NDVI for wheat comprising all stages and individual ones (tillering, stem elongation and heading) combined. Colors represent different studies, and the type of symbols refer to the crop growth stage (time).

Despite considerable progress, there are still many relevant research knowledge gaps in drone-based crop research. Many studies do not use the same VIs to analyze a specific plant trait and/or phenological stage. In addition, numerous studies provided metrics (R^2 and/or RMSE) of the relationship between plant trait and VI, but often omitted the corresponding data, restricting the future use of those studies.

Future updates to this dataset could include newly published studies and previously unavailable data (with potential for more contribution from different authors). The goal is to continually expand the dataset to encourage collaboration, open science, and inclusion of more data for more comprehensive UAV-VI crop trait estimates. Additionally, the dataset could be expanded to include other plant traits such as other nutrient deficiencies (e.g., potassium), drought status, and pest and disease detection. Drone-based imagery data can help detect changes in crop N status early in the season, permitting to adjust via interventions. Improving the ability to more precisely and dynamically correct crop N deficiencies will help farmers focus on a more sustainable approach to monitor large areas in a short period of time, improving farming profitability and reducing the environmental footprint.

2.6 Code Availability

Scripts using R programming language are provided to produce figures. Additional code and related files are available at figshare repository[65]: https://figshare.com/s/177cdcd70963a415925b.

Acknowledgements

The research to create this database was funded by the Coordination for the Improvement of Higher Education Personnel - Brazil (CAPES) - Finance Code 001, sandwich program. This is a contribution no. 23-XYZ for the Kansas Agricultural Experiment Station.

Author contributions

The manuscript design was a collaborative effort with contributions from all authors. Diogo Castilho and Danilo Tedesco worked on the data collection process and were guided by Ignacio Ciampitti and Carlos Hernandez. Diogo Castilho wrote the original draft of the manuscript, and all authors reviewed the final version of the manuscript.

Competing interests

The authors declare no competing interests.

2.7 References

1. Yu, J., Wang, J. & Leblon, B. Evaluation of soil properties, topographic metrics, plant height, and unmanned aerial vehicle multispectral imagery using machine learning methods to estimate canopy nitrogen weight in corn. *Remote Sens.* **13**, (2021).
2. Zhang, J. *et al.* In-season variable rate nitrogen recommendation for wheat precision production supported by fixed-wing UAV imagery. *Precis. Agric.* **23**, 830–853 (2022).
3. Benincasa, P. *et al.* Reliability of ndvi derived by high resolution satellite and uav compared to in-field methods for the evaluation of early crop n status and grain yield in Wheat. *Exp. Agric.* **54**, 604–622 (2017).
4. Han, S. *et al.* Monitoring Key Wheat Growth Variables by Integrating Phenology and UAV Multispectral Imagery Data into Random Forest Model. *Remote Sens.* **14**, (2022).
5. Javed, T. *et al.* Recent Advances in Agronomic and Physio-Molecular Approaches for Improving Nitrogen Use Efficiency in Crop Plants. *Front. Plant Sci.* **13**, 1–21 (2022).
6. Arroyo, J. A. *et al.* Assessing nitrogen nutrition in corn crops with airborne multispectral sensors. *Lect. Notes Comput. Sci. (including Subser. Lect. Notes Artif. Intell. Lect. Notes Bioinformatics)* **10351 LNCS**, 259–267 (2017).
7. Zheng, H. *et al.* Combining unmanned aerial vehicle (UAV)-based multispectral imagery and ground-based hyperspectral data for plant nitrogen concentration estimation in rice. *Front. Plant Sci.* **9**, 1–13 (2018).
8. Li, M. *et al.* Retrieval of Nitrogen Content in Apple Canopy Based on Unmanned Aerial Vehicle Hyperspectral Images Using a Modified Correlation Coefficient Method. *Sustain.* **14**, (2022).
9. Wang, L. *et al.* Estimation of paddy rice nitrogen content and accumulation both at leaf and plant levels from uav hyperspectral imagery. *Remote Sens.* **13**, 1–21 (2021).
10. Näsi, R. *et al.* Estimating biomass and nitrogen amount of barley and grass using UAV and aircraft based spectral and photogrammetric 3D features. *Remote Sens.* **10**, 1–32 (2018).
11. Chen, P. & Wang, F. Effect of crop spectra purification on plant nitrogen concentration estimations performed using high-spatial-resolution images obtained with unmanned aerial vehicles. *F. Crop. Res.* **288**, 108708 (2022).
12. Lebourgeois, V., Bégué, A., Labbé, S., Houlès, M. & Martiné, J. F. A light-weight multi-spectral aerial imaging system for nitrogen crop monitoring. *Precis. Agric.* **13**, 525–541 (2012).
13. Xiang, H. & Tian, L. An automated stand-alone in-field remote sensing system (SIRSS) for in-season crop monitoring. *Comput. Electron. Agric.* **78**, 1–8 (2011).
14. Barbedo, J. G. A. A review on the use of unmanned aerial vehicles and imaging sensors for monitoring and assessing plant stresses. *Drones* **3**, 1–27 (2019).

15. Almeida-Ñauñay, A. F. *et al.* Optimization of soil background removal to improve the prediction of wheat traits with UAV imagery. *Comput. Electron. Agric.* **205**, (2023).

16. Cai, Y. *et al.* Detecting In-Season Crop Nitrogen Stress of Corn for Field Trials Using UAV-and CubeSat-Based Multispectral Sensing. *IEEE J. Sel. Top. Appl. Earth Obs. Remote Sens.* **12**, 5153–5166 (2019).

17. Li, J., Zhang, F., Qian, X., Zhu, Y. & Shen, G. Quantification of rice canopy nitrogen balance index with digital imagery from unmanned aerial vehicle. *Remote Sens. Lett.* **6**, 183–189 (2015).

18. Kefauver, S. C. *et al.* Comparative UAV and field phenotyping to assess yield and nitrogen use efficiency in hybrid and conventional barley. *Front. Plant Sci.* **8**, 1–15 (2017).

19. Kou, J. *et al.* Predicting Leaf Nitrogen Content in Cotton with UAV RGB Images. *Sustain.* **14**, (2022).

20. Oliveira, R. A. *et al.* Machine learning estimators for the quantity and quality of grass swards used for silage production using drone-based imaging spectrometry and photogrammetry. *Remote Sens. Environ.* **246**, 111830 (2020).

21. Heinemann, P. & Schmidhalter, U. Spectral assessments of N-related maize traits: Evaluating and defining agronomic relevant detection limits. *F. Crop. Res.* **289**, 108710 (2022).

22. Qiu, Z. *et al.* Estimation of nitrogen nutrition index in rice from UAV RGB images coupled with machine learning algorithms. *Comput. Electron. Agric.* **189**, 106421 (2021).

23. Gabriel, J. L. *et al.* Airborne and ground level sensors for monitoring nitrogen status in a maize crop. *Biosyst. Eng.* **160**, 124–133 (2017).

24. Li, X. *et al.* Sugarcane Nitrogen Concentration and Irrigation Level Prediction Based on UAV Multispectral Imagery. *Sensors* **22**, (2022).

25. Richardson, A. D., Duigan, S. P. & Berlyn, G. P. An evaluation of noninvasive methods to estimate foliar chlorophyll content. *New Phytol.* **153**, 185–194 (2002).

26. Gitelson, A. A., Gritz, Y. & Merzlyak, M. N. Relationships between leaf chlorophyll content and spectral reflectance and algorithms for non-destructive chlorophyll assessment in higher plant leaves. *J. Plant Physiol.* **160**, 271–282 (2003).

27. Yin, C. *et al.* Hyperspectral UAV Images at Different Altitudes for Monitoring the Leaf Nitrogen Content in Cotton Crops. *Remote Sens.* **14**, 1–19 (2022).

28. Lee, H., Wang, J. & Leblon, B. Using linear regression, random forests, and support vector machine with unmanned aerial vehicle multispectral images to predict canopy nitrogen weight in corn. *Remote Sens.* **12**, (2020).

29. Lee, H., Wang, J. & Leblon, B. Intra-Field Canopy Nitrogen Retrieval from Unmanned Aerial Vehicle Imagery for Wheat and Corn Fields. *Can. J. Remote Sens.* **0**, 454–472 (2020).

30. Xu, X. *et al.* Estimating leaf nitrogen content in corn based on information fusion of multiple-sensor imagery from uav. *Remote Sens.* **13**, 1–17 (2021).

31. Li, G. S. *et al.* Prediction of plant nutrition state of rice under water-saving cultivation

and panicle fertilization application decision making. *Agronomy* **11**, (2021).

32. Geipel, J., Link, J., Wirwahn, J. A. & Claupein, W. A programmable aerial multispectral camera system for in-season crop biomass and nitrogen content estimation. *Agric.* **6**, 1–19 (2016).

33. Argento, F. *et al.* Site-specific nitrogen management in winter wheat supported by low-altitude remote sensing and soil data. *Precis. Agric.* **22**, 364–386 (2021).

34. Ballester, C., Hornbuckle, J., Brinkhoff, J., Smith, J. & Quayle, W. Assessment of in-season cotton nitrogen status and lint yield prediction from unmanned aerial system imagery. *Remote Sens.* **9**, 1–18 (2017).

35. Caturegli, L. *et al.* Normalized Difference Vegetation Index versus Dark Green Colour Index to estimate nitrogen status on bermudagrass hybrid and tall fescue. *Int. J. Remote Sens.* **41**, 455–470 (2019).

36. Chen, Z. *et al.* In-season diagnosis of winter wheat nitrogen status in smallholder farmer fields across a village using unmanned aerial vehicle-based remote sensing. *Agronomy* **9**, (2019).

37. Junior, A. S. D. A. *et al.* REMOTE DETECTION OF WATER AND NUTRITIONAL STATUS OF SOYBEANS USING UAV-BASED IMAGES. *Eng. Agric.* **4430**, 9–23 (2022).

38. Fassa, V., Pricca, N., Cabassi, G., Bechini, L. & Corti, M. Site-specific nitrogen recommendations' empirical algorithm for maize crop based on the fusion of soil and vegetation maps. *Comput. Electron. Agric.* **203**, (2022).

39. Fu, Y. *et al.* Winter wheat nitrogen status estimation using uav-based rgb imagery and gaussian processes regression. *Remote Sens.* **12**, 1–27 (2020).

40. Fu, Z. *et al.* Combining UAV multispectral imagery and ecological factors to estimate leaf nitrogen and grain protein content of wheat. *Eur. J. Agron.* **132**, 126405 (2022).

41. Heinemann, P., Haug, S. & Schmidhalter, U. Evaluating and defining agronomically relevant detection limits for spectral reflectance-based assessment of N uptake in wheat. *Eur. J. Agron.* **140**, 126609 (2022).

42. Jiang, J. *et al.* Combining fixed-wing UAV multispectral imagery and machine learning to diagnose winter wheat nitrogen status at the farm scale. *Eur. J. Agron.* **138**, 126537 (2022).

43. Li, F. *et al.* Evaluating hyperspectral vegetation indices for estimating nitrogen concentration of winter wheat at different growth stages. *Precis. Agric.* **11**, 335–357 (2010).

44. Li, J., Shi, Y., Veeranampalayam-Sivakumar, A. N. & Schachtman, D. P. Elucidating sorghum biomass, nitrogen and chlorophyll contents with spectral and morphological traits derived from unmanned aircraft system. *Front. Plant Sci.* **9**, 1–12 (2018).

45. Liu, S. *et al.* Diagnosis of nitrogen status in winter oilseed rape (Brassica napus L.) using in-situ hyperspectral data and unmanned aerial vehicle (UAV) multispectral images. *Comput. Electron. Agric.* **151**, 185–195 (2018).

46. Luo, S. *et al.* Remotely Sensed Prediction of Rice Yield at Different Growth Durations Using UAV Multispectral Imagery. *Agriculture* **12**, 1447 (2022).

47. Maresma, Á., Ariza, M., Martínez, E., Lloveras, J. & Martínez-Casasnovas, J. A. Analysis of vegetation indices to determine nitrogen application and yield prediction in maize (zea mays l.) from a standard uav service. *Remote Sens.* **8**, (2016).

48. Namoi, N. *et al.* Aerial Imagery Can Detect Nitrogen Fertilizer Effects on Biomass and Stand Health of Miscanthus × giganteus. *Remote Sens.* **14**, (2022).

49. Osco, L. P. *et al.* Leaf nitrogen concentration and plant height prediction for maize using UAV-based multispectral imagery and machine learning techniques. *Remote Sens.* **12**, 1–17 (2020).

50. Pipatsitee, P., Tisarum, R. & Taota, K. Effectiveness of vegetation indices and UAV-multispectral imageries in assessing the response of hybrid maize (Zea mays L.) to water deficit stress under field environment. *Env. Monit Assess* **195**, (2023).

51. Rodene, E. *et al.* A UAV-based high-throughput phenotyping approach to assess time-series nitrogen.pdf. *Plant Phenome J.* 12 (2021) doi:10.1002/ppj2.20030.

52. Vergara-Díaz, O. *et al.* A novel remote sensing approach for prediction of maize yield under different conditions of nitrogen fertilization. *Front. Plant Sci.* **7**, 1–13 (2016).

53. Viljanen, N. *et al.* A novel machine learning method for estimating biomass of grass swards using a photogrammetric canopy height model, images and vegetation indices captured by a drone. *Agric.* **8**, (2018).

54. Walsh, O. S. *et al.* Assessment of UAV Based Vegetation Indices for Nitrogen Concentration Estimation in Spring Wheat. *Adv. Remote Sens.* **07**, 71–90 (2018).

55. Walsh, O. S. *et al.* Wheat yield and protein estimation with handheld- and UAV-based reflectance measurements. *Agrosystems, Geosci. Environ.* **5**, 1–14 (2022).

56. Walsh, O. S. *et al.* Wheat Yield and Protein Estimation with Handheld and Unmanned Aerial Vehicle-Mounted Sensors. *Agronomy* **13**, 1–14 (2023).

57. Wang, H., Mortensen, A. K., Mao, P., Boelt, B. & Gislum, R. Estimating the nitrogen nutrition index in grass seed crops using a UAV-mounted multispectral camera. *Int. J. Remote Sens.* **40**, 2467–2482 (2018).

58. Wang, W. *et al.* AAVI: A Novel Approach to Estimating Leaf Nitrogen Concentration in Rice from Unmanned Aerial Vehicle Multispectral Imagery at Early and Middle Growth Stages. *IEEE J. Sel. Top. Appl. Earth Obs. Remote Sens.* **14**, 6716–6728 (2021).

59. Wang, W. *et al.* An assessment of background removal approaches for improved estimation of rice leaf nitrogen concentration with unmanned aerial vehicle multispectral imagery at various observation times. *F. Crop. Res.* **283**, 108543 (2022).

60. Xu, Y. *et al.* Sustainability trait modeling of field-grown switchgrass (Panicum virgatum) using uav-based imagery. *Plants* **10**, 1–22 (2021).

61. Xu, L. *et al.* An improved approach to estimate ratoon rice aboveground biomass by integrating UAV-based spectral, textural and structural features. *Precis. Agric.* **23**, 1276–1301 (2022).

62. Yang, M. *et al.* Assessment of Water and Nitrogen Use Efficiencies Through UAV-Based Multispectral Phenotyping in Winter Wheat. *Front. Plant Sci.* **11**, 1–16 (2020).

63. Zheng, H. *et al.* Evaluation of RGB, color-infrared and multispectral images acquired

from unmanned aerial systems for the estimation of nitrogen accumulation in rice. *Remote Sens.* **10**, (2018).

64. Zheng, H. *et al.* Enhancing the nitrogen signals of rice canopies across critical growth stages through the integration of textural and spectral information from unmanned aerial vehicle (UAV) multispectral imagery. *Remote Sens.* **12**, (2020).

65. Castilho, D., Tedesco, D., Hernandez, C., Madari, B. E. & Ciampitti, I. A global dataset for assessing nitrogen-related plant traits using drone imagery in major field crop species. *figshare* https://figshare.com/s/177cdcd70963a415925b (2023).

66. Lajeunesse, M. J. Automated, semi-automated, and manual extraction of numerical data from scientific images, plot, charts, and figures. *R package version 0.1* https://cran.r-project.org/package=juicr (2021).

67. Zhao, Z. *et al.* A reappraisal of the critical nitrogen concentration of wheat and its implications on crop modeling. *F. Crop. Res.* **164**, 65–73 (2014).

68. Ratjen, A. M., Lemaire, G., Kage, H., Plénet, D. & Justes, E. Key variables for simulating leaf area and N status: Biomass based relations versus phenology driven approaches. *Eur. J. Agron.* **100**, 110–117 (2018).

CAPÍTULO 2

PLANNING AND OPTIMIZATION OF NITROGEN FERTILIZATION IN CORN BASED ON MULTISPECTRAL IMAGES AND LEAF NITROGEN CONTENT USING UNMANNED AERIAL VEHICLE (UAV)[1]

Diogo Castilho[2,3]; Beata Emoke Madari[2,3]; Maria da Conceição Santana Carvalho[3]; João Vitor Silva Costa[4]; Manuel Eduardo Ferreira[4]

---

[1] Capítulo submetido como artigo ao periódico científico Precision Agriculture. Submetido em 07 dez. 2023.

[2] Programa de Pós-graduação em Agronomia (PPGA), Universidade Federal de Goiás (UFG), Goiânia, Goiás, Brasil.

[3] Embrapa Arroz e Feijão, Santo Antônio de Goiás, Goiás, Brazil.

[4] Laboratório de Processamento de imagens e Geoprocessamento (LAPIG), IESA, UFG, Goiânia, Goiás, Brasil.

ABSTRACT

Nitrogen (N) is one of the factors that most affect corn yield. An alternative method in assessing N status is to measure the spectral reflectance of plant canopy by remote sensing. Corn images provided by unmanned aerial vehicle (UAV) offer a great advantage given their high spatial and temporal resolution. In order to (1) correlate multispectral images by means of vegetation indices, leaf N content (LNC) and yield at V6, V11, and R1 corn growth stages, and (2) to develop a model to predict top-dressing N rate to be applied at V5-V6, two experiments were carried out in Goiás State, Brazil. The experiment consisted of ten N rates ranging from 0 to 300 kg N ha^{-1} surface-applied at V5. The aerial imagery took place at V6, V11 and R1 stages. Leaf samples were collected on the day of the flight to assess leaf N content. The first experiment provided useful information to estimate N rate at V5 stage using VIs such as Green Normalized Difference Vegetation Index (GNDVI), Green to Near–Infrared Band Ratio (GN) and Transformed Chlorophyll Absorption in Reflectance Index (TCARI). It was also possible to estimate N rates based on leaf N content and VIs using GNDVI, GN, and TCARI. GNDVI, GN, Soil Adjusted Vegetation Index (SAVI), Green Soil Adjusted Vegetation Index (GSAVI) and Ratio Vegetation Index (RVI) were the most accurate indices to predict grain yield at V6, V11 and R1 stages, emphasizing the V6 stage, where the highest correlations were found ($R^2 \geq 0.70$).

Keywords: spectral reflectance, UAV, N recommendation, vegetation indices, yield.

3.1 Introduction

In traditional crop production practices, the fertility of farmlands on a certain farm is usually assumed to be homogeneous, thus a uniform nitrogen (N) management strategy is adopted, while the actual N status of soil and crop often exhibits large spatial and temporal variability over fields (Zhang et al., 2022). Rather than applying localized fertilizer amendments, growers use sparse data to guide the application of fertilizers to many acres of crops, using a common prescription, resulting in suboptimal growth and unnecessary nitrate leaching, runoff of N and nitrous oxide emissions, a greenhouse gas with a high global warming potential (Snyder et al., 2009; Quemada et al., 2013; Chancia et al., 2021).

The proper application of N fertilizers is the key strategy to secure optimal crop yield (Han et al., 2022). The best indication of the nutrient status of the plant is the leaf N content (LNC), however the traditional means of measuring leaf N are low, time-consuming, laborious, therefore do not meet the needs of rapid, real-time monitoring (Blackmer and Schepers 1996). Obtaining LNC remotely and effectively has always been an urgent problem

to be solved to either boost higher yield potential zones or reduce inputs (Marang et al., 2021; Li et al., 2022).

Methods for estimating the applicable N rate are based on soil tests (Magdoff 1991), tissue N concentration (Tyner & Webb 1946), chlorophyll concentration (Varvel et al., 1997) and expected grain yield (Sousa & Lobato 2004). If these methods are used together with new rapid techniques, N use efficiency can increase considerably. The constant increase in N prices and the environmental impact has stimulated interest in reducing N rates. At the same time, the increase in the price of corn in the internal and external market has generated incentives for the use of technologies that allow the maximization of production.

Unmanned aerial vehicles (UAVs) have attracted considerable scientific and public attention in recent years, as they have the advantage of being flexible to manipulate, acting as a rapid, nondestructive and efficient method (Jiang et al., 2020; Chen & Wang 2022). Their use offers the possibility of obtaining field data in an easy and profitable way, resulting in images with high spatial and temporal resolution (García-Martínez et al., 2020; Li et al., 2022).

The major advantage of using UAV is that large populations of plants can be assessed quickly, while also reducing inaccuracies resulting from sampling a limited subset of plants (Costa et al., 2021). Remote monitoring of crop nutrient status can provide on-demand, spatial information to improve crop yield and minimize over-application of fertilizers if integrated into existing precision agriculture technology used on-board commercial tractors and implements (Montgomery et al., 2020). UAVs have overcome the deficiencies of ground and high-altitude remote sensing, providing strong support for crop information monitoring technology of precision agriculture (Fu et al., 2020).

Evidence suggests that estimating N in leaf or canopy based on spectral properties may be as accurate as measuring soil N to estimate N supply (Scharf et al., 2006). Measuring spectral reflectance of canopy leaves with multispectral cameras carried by UAVs may be an alternative method in assessing N status of plants (Schepers et al., 1992; Bausch and Duke 1996; Goel et al., 2003; Kyveryga et al., 2012). With such sensors it is also possible to estimate yield in most corn phenological stages (Blackmer and Schepers 1996; Maresma et al., 2016).

There are a growing number of vegetation indices (VIs) to estimate chlorophyll concentration, LNC, dry mass, and yield. The indices are calculated by combining reflectance on the wavelengths located in the visible, red-edge and near infrared ranges

(Gabriel et al., 2017). Sripada et al., (2006) studied 26 VIs to estimate N rate to be applied at V7 stage of corn. Others separated the VIs into structural indices (e.g., Normalized Difference Vegetation Index – NDVI, Renormalized Difference Vegetation Index – RDVI, Optimized Soil Adjusted Vegetation Index – OSAVI) and chlorophyll indices (e.g., Red Edge Reflectance Index, Double-Peak Canopy Nitrogen Index – DCNI, TCARI, TCARI/OSAVI) (Gabriel et al., 2017). Still others separate VIs into N (e.g., DCNI), leaf pigment (e.g., TCARI, TCARI/OSAVI) and amount of green content in the leaf (e.g., NDVI, OSAVI) (Cilia et al., 2014).

Several indices, such as Difference Vegetation-Index (DVI) and SAVI, have been proposed as ideal for correcting soil influence (Tucker 1979; Huete 1988). Another method for soil correction is the use of relative indices. Bausch & Duke (1996) were the first to use this method defined as the Nitrogen Reflectance Index (NRI), based on the NIR/G ratio (NIR and green reflectance ratio) of an area of interest with NIR/G from an area where there is no N limitation (reference area).

The importance of VIs as estimators of LNC is mainly because the VIs enhance some characteristics related to biological variables, such as chlorophyll content and biomass, which are highly correlated with LNC and plant height (Osco et al., 2020). LNC is the major index for representing the plant's leaf N nutrition, and through monitoring the LNC, proper fertilizer-N measures can be enacted (Liu et al., 2016). LNC at early growth stages is a good indicator for N fertilizer application, and at later growth stages is highly related to the final grain quality. Quantification of LNC therefore provides important information for the production of high-yield and good-quality crops (Zheng et al., 2018; Xu et al., 2021).

While much work has been done demonstrating that a UAV with passive multispectral sensors can detect N stress in crops, few studies have been done to transform these multispectral sensor readings into a practical N recommendation system to be applied in farming operations. Few studies used the simplified Holland and Schepers algorithm for corn (Thompson & Puntel 2020), nitrogen fertilizer optimization algorithm (NFOA) for rice (Yang et al., 2022), modified sufficiency index algorithm (MSIA) for wheat (Zhang et al., 2022), a two-step approach for modelling optimal N rate for winter wheat (Piikki et al., 2022), standard farmers´ N application for winter wheat (Argento et al., 2020), plant N uptake and N nutrition index estimated by random forest regression using band reflectance for potato (Peng et al., 2021), and linear, quadratic, linear/quadratic-plateau model for corn (Sripada et al., 2005, Gabriel et al., 2017; Maresma et al., 2016, 2018). All studies above

highlight the importance of using regional optimum topdressing N application or farmer´s traditional management to compare UAV-sensor based variable rate N application. These methods can reduce the production cost and increase the net income by reducing N rates with no yield difference compared to the farmers' traditional management. Although they achieved the same yield using UAV-based sensor compared to farmer´s recommendation using less N inputs, only one VI was used to estimate N rate (Thompson & Puntel 2020; Zhang et al., 2022). The equation utilized was developed to Nebraska state. It requires data such as expected yield, soil organic matter, N credits, soil nitrate-N concentration, grain N content, plant N uptake, and N nutrition index prior to use the UAV sensor (Thompson & Puntel 2020, Peng et al., 2021, Yang et al., 2022), which makes this approach difficult and may not be adequate to other regions. Furthermore, some studies have not validated their methods (Yang et al., 2022). Regardless the method used, prior to implementing these technics, experimentation is needed to calibrate them, preferably, for the site and variety of interest. As several factors can affect the spectral reading (Schepers et al., 1992), the transfer of a method to different sites with different edaphic and climatic conditions as well as varieties may prove to be difficult (Scharf & Lory 2009). It is clear that no one method can be used individually, but a combined approach might help in improving N use efficiency (Sharma & Bali 2018).

Template models such as linear-plateau or quadratic-plateau can have advantages over the others once these utilize VIs to correlate with LNC, yield or N rate. Studies that utilized these models conducted the UAV flights at later corn stages (above V12) which can be too late to identify and correct the N deficiency, furthermore estimating N rate at initial stages of corn growth is of great importance for the final yield (Benincasa et al., 2017) as corn absorbs more than 60% of the N until the VT stage (Ritchie et al., 1997). In Brazil, studies are still scarce using only a few VIs such as NDVI (Santos et al., 2020), a fact that limits the reliable use of methods based on the analysis of reflectance spectra obtained by remote sensors, and on their use in larger corn fields.

The objectives of this study were (1) to develop a model to predict top-dressing N rate required for corn at V6 stage using N rate and/or LNC; (2) to correlate VIs with LNC (g kg^{-1}) and yield (kg ha^{-1}) at V6, V11 and R1 stages; (3) to validate the prediction model for N rate estimation at V6 stage.

3.2 Materials and methods

The methodology consisted of three distinct phases: (a) conducting a field survey to gather relevant data, (b) performing chemical analysis on leaf tissue samples, and (c) utilizing digital image processing techniques for data analysis. Each phase comprised specific steps, which were visually represented in a workflow diagram (Fig. 1) and further elaborated upon below.

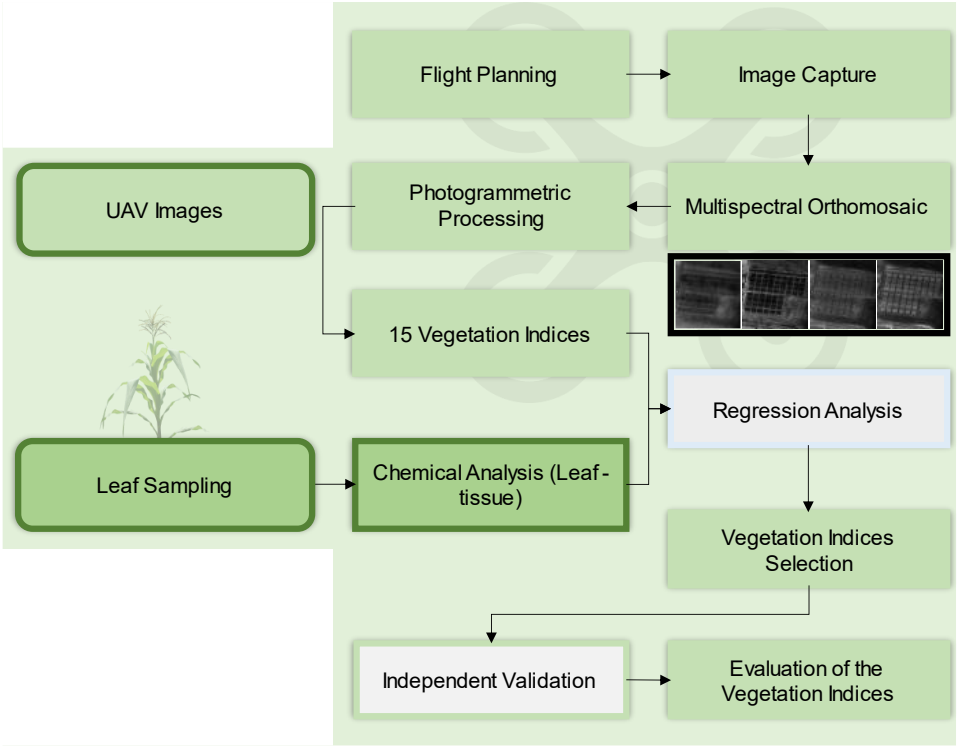

Fig. 1 Workflow diagram of the process performed in this study

3.2.2 Experimental Site and Management

The study was conducted in the experimental farm of Embrapa Rice and Beans, in Santo Antônio de Goiás – Goiás State, Brazil (16°29'10.5"S, 49°17'53.7"W) (Fig. 2). The first experiment was planted on December 14th, 2020, with the Pioneer P307 VHY hybrid. Corn emergence occurred five days after planting. The experimental site covered approximately 8600 m^2, located under a central pivot irrigation system, which was used only during summer dry spells. The soil of the experimental area was a Rhodic Ferrosol and had homogeneous distribution of its characteristics (Table 1).

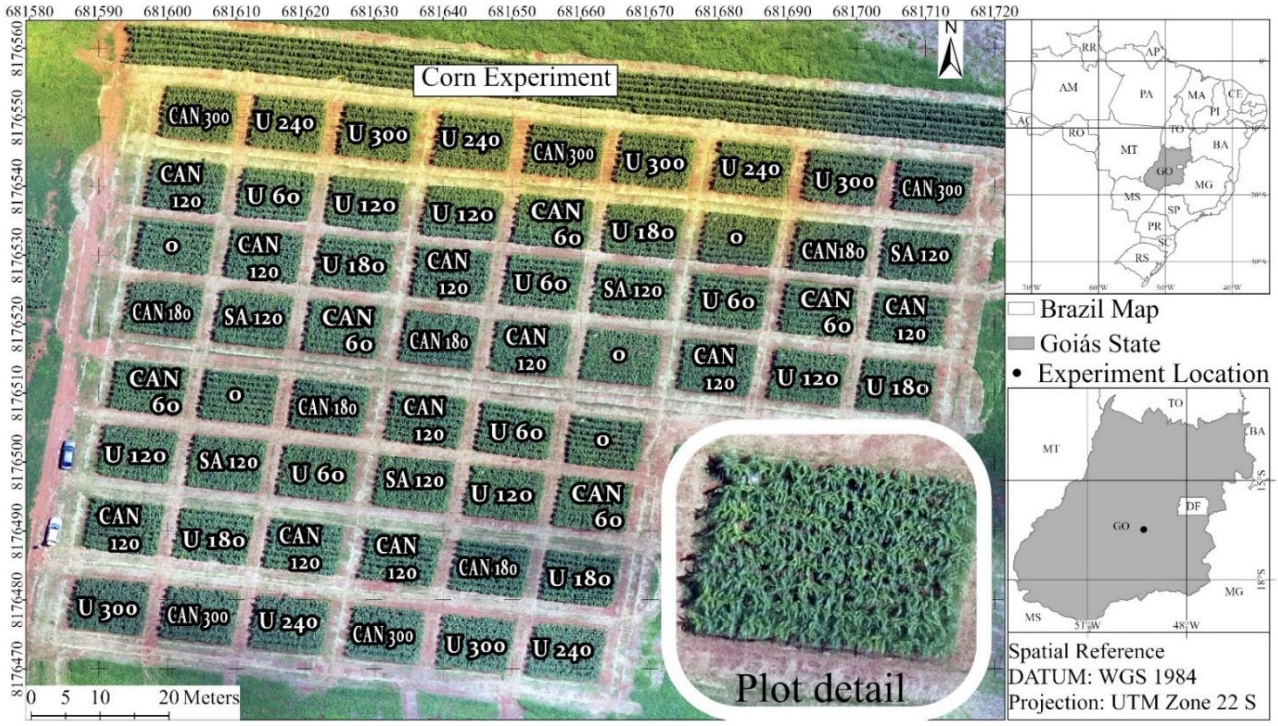

Fig. 2 Location of the study area and detail of the experimental plots. The image of the experiment was obtained using RGB camera on 28 January 2021, at V11 stage. The plot labels refer to N source: U – Urea (46% N) and CAN – Calcium Ammonium Nitrate (27% N). Numbers followed by U or CAN represent N rate applied at V5 stage (60, 120, 180, 240 and 300 kg N ha^{-1}). Zero (0) represents the control (0 kg N ha^{-1})

Table 1 Soil texture and chemical properties of the soil used in the study

Depth	pH	Ca	Mg	K	Al	H + Al	P (melich)	S	Zn	B	Cu	Fe	Mn	Org. Matter
(m)	($CaCl_2$)	(cmolc dm^{-3})					(ppm)							(g dm^{-3})
0 – 0.2	5.4	3.9	1.7	0.34	0.0	2.3	9.2	7.1	10.2	0.3	2.1	40.5	9.6	26
0.2 – 0.4	4.8	1.6	0.7	0.15	0.2	3.3	3.4	11.0	2.8	0.2	2.1	1.8	8.3	22

The experiment was implemented in 2020 and 2021 cropping season to study N use efficiency in rotation of corn (*Zea mays*), soybean (*Glycine max*) and common beans (*Phaseolus vulgaris*) using two types of N fertilizers, urea containing 46% N and calcium ammonium nitrate (CAN) containing 27% N. Our first part of our study, aimed to develop a model to predict top-dressing N rate required for corn at V6 stage using LNC. UAV flight dates were adjusted to the field leaf sampling dates (Table 2).

Table 2 Synthesis of field management and data acquisition calendar

Year	Seedling	N Fertilizer	UAV Flight	Field Sampling	Growth Stage	Harvest Date
2020	14 December	6 January	13 January	13 January	V6	28 April 2021
			28 January	28 January	V11	
			23 February	23 February	R1	

			23 December		V6	
2021	23 November	18 December	05 January	-	V11	05 April 2022
			27 January		R1	

Pre- and post-emergence herbicides were used. In pre-emergence, 2.5 L ha^{-1} of glyphosate (48%) was applied 7 days before planting. In post emergence, 2 L ha^{-1} of Atrazine (50%) and 800 ml ha^{-1} of Nicosulfuron (6%) were applied at V3 to control weeds. To control corn leafhopper, 150 g ha^{-1} of Imidacloprid (70%) and 500 g ha^{-1} of Acephate (75%) were applied at V5 and V8, respectively.

The second part, to validate the prediction model for N rate estimation at V6 stage, was done from November 2021 to April 2022 using the same management practices.

3.2.3 Experimental design and treatments

The experimental design used completely randomized blocks with ten fertilizer treatments and five repetitions, referring to the rates and sources of N. N was applied manually at V5 stage (60, 120, 180, 240 and 300 kg N ha^{-1} as urea and 60, 120, 180 and 300 kg N ha^{-1} as CAN), plus the control treatment (0 kg N ha^{-1}) totalizing 50 plots. Two days after planting YaraBasa (6N-27P-6K with sulfur, calcium and micronutrients) at 300 kg ha^{-1} and KCl (60% K_2O) at 170 kg ha^{-1} rates were applied. Thus, all the 50 plots received 18 kg N ha^{-1} each at planting, including the control plots.

Plots with 300 kg N ha^{-1} were used as reference area to calculate yield, LNC and N rate for the other treatments in the study. Each plot contained 8 rows of 10 m length, measuring 0.90 m between rows and 0.17 m within rows (plot dimensions were 10 x 7.2 m). The buffer areas between plots were 3 m.

3.2.4 Remote sensing: data acquisition and analysis

Seven days after top-dressing N application (V5 stage), a digital multi-spectral camera Parrot Sequoia (Fig. 3) mounted on an UAV (Sensefly – Bluegrass) was used to acquire multispectral aerial images (“TIF” format) of the experiment. The flight was conducted under optimum weather condition at an altitude of 70 m above ground (V6, V11 and R1 stages). The time of flight was less than 20 min between 10:00 and 12:00h a.m. on sunny days, without clouds on January 13th, 28th, and February 23rd of 2021 (Table 2). Before the

flight, a calibration plate that accompanies the Parrot Sequoia was registered to carry out the radiometric calibration of images in a later process. Flight planning was generated using the Pix4D Capture software with a side and front overlap of 70%. Orthomosaic photos were generated using the Pix4Dmapper Pro software (Pix4D SA, Lausanne, Switzerland).

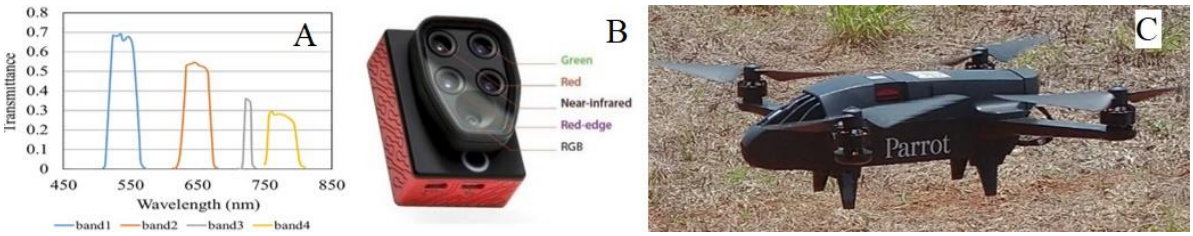

Fig. 3 A: Parrot Sequoia sensor spectral response function. The central wavelengths of the bands are 550 nm (40 nm) Green, 660 nm (40 nm) Red, 735 nm (10 nm) Red-Edge, and 790 nm (40 nm) NIR, adapted from Deng et al., (2018); B: Parrot Sequoia multispectral camera; C: Bluegrass UAV, from Sensefly

Bluegrass is a self-operating, autonomous UAV weighing 1850 g with the sequoia camera included. It is used to capture high spatial resolution aerial photos for the construction of accurate orthomosaics (georeferenced) in addition to 3D surface models. According to the manufacturer, it can cover about 30 ha in a single automated mapping flight, at an altitude of 70 m, with a spatial resolution of 0.066 m pixel^{-1} (considering only the use of the multispectral sensors).

The Parrot Sequoia camera is composed of two photographic sensors: one multispectral, composed of four independent synchronous bands, positioned in the green (G), red (R), red-edge (RE) and near infrared (NIR) bands, and another comprising a RGB camera. At the top of the drone, there is a sensor that continuously captures the solar irradiance, for radiometric calibration of the multispectral bands. The complete sensor weighs approximately 100 g, powered by the drone's own battery.

Four 1.2 Megapixel spectral images (10 bits of radiometric resolution) were captured in each shot (in addition to an RGB image), with a spatial resolution of 0.035 m pixel^{-1} for the multispectral bands. The RGB image was not used in this study, due to the drone's shaking during the flight, which compromised the quality of this record.

Pix4DMapper was utilized for radiometric calibration. To ensure accurate measurements, a calibrated reflectance plate was imaged with the Parrot Sequoia camera prior to the flight. Additionally, the camera's built-in sunshine sensor was employed during the flight to assess the local light conditions. By employing the calibrated reference plate, the software was able

to calibrate and rectify the reflectance values of the images based on the provided calibration plate values. This calibration process considered both the light conditions during image capture and specific sensor characteristics.

Fifteen VIs reported in the literature were calculated using the values of the single bands extracted from the NIR, RE, R and G (Table 3). The ArcGIS Pro 2.8.0 (Esri Inc. 2021) software was used to extract the response of the different N treatments for each VI and individual bands. Polygons in vector format (shapefile) were created for each experimental plot (45 m^2) to generate the average reflectance of each VI, NIR, RE, R and G using the "Zonal Statistics as Table" ArcGIS Pro tool. To generate the VIs, the "Raster Calculator" tool was applied to insert the formulas for the respective vegetation indices (Table 3) along with the orthomosaics generated in each individual band of the Sequoia sensor. Relative bands (Rel NIR, Rel R and Rel G) and VIs (e.g., R_GDVI) were calculated as the ratio of the spectral value of a plot of interest to the average of the spectral value of plots that received the highest N rate (300 kg N ha^{-1}).

Table 3 Calculated vegetation indices

Vegetation Index	Formula	Reference
Normalized Difference Vegetation Index (NDVI)	NDVI = (NIR – RED) / (NIR + RED)	(Rouse et al., 1974)
Green Normalized Difference Vegetation Index (GNDVI)	(NIR – GREEN) / (NIR + GREEN)	(Gitelson et al., 1996)
Red to NIR band ratio (RN)	Red / NIR	(Scharf and Lory 2009)
Green to Near–Infrared Band Ratio (GN)	Green / NIR	(Scharf and Lory 2009)
Soil Adjusted Vegetation Index (SAVI)	$\frac{1.5 \text{ x NIR} - \text{R}}{\text{NIR} + \text{R} + 0.5}$	(Huete 1988)
Modified Soil Adjusted Vegetation Index (MSAVI)	$\frac{2\,x\,NIR + 1 - \sqrt{(2\,x\,NIR + 1)^2 - 8\,x\,(NIR - R)}}{2}$	(Qi et al., 1994)
GSAVI	$\frac{1.5 \text{ x NIR} - \text{Green}}{(\text{NIR} + \text{Green} + 0.5)}$	(Sripada et al., 2006)
Nitrogen Reflectance Index (NRI)	$\frac{\text{NIR/G interest area}}{\text{NIR/G reference area}}$	(Bausch and Duke 1996)
Modified Chlorophyll Absorption Ratio Index (MCARI)	((RE − Red) − 0.2 (RE − Green)) (RE / Red)	(Daughtry et al., 2000)
Transformed Chlorophyll Absorption in	3 ((RE − Red) − 0.2(RE − Green) (RE / Red))	(Haboudane et al., 2002)

Reflectance Index (TCARI)		
Optimized Soil Adjusted Vegetation Index (OSAVI)	1.16 (NIR − Red) / (NIR + Red +0.16)	(Zou and Mõttus 2017)
TCARI/OSAVI	TCARI / OSAVI	(Haboudane et al., 2002)
TCARI / MSAVI	TCARI / MSAVI	(Haboudane et al., 2002)
Ratio Vegetation Index (RVI)	NIR / RED	(Jordan 1969)
Difference Vegetation Index (DVI)	NIR – RED	(Tucker 1979)

Reflectance of Green, Red, RE (Red Edge) and NIR (Near-infrared).

3.2.5 Yield and leaf N content estimation

Grain yield was measured in the three central rows (2.70 x 3.00 m) of each plot, which were manually harvested at the physiological maturity stage (R6). Grain moisture was adjusted to 13%. The yield response to N rate and spectral images were correlated.

Leaf samples for the determination of LNC (g kg^{-1}) were collected at V6, V11 and R1 stages on the day of spectral acquisition. These samples were obtained from 15 plants at random in each plot at each of the three phenological stages. At V6 and V11, the leaf sample obtained was the last fully expanded leaf (visible collar). At R1, the leaf sampled was the opposite and below the first upper ear. The midrib was discarded, and the leaves were dried at 65 degrees Celsius until they reached constant weight. Subsequently, the samples were ground for determining LNC, applying the Dumas combustion method (Keeney & Bremner 1967) using the Rapid N cube by Elementar (Frankfurt, Germany).

Regression analysis was used to identify VIs that were useful in predicting LNC and yield. The linear model was preferentially used to the quadratic model if it resulted in a higher or equal regression coefficient.

3.2.6 Statistical Analysis

To analyze the VIs according to the different N treatments, an area of approximately 45 m^2 was used in each treatment using ArcGis Pro 2.8.0 software (Esri Inc. 2021), excluding the edge of each corn plot. Pixels presenting bare soil within the plot were eliminated at the V6 stage following the methods described in Thompson & Puntel (2020). In the following corn

stages, there was no presence of bare soil as the corn canopy closed the space between rows before V11 stage. A multiple comparison analysis, using the Tukey Honest Significant Difference (HSD) test at a significance level of 0.05, was performed. For each treatment, this analysis compared mean VIs values, distinguishing different significant groups. SigmaPlot 12.0 software (Systat Software, 2011), and easyreg package (Arnhold 2019) in RStudio were utilized for the statistical analysis.

Linear, linear-plateau, quadratic and quadratic-plateau regression analyses were also performed: (1) between VIs and LNC measured under different N rates, to determine the economic optimal N rate (Maresma et al., 2018), and (2) between VIs and yield, to determine the usefulness of VIs to predict grain yield at V6, V11 and R1 growth stages.

3.2.7 Validation Trial

To validate the first part of the study, a validation trial was conducted in an adjacent area, under the same edaphic and climatic conditions, between December 2021 and April 2022, in an area of approximately 1600 m^2. Eight complete random treatments were installed based on the VIs that best correlated in the first experiment with N rates applied and LNC for each of the two N sources used (urea and CAN). N fertilization was conducted according to the results obtained in the first experiment, aiming for maximum yield of the area with the following combinations: 1) GNDVI with LNC using CAN; 2) GN with LNC using CAN; 3) GNDVI with LNC using urea; 4) TCARI with LNC using urea; 5) GNDVI with N rate using CAN; 6) GN with N rate using CAN; 7) GNDVI with N rate using urea; and 8) GN with N rate using urea, with four repetitions totalizing 32 plots (7.2 x 5.0 m each), with 14 corn rows per plot (0.50 m between rows and 0.30 m within rows). The buffer between the plots was 1m (Fig. 4). Corn was hand harvested at physiological maturity stage. Grain yield was measured in the four central rows (2 x 3 m) of each plot and subsequently, the grain was adjusted to 13% moisture content.

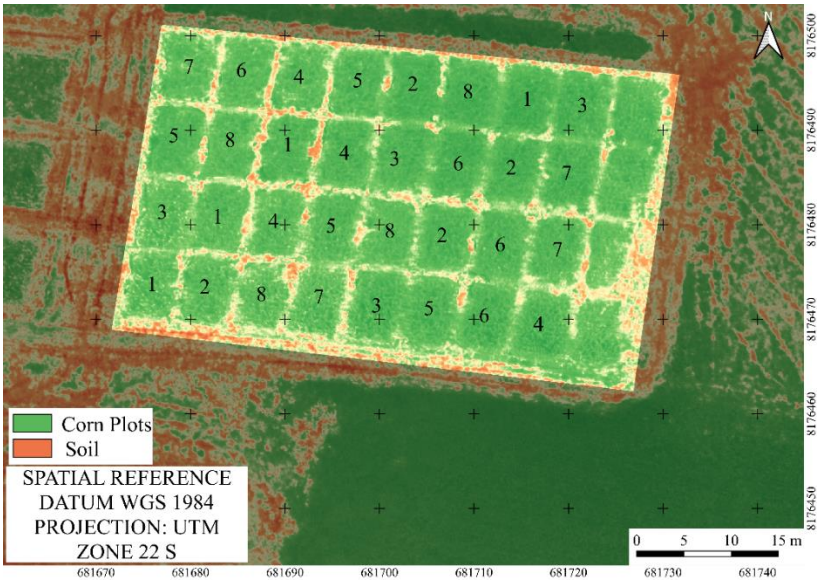

Fig. 4 Validation trial with eight treatments and four replications (32 plots), allocated adjacent to the first experiment. Image obtained with the Bluegrass drone using Parrot Sequoia multispectral camera, with the red band, applying false color composition through ArcGis Pro 2.8.0 software. CAN: Calcium ammonium nitrate; LNC: leaf N content. Treatments: (1) GNDVI with LNC using CAN; (2) GN with LNC using CAN; (3) GNDVI with LNC using urea; (4) TCARI with LNC using urea; (5) GNDVI with N rate using CAN; (6) GN with N rate using CAN; (7) GNDVI with N rate using urea; (8) GN with N rate using urea

Corn was sown on 23 November 2021 and harvested on 05 April 2022. Fertilization at planting consisted of KCl (52 kg ha^{-1}, 58% K_2O) and Super Triple (250 kg ha^{-1} with 41% P_2O_5). No N was applied at planting. After obtaining the orthomosaic images at V5 (23 December 2021), top-dressing of N in the calculated rates was performed manually on the following day.

3.3 Results

Visual representation of VIs GNDVI, OSAVI and NDVI at V6 stage can be seen in Fig. 5. Higher values of VIs were verified in plots that received more than 120 kg N ha^{-1} for all N sources. The large presence of bare soil at V6 was visible.

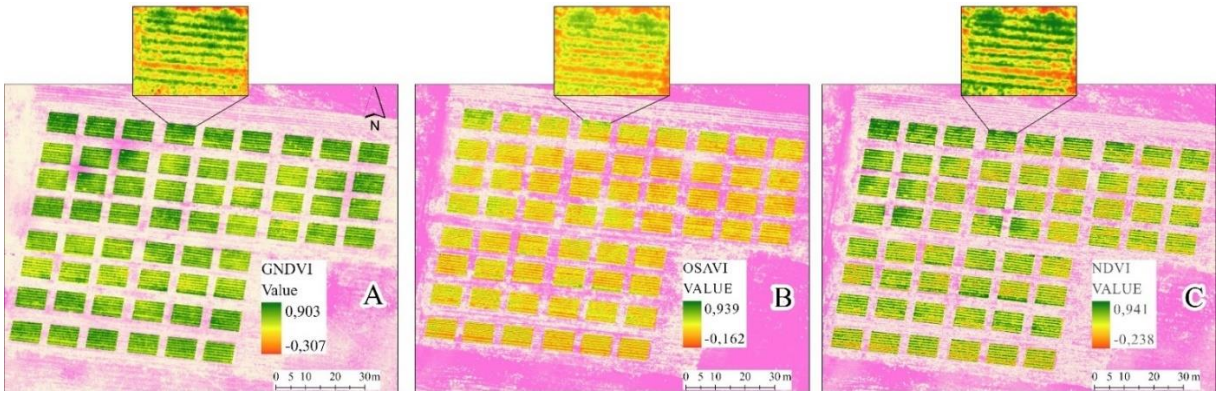

Fig. 5 Vegetation indices A: GNDVI, B: OSAVI and C: NDVI at V6 corn stage. The identification of N rates applied in each plot can be seen in Fig. 2. Detail of a plot where 240 kg N ha^{-1} was surface-applied, showing the presence of the soil in reddish color for three highlighted VIs

Reflectance values in the visible region (Green – 550 nm and Red – 660 nm) were below 10% in all stages evaluated (Online Resource 1). Soil reflectance data were then eliminated using ArcGis Pro software ("supervised classification" tool) to separate what was soil from corn. Thus, a graph was generated allowing us to see the decline between the green and red region, giving the characteristic of plant presence in that region. The control treatment (0 kg N ha^{-1}) had the highest reflectance in the red region (5; 3.77; and 3.71, for V6, V11 and R1 stages, respectively), indicating less use of sunlight and consequently resulting in lower yield. In all stages, the control treatment reflected more light in the visible wavelength and less in the NIR region than the treatment with the highest N rate (300 kg N ha^{-1}), allowing us to distinguish plots that received a lower N rate from plots that received the high N rate.

Online Resource 1 shows the average values of VIs, LNC (g kg^{-1}) and yield (kg ha^{-1}) with different treatments applied in the plots. The treatments are placed according to the total N rate applied at V5 separated by phenological stage (V6, V11 and R1).

For all variables considered, treatments with N rate were grouped in one to four homogeneous groups within each stage. Of these, the control treatment (0 kg N ha^{-1}) presented the lowest values for GNDVI, GN, TCARI, TCARI/OSAVI and TCARI/MSAVI VIs at V6, being totally different from the other N treatments. In the case of LNC, it was also possible to differentiate the control treatment from others at 60 kg N ha^{-1} at V6. Of the nine remaining indices, three VIs (NDVI, RN, MCARI) were only different from the control at a rate of 120 kg N ha^{-1} or higher, and one (RVI) at a rate of 240 kg N ha^{-1} or higher. The remaining VIs (SAVI, MSAVI, GSAVI, OSAVI and DVI) were homogenous at any N rate. At the V11 stage, the control presented the lowest values for twelve vegetation indices:

NDVI, GNDVI, RN, GN, SAVI, GSAVI, MCARI, TCARI, OSAVI, TCARI/OSAVI, TCARI/MSAVI and RVI, in addition to the LNC, identifying the treatments equal to or above 60 kg N ha^{-1}. For two remaining indices, MSAVI and DVI, it was only possible to differentiate the control from the 120 and 180 kg N ha^{-1} rate, respectively. At R1 stage, the control treatment presented the lowest values only for GNDVI, identifying the treatments equal to or above 240 kg N ha^{-1}.

For the results obtained in the treatment of 300 kg N ha^{-1}, it was expected that this treatment might have been expected to be in the upper part of the homogeneous group classification (group "a" or "ab") for the different variables considered. However, it was not, even though this treatment produced the highest yield together with the 240 kg N ha^{-1} treatment (8239 kg ha^{-1}). Indices that contain the green spectrum region in their composition, GSAVI, GN and GNDVI, were the ones that best differentiated the treatments 240 and 300 kg N ha^{-1} at V6 stage.

With regard to yield, treatments of 240 and 300 kg N ha^{-1} showed the greatest responses to N rate applied at V6 (8314 and 8239 kg ha^{-1}, respectively), being classified in group "a".

LNC increased linearly ($p<0.05$) with increasing N rate in the evaluated stages (Online Resource 1). At V6 and V11 stages, the control treatment showed the lowest values when compared to the other N rates. At the R1 stage, however, it was not possible to differentiate the control from the other rates. At the V6 stage, the levels of LNC were between 26.9 and 42 g kg^{-1}. At the V11 stage, LNC were between 26.4 and 35.2 g kg^{-1}.

3.3.1 Predicting N rate at V5 from spectral images, based on N rate applied

The spectral images obtained at V6 (one week after N application) provide the N rate at V5 based on the variables using linear, linear-plateau, quadratic and quadratic-plateau models. Higher N rate (urea source) presented higher yields (240 and 300 kg N ha^{-1}) being significantly affected by N rate applied at V5, yielding 8314 and 8239 kg ha^{-1}, respectively. As for the treatments using CAN, there was no difference in yield between 120 and 300 kg N ha^{-1} rate, yielding 7114 and 7981 kg ha^{-1}, respectively (Fig. 6). There was no difference between the control, 60 and 120 kg N ha^{-1}.

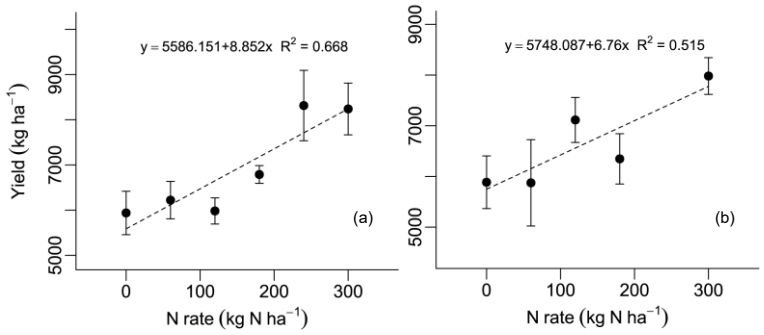

Fig. 6 Linear model of yield response to N rate in the form of urea (a) and in the form of calcium ammonium nitrate (CAN) (b), applied at V5 stage. Each point is the average of 5 replications. Error bars represent standard deviation at $p < 0.01$

The coefficients of determination (r^2 or R^2) of the relationships between the optimal N rate (urea, CAN and both applied at V5), absolute bands (G, Red, RE and NIR), VIs, and relative VIs are shown in table 4.

Among four mathematical models (linear, linear-plateau, quadratic and quadratic-plateau) used to predict the relationship between optimal N rate and VIs, the linear, quadratic and quadratic-plateau models showed consistently significant relationships. For the individual spectral bands (NIR, Red Edge, Red and Green), the NIR and Green were the only ones that showed significance with the applied N rate (urea source), albeit with a low R^2= 0.21 and R^2=0.20, respectively. When using the VIs, the coefficients of determination of the models increased considerably. The union of the two N sources did not bring a significant increase in the prediction of N rate to be applied at V5 in any of the VIs used (Table 4 – both), as well as in the relative VIs; therefore, the two N sources were tested separately.

When using urea for the linear model, GNDVI (r^2 = 0.62), GN (r^2 = 0.62), TCARI/OSAVI (r^2 = 0.54), TCARI/MSAVI (r^2 = 0.62), NRI (r^2 = 0.54), R_GNDVI (r^2 = 0.51) and R_GN (r^2 = 0.54) VIs had the highest significant coefficients with ideal N rate. For the quadratic model, the GNDVI (R^2 = 0.64), GN (R^2 = 0.64), TCARI (R^2 = 0.55), TCARI/OSAVI (R^2 = 0.57), TCARI/MSAVI (R^2 = 0.62), NRI (R^2 = 0.57), R_GNDVI (R^2 = 0.54) and R_GN (R^2 = 0.57) VIs had significant coefficients with ideal N rate (Table 4). In general, the quadratic regression model behaved significantly similar to the linear model while increasing the complexity. Thus, only the linear model was used for further analysis and discussion. The linear model was used in comparison with the quadratic-plateau model as there was no yield saturation with increasing N rate at V5 stage.

When using CAN as N source, for the linear-plateau model the GNDVI (R^2 = 0.74), GN (R^2 = 0.75), TCARI/OSAVI (R^2 = 0.55), TCARI/MSAVI (R^2 = 0.55), R_GNDVI (R^2 = 0.70)

and R_GN (R^2 = 0.75) VIs had the highest significant relationships with optimal N rate. For the quadratic-plateau model, the GNDVI (R^2 = 0.74), GN (R^2 = 0.75), TCARI/OSAVI (R^2 = 0.55), TCARI/MSAVI (R^2 = 0 .54), R_GNDVI (R^2 = 0.63) and R_GN (R^2 = 0.61) VIs had significant relationships with ideal N rate (Table 4). In general, the linear-plateau regression model behaved significantly similar to the quadratic-plateau model while increasing the complexity. As a result, only the linear-plateau model was used for further analysis and discussion. The linear-plateau model was used for the CAN with the GNDVI and GN VIs, as there was no yield increase above 120 kg N ha^{-1} and the VIs also had saturation in this region close to the rate applied at V5 (Fig. 7).

Table 4 Regression analysis of the optimal N rate (kg N ha^{-1}) applied at V5, using urea, calcium ammonium nitrate (CAN) and both, with near infrared (NIR), red (R), Red Edge (RE), green (G) and the various spectral indices of vegetation (VIs), as well as the relative vegetation indices (Rel average VI of the plot of interest divided by the average of the same VI in plots that were applied 300 kg N ha^{-1}). The significance and coefficient of determination (r^2 or R^2) for the linear, linear-plateau, quadratic and quadratic-plateau models are presented

Vegetation Index	Model			
	Linear	Linear-plateau	Quadratic	Quadratic-plateau
	r^2	R^2		
	Urea – CAN – Both			
NIR	NS – NS – 0.12*	NS – NS – NS	0.21* – NS – 0.14*	NS – NS – NS
Red Edge	NS – NS –NS	NS – NS – NS	NS – NS – NS	NS – NS – NS
Red	NS – NS – NS	NS – NS – NS	NS – NS – NS	NS – NS – NS
Green	NS – NS – NS	NS – NS – NS	0.20* – NS – NS	0.21* – NS – NS
NDVI	0.27* – 0.18* – 0.23**	NS – NS – 0.28**	0.28* – 0.43* – 0.30**	NS – 0.44* – 0.30**
GNDVI	0.62** – 0.59** – 0.52**	NS – 0.74** – NS	0.64** – 0.72** – 0.57**	0.64** – 0.74** – 0.57**
RN	0.29* – 0.17* – 0.22**	NS – NS – 0.29**	0.29* – 0.43* – 0.31**	0.29* – 0.43* – 0.30**
GN	0.62** – 0.58** – 0.52**	NS – 0.75** – NS	0.64** – 0.73** – 0.57**	0.64** – 0.75** – 0.57**
SAVI	0.22* – NS – 0.13*	NS – NS – NS	0.26* – NS – 0.13*	NS – NS – NS
MSAVI	0.22* – NS – 0.16*	NS – NS – NS	0.27* – NS – 0.16*	NS – NS – NS
GSAVI	0.37* – 0.29* – 0.29**	NS – NS – NS	0.38* – 0.30* – 0.29**	NS – 0.30* – NS
MCARI	0.43* – 0.64* – 0.30**	0.48** – 0.36* – 0.32**	0.48** – 0.40* – 0.34**	0.48** – 0.44* – 0.34**
TCARI	0.50** – 0.32* – 0.31**	0.54** – NS – 0.33**	0.55** – 0.42* – 0.37**	0.55** – 0.47** – 0.37**
OSAVI	0.27* – NS – 0.16*	NS – NS – NS	0.29* – NS – 0.16*	NS – NS – 0.16*
TCARI/OSAVI	0.54** – 0.32* – 0.34**	NS – 0.55** – 0.39**	0.57** – 0.49** – 0.42**	0.57** – 0.55** – 0.42**
TCARI/MSAVI	0.62** – 0.64* – 0.38**	NS – 0.55** – 0.41**	0.62** – 0.49** – 0.43**	0.62** – 0.54** – 0.43**
RVI	0.38** – NS – 0.22**	NS – NS – 0.27**	0.38* – 0.45* – 0.29**	0.38* – NS – 0.28**
DVI	0.18* – 0.19* – 0.17*	NS – NS – NS	0.23* – 0.19* – 0.17*	NS – 0.19* – NS
NRI	0.54** – 0.47** – 0.28**	NS – NS – NS	0.57** – 0.59** – 0.31**	NS – 0.58** – NS
Rel_NIR	NS – NS – NS	NS – NS – NS	0.36* – NS – NS	NS – NS – NS
Rel_Red_Edge	NS – NS – NS	NS – NS – NS	NS – NS – NS	NS – NS – NS
Rel_Red	NS – NS – 0.11*	NS – NS – NS	NS – NS – 0.14*	NS – NS – 0.16*
Rel_Green	0.28* – NS – 0.14*	0.36* – NS – NS	0.39* – NS – 0.20*	0.38* – NS – 0.21*
Rel_NDVI	0.33* – NS – 0.16*	NS – NS – NS	0.38* – NS – 0.16*	NS – NS – 0.16*
Rel_GNDVI	0.51** – 0.59** – 0.61**	NS – 0.70** – NS	0.54** – 0.70** – 0.62**	NS – 0.71** – 0.63**

Rel_RN	0.22* – 0.21* – 0.18*	NS – NS – NS	0.31* – 0.28* – 0.18*	NS – 0.27* – 0.18*
Rel_GN	0.54** – 0.58** – 0.59**	NS – 0.75** – NS	0.57** – 0.73** – 0.61**	NS – 0.75** – 0.61**
Rel_SAVI	0.20* – NS – NS	NS – NS – NS	0.43** – NS – NS	NS – NS – NS
Rel_MSAVI	0.20* – NS – 0.09*	NS – NS – NS	0.42* – NS – 0.10*	NS – NS – NS
Rel_GSAVI	0.28* – NS – 0.23**	NS – NS – NS	0.43* – NS – 0.25**	NS – NS – NS
Rel_MCARI	0.16* – 0.46* – 0.50**	NS – NS – NS	0.16* – 0.67** – 0.53**	NS – 0.65** – 0.53**
Rel_TCARI	0.17* – 0.37* – 0.45**	NS – NS – 0.46**	NS – 0.61** – 0.53**	NS – 0.57** – 0.55**
Rel_OSAVI	0.30* – NS – 0.11*	NS – NS – NS	0.40* – NS – 0.12*	NS – NS – NS
Rel_TCARI/OSAVI	0.18* – 0.50** – 0.48**	NS – NS – 0.49**	0.24* – 0.70** – 0.53**	NS – 0.68** – 0.54**
Rel_TCARI/MSAVI	0.22* – 0.43* – 0.45**	NS – NS – NS	0.29* – 0.60** – 0.48**	NS – 0.58** – 0.48**
Rel_RVI	0.39* – 0.32* – 0.25**	NS – NS – NS	0.49** – 0.44* – 0.48**	NS – 0.43* – 0.48**
Rel_DVI	NS – NS – 0.10*	NS – NS – NS	0.29* – NS – 0.13*	NS – NS – NS

CAN: Calcium ammonium nitrate; *p ≤ 0.05; **p ≤ 0.01; NS: not significant

Regression analyses for the VIs composed of the NIR and G bands (GNDVI, GN, R_GNDVI, R_GN) showed better relationships with N rate applied at V5, compared with VIs composed of the NIR and R bands (NDVI, SAVI, OSAVI, RVI). Models showing the relationship between N rate at V5, and the best VIs are shown in Fig. 7 for urea and CAN N sources.

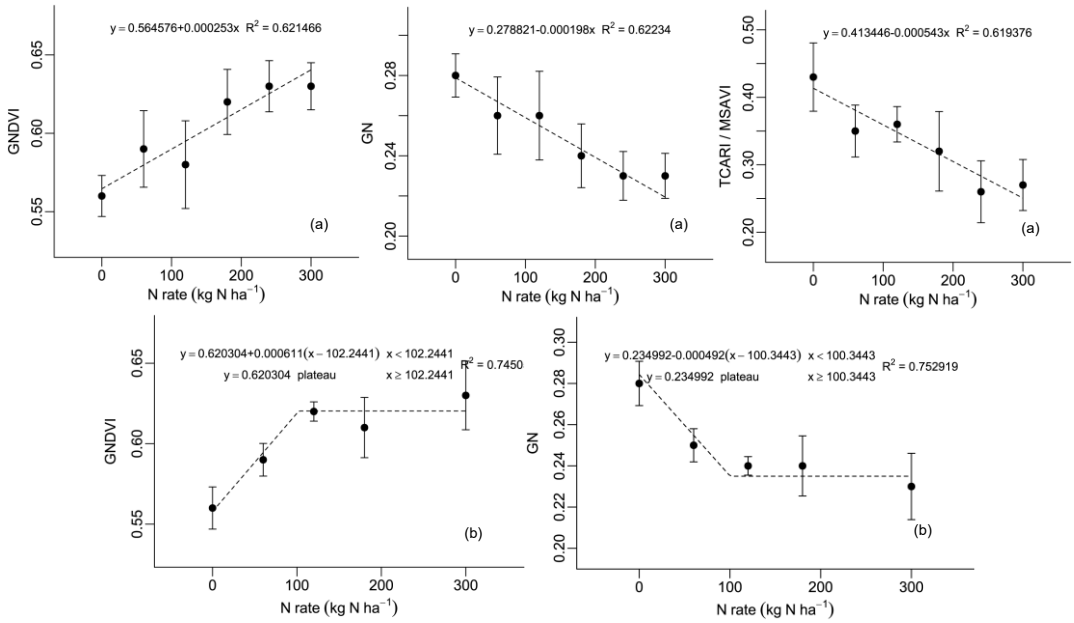

Fig. 7 The five best estimators of N rate to apply at V5 stage for urea (GNDVI-a, GN-a and TCARI/MSAVI-a), and calcium ammonium nitrate (GNDVI-b and GN-b)

3.3.2 Predicting N rate at V5 from spectral images, based on leaf N content

The LNC of corn reached the highest levels at the rate of 223.09 and 139.90 kg N ha^{-1} for urea (40.20 g kg^{-1}) and CAN (41.91 g kg^{-1}), respectively. The results were significantly

affected by the rate applied at V5 (Fig. 8). The lowest LNC levels were observed in the control treatment for the two N sources.

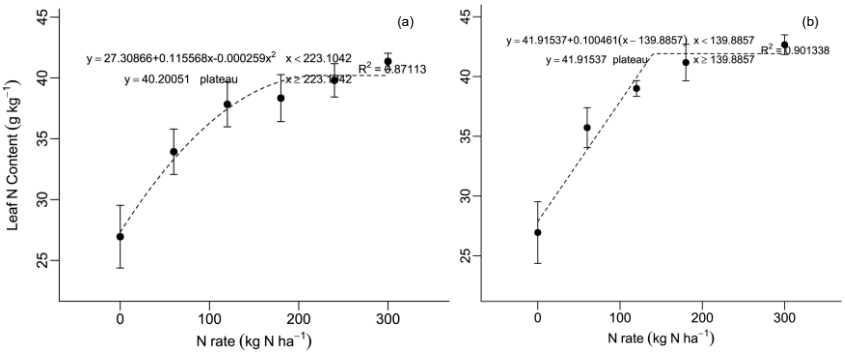

Fig. 8 Leaf N content (g kg^{-1}) and top-dressed N rate applied at V5 corn stage for urea (a), and calcium ammonium nitrate (CAN) (b) N sources. The quadratic-plateau models, for urea (a), and linear-plateau for CAN (b), were the ones that best fit the data. Each point refers to the average of 5 leaves per plot. The bars refer to the standard deviation of the mean

There was no yield increase above LNC of 40.80 g kg^{-1}, reaching the plateau at 7433.34 kg ha^{-1} using urea (Fig. 9a). This yield value did not differ statistically from yields observed at rate of 240 and 300 kg N ha^{-1} applied in V5 (8313.95 and 8239.23 kg ha^{-1}, respectively), thus, LNC obtained at V5 stage can accurately estimate the N rate to be applied at this stage. In the case of CAN, there was no yield increase above the LNC of 42.97 g kg^{-1}, reaching saturation at 8679 kg ha^{-1} (Fig. 9b). This yield value does not differ statistically from yields observed at rate of 120 and 300 kg N ha^{-1} applied at V5, which also makes the LNC useful to estimate top-dress N rate at this stage.

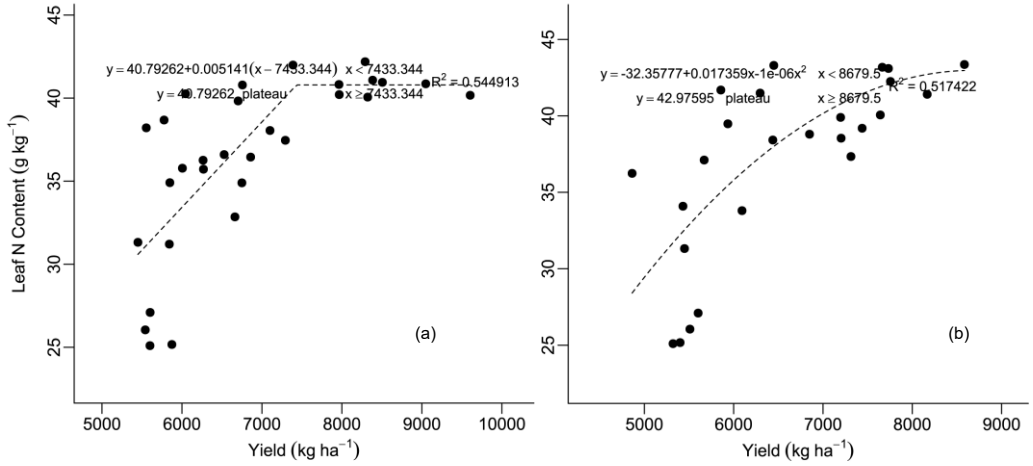

Fig. 9 Leaf N content (g kg^{-1}) obtained at V5 stage and grain yield for urea (a), and calcium and ammonium nitrate (b) N sources. Linear-plateau models for urea and quadratic-plateau models for CAN were used to correlate the two variables

The determination coefficients (r^2 or R^2) of the relationships between the LNC of the last fully expanded corn leaf collected at V5, individual spectral bands, and VIs are presented in table 5.

Among four different mathematical models (linear, linear-plateau, quadratic and quadratic-plateau) used to predict the relationship between optimal N rate and VIs, the linear, quadratic and quadratic-plateau models showed consistently significant relationships. For the individual spectral bands (NIR, Red Edge, Red and Green), the green band was the only one that showed a significant correlation with LNC, using the linear model for urea source; however, it showed a low correlation coefficient (r^2=0.19). The other individual spectral bands did not correlate with LNC at V5. When using the VIs, the coefficients of the models increased considerably. The union of two N sources with LNC at V5 did not bring a significant increase in the prediction of N rate to be applied in any of the VIs used, as well as the relative VIs (Rel_VIs); thus, the two N sources were tested separately.

When using urea as N source, the linear model had the highest significant correlation coefficients with LNC, GNDVI (r^2 = 0.55), GN (r^2 = 0.55), TCARI (r^2 = 0.60), TCARI/OSAVI (r^2 = 0.55), and TCARI/MSAVI (r^2 = 0.55). For the quadratic model, the GNDVI (R^2 = 0.55), GN (R^2 = 0.55), TCARI (R^2 = 0.63), TCARI/OSAVI (R^2 = 0.57), TCARI/MSAVI (R^2 = 0.57), Rel_MCARI (R^2 = 0.63) and Rel_TCARI (R^2 = 0.63) had significant relationships with LNC (Table 5). In general, the quadratic regression model behaved better to predict LNC compared to the linear model when using the TCARI. The linear regression model behaved better for the GNDVI.

When using CAN as N source, for the quadratic-plateau model, the GNDVI (R^2 = 0.71) had the highest significant relationship with LNC. For the quadratic model, GN (R^2 = 0.70) showed the highest significant relationship with LNC (Table 5).

Table 5 Regression analysis of leaf N content (g kg^{-1}) with near infrared (NIR), red (R), Red Edge (RE), green (G) and the various vegetation indices (VIs), as well the relative vegetation indices (Rel_VI, average VI of the plot of interest, divided by the average of the same VI in plots that were applied 300 kg N ha^{-1}). Data shown are from urea N source, calcium ammonium nitrate (CAN) and the two together (both). The significance and coefficient of determination (r^2 or R^2) for linear, linear-plateau, quadratic, and quadratic-plateau are presented

	Model			
Vegetation Index	**Linear**	**Linear-plateau**	**Quadratic**	**Quadratic-plateau**
	r^2	**R^2**		
	Urea – CAN – Both			
NIR	NS – NS – NS	NS – NS – NS	NS – NS – NS	NS – NS – NS

Red Edge	NS – NS –NS	NS – NS – NS	NS – NS – NS	NS – NS – NS
Red	NS – NS – NS	NS – NS – NS	NS – NS – NS	NS – NS – NS
Green	0.19* – NS – NS	NS – NS – NS	NS – NS – NS	NS – NS – NS
NDVI	0.17* – 0.28* – 0.26**	0.21* – 0.33* – 0.28**	0.22* – 0.31* – 0.30**	0.22* – 0.31* – 0.30**
GNDVI	0.55** – 0.66** – 0.51**	NS – NS – NS	0.55** – 0.71** – 0.54**	0.55** – 0.71** – 0.54**
RN	0.17* – 0.24* – 0.24**	NS – NS – NS	NS – 0.24* – 0.24**	NS – 0.24* – NS
GN	0.55** – 0.67** – 0.51**	NS – NS – NS	0.55** – 0.70** – 0.54**	NS – NS – NS
SAVI	NS – NS – NS	NS – NS – NS	NS – NS – NS	NS – NS – NS
MSAVI	NS – NS – 0.08*	NS – NS – NS	NS – NS – NS	NS – NS – NS
GSAVI	0.20* – 0.23* – 0.20*	NS – NS – NS	0.20* – 0.23* – 0.21*	0.20* – 0.23* – 0.21*
MCARI	0.51** – 0.35* – 0.33**	NS – NS – NS	0.62** – 0.47** – 0.44**	NS – NS – 0.33**
TCARI	0.60** – 0.37* – 0.37**	NS – NS – NS	0.63** – 0.47** – 0.44**	NS – NS – NS
OSAVI	NS – NS – 0.09*	NS – NS – NS	NS – NS – 0.13*	NS – NS – 0.12*
TCARI/OSAVI	0.55** – 0.39** – 0.39**	NS – NS – NS	0.57** – 0.46** – 0.45**	NS – NS – NS
TCARI/MSAVI	0.55** – 0.39** – 0.40**	NS – NS – NS	0.57** – 0.48** – 0.48**	NS – NS – NS
RVI	0.26* – 0.25* – 0.23**	NS – NS – 0.27**	0.27* – 0.26* – 0.26**	0.27* – 0.26* – 0.26**
DVI	NS – NS – 0.09*	NS – NS – NS	NS – NS – NS	NS – NS – NS
NRI	0.41** – 0.50** – 0.16*	NS – NS – NS	0.42** – 0.50** – 0.22*	0.42** – 0.50** – 0.38**
Rel_NIR	NS – NS – NS	NS – NS – NS	NS – NS – NS	NS – NS – NS
Rel_Red_Edge	NS – NS – NS	NS – NS – NS	NS – NS – NS	NS – NS – NS
Rel_Red	NS – NS – NS	NS – NS – NS	NS – NS – NS	NS – NS – NS
Rel_Green	0.26* – NS – 0.11*	NS – NS – NS	0.30* – NS – 0.12*	NS – NS – NS
Rel_NDVI	NS – NS – NS	NS – NS – NS	NS – NS – NS	NS – NS – NS
Rel_GNDVI	0.48** – 0.65** – 0.49**	NS – NS – NS	0.49** – 0.67** – 0.50**	0.49** – 0.67** – 0.50**
Rel_RN	NS – NS – 0.09*	NS – NS – NS	NS – NS – NS	NS – NS – NS
Rel_GN	0.48** – 0.67** – 0.47**	NS – NS – NS	0.49** – 0.70** – 0.48**	NS – NS – NS
Rel_SAVI	NS – NS – NS	NS – NS – NS	NS – NS – NS	NS – NS – NS
Rel_MSAVI	NS – NS – NS	NS – NS – NS	NS – NS – NS	NS – NS – NS
Rel_GSAVI	NS – NS – 0.14*	NS – NS – NS	NS – NS – 0.15*	NS – NS – 0.15*
Rel_MCARI	0.51** – 0.35* – 0.43**	NS – NS – NS	0.63** – 0.47** – 0.55**	NS – NS – NS
Rel_TCARI	0.62** – 0.37* – 0.32**	NS – NS – NS	0.63** – 0.50** – 0.47**	NS – NS – NS
Rel_OSAVI	NS – NS – NS	NS – NS – NS	NS – NS – NS	NS – NS – NS
Rel_TCARI/OSAVI	0.52** – 0.40** – 0.43**	NS – NS – NS	0.53** – 0.46** – 0.49**	NS – NS – NS
Rel_TCARI/MSAVI	0.48** – 0.43** – 0.38**	NS – NS – NS	0.50** – 0.48** – 0.44**	NS – NS – NS
Rel_RVI	0.21* – 0.24* – 0.16*	NS – NS – NS	NS – 0.25* – 0.16*	NS – 0.25* – 0.16*
Rel_DVI	NS – NS – NS	NS – NS – NS	NS – NS – NS	NS – NS – NS

CAN: Calcium ammonium nitrate; *p ≤ 0.05; **p ≤ 0.01; NS: not significant

These results bring reliability to estimate LNC in corn at V5 stage and define strategies regarding the N rates using VIs such as GNDVI, TCARI and GN. When Rel_VIs was used, there was no considerable improvement compared to VIs. The linear, quadratic and quadratic-plateau models, showing the relationship between LNC and the best VIs are shown in Fig. 10.

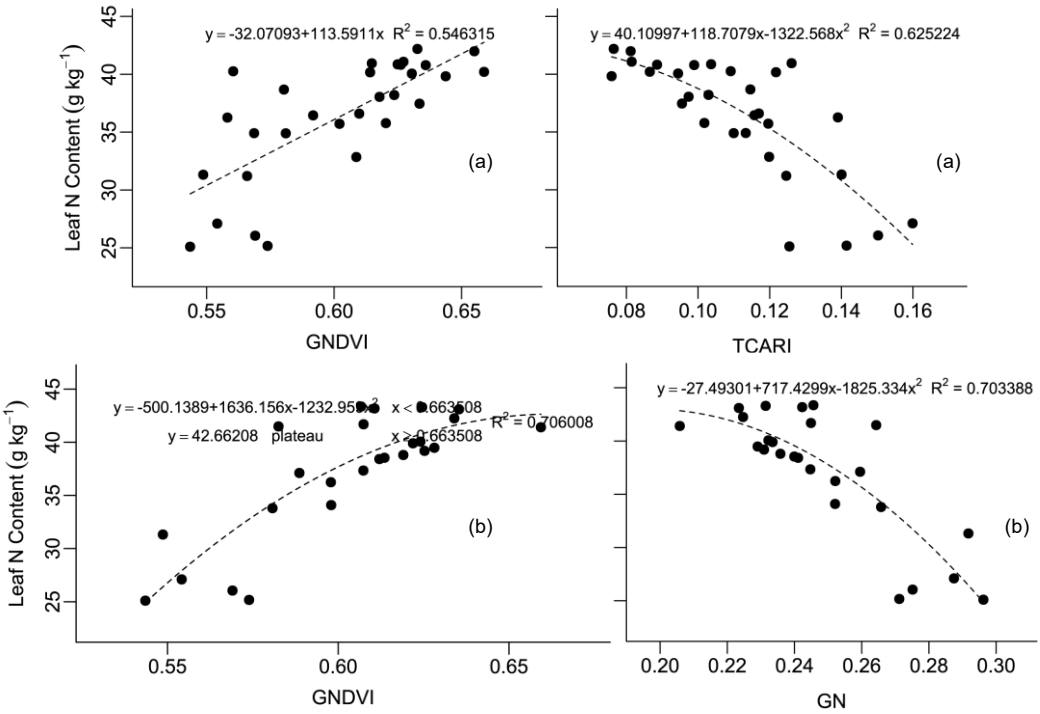

Fig. 10 Vegetation indices (VIs) GNDVI and TCARI for urea (a), and GNDVI and GN for calcium ammonium nitrate (b), which best estimated the leaf N content at V5 stage

A gradual increase in GNDVI was associated with an increase in the economic optimal N rate as for GN and TCARI VIs, the opposite was observed. The narrow range of GNDVI (0.54–0.67) and TCARI (0.08–0.16) values in the case of urea and GNDVI (0.54–0.67) and GN (0.21 –0.29) in the case of CAN, which are responsive to N rate is a concern, as even small variations in the values of these VIs can significantly change the predicted LNC in the model. So, a validation trial was conducted to verify if these VIs can estimate N rate at V5 corn stage.

3.3.4 Validation trial

The VIs best related to applied N rate (Fig. 7) and LNC (Fig. 10) were used for validation. The reflectance of each treatment was obtained at V5 to estimate the N rate as urea and CAN (Table 6).

Table 6 Treatments used in the validation with their respective mean reflectance, mean standard deviation (SD) amount of N applied (kg ha^{-1}) at V5-V6, and yield for each treatment compared to the first experiment. The treatments were applied one day after image acquisition in the area

Treatment	Reflectance	SD	N applied (kg N ha^{-1})	Yield (kg ha^{-1})
GNDVI x N rate – urea	0.450	0.085	**224**	7397 a
GN x N rate – urea	0.281	0.030	**188**	7475 a
1º experiment (N rate to reach high yield = **240** kg N ha^{-1})				7560 a
GNDVI x N rate – CAN	0.548	0.046	**101**	7437 a
GN x N rate – CAN	0.383	0.025	**120**	7617 a
1º experiment (N rate to reach high yield = **120** kg N ha^{-1})				7414 a
GNDVI x LNC – urea	0.574	0.024	**162**	7437 a
TCARI x LNC – urea	0.130	0.008	**166**	7617 a
1º experiment (N rate to reach high yield = **223** kg N ha^{-1})				7558 a
GNDVI x LNC – CAN	0.554	0.022	**119**	6711 a
GN x LNC – CAN	0.279	0.032	**91**	6673 a
1º experiment (N rate to reach high yield = **140** kg N ha^{-1})				6716 a

CAN: calcium ammonium nitrate; LNC, Leaf N Content; SD, Standard Deviation; yield followed by the same letter do not differ at $p<0.05$

Top-dressed N applications at V5-V6 stage were calculated based on the highest yield obtained to the N rate applied from urea and CAN. Although there may be no advantages in applying N rate to reach higher yield due to the economic return, our experiment demonstrated the ability of VIs to estimate N rate, obtaining a grain yield similar to the best N rate used in the first experiment to obtain high yield (Table 6). Using GNDVI and GN VIs with LNC, for CAN N source, yielded 6711.52 and 6673.48 kg ha^{-1}, respectively, not differing from the optimal yield of 6716.24 kg ha^{-1} obtained with 140 kg N ha^{-1} in the first experiment (Fig. 9b). The best VIs related to LNC for the urea N source were GNDVI and TCARI, yielding 7437.54 and 7617.43 kg ha^{-1}, respectively, not differing from the optimal yield of 7558.14 kg ha^{-1} obtained with 223 kg N ha^{-1} in the first experiment (Fig. 9a). Using the GNDVI and GN VIs with the rate of N applied as CAN, the yield was 7437.21 and 7617.32 kg ha^{-1}, respectively, not differing from the optimal yield of 7414.28 kg ha^{-1} obtained with the rate of 120 kg N ha^{-1} in the first experiment (Fig. 8b). The best VIs related to the applied N rate from the urea were GNDVI and GN, yielding 7397.25 and 7475.48 kg ha^{-1}, respectively, not differing from the optimal yield of 7560.50 kg ha^{-1} obtained with 240 kg N ha^{-1} in the first experiment (Fig. 8a). Regardless the VI and plant variable used, the economy of N application is one of the major benefits of using these methods. The economy of N application ranged from 6.6 to 35% as compared to the traditional method used in the first experiment to achieve high yield.

3.3.5 Relationship between VIs and yield at V5, V11 and R1 growth stages

Online Resource 1 also presents the results of linear and quadratic regression analysis, relating VIs to grain yield. In general, quadratic regression models significantly improved yield prediction over linear models. The V6 stage allowed strong correlations with a high range of spectral indices (sixteen indices with a $R^2 > 0.67$), when using urea as N source. As for CAN at V6, the NIR and DVI obtained close relationships with yield ($R^2 = 0.84$). For the V11 stage using urea, the best correlations were observed with six indices (all with $R^2 > 0.70$). For CAN as N source. the GNDVI, GN and MCARI presented $R^2 = 0.99$. At R1, the best correlation occurred with three indices ($R^2 > 0.75$) for urea, while TCARI/OSAVI and TCARI/MSAVI reached $R^2 = 0.98$ for CAN. For LNC, there was no significance in any of the N sources and physiological stages of corn, except for CAN at R1, where it presented a high significance of 0.98.

3.4 Discussion

3.4.1 Enhancing crop nitrogen management and yield through UAV-based sensing and vegetation indices

Unmanned aerial vehicles equipped with remote sensing technologies and vegetation indices offer promising solutions. The V6 stage would have the worst performance among the evaluated stages, due to the influence of the soil reflectance manifested in high reflectance in the red region and the absence of reflectance decline between the green and red region (data not shown) (Deng et al., 2018; Chen and Wang 2022), which is a characteristic of healthy plants (Scharf and Lory 2009). This would have happened if the reflectance in each plot had not removed the soil, where at this growth stage it is still possible to see the bare soil in the image generated by the UAV.

The adequate levels of LNC at R1 stage range from 27.5 to 32.5 g kg^{-1} and from 27 to 35 g kg^{-1}, according to Malavolta et al., (1997) and Raij et al., (1996), respectively. For the R1 stage, only the rate of 300 kg reached leaf N levels close to those of Malavolta et al., (1997) and Raij et al., (1996) with a maximum value of 26.30 g kg^{-1} at 300 kg N ha^{-1} (Online Resource 1). These results are corroborated by Silva et al., (2005), who also found LNC at the R1 stage lower than those described as adequate, attributing this effect to the hybrid used.

Usually, the main causes of LNC variations in corn are factors related to corn genetics, soil fertility and, mainly, changes in climatic conditions (Jakelaitis et al., 2005; Silva et al., 2005). According to Gabriel et al., (2017), when leaf N levels reach the maximum concentration, the corn plant tends to increase biomass instead of increasing leaf N concentration.

Individual bands correlated well with yield at V6 (NIR and Red Edge), V11 (NIR) and R1 (Green) stages. Green band composite indices were highly correlated with grain yield. Other authors have also pointed out that green-based vegetation indices are particularly useful for assessing N status at the V6 stage or at later stages of corn growth (Schepers et al., 1992; Blackmer and Schepers 1996; Bausch and Khosla 2010; Maresma et al., 2016, 2018), although Maresma et al., (2016) also established a high correlation between NDVI and yield (R^2 = 0.92) at V12, with a flight altitude of 120 m, demonstrating that the red region can still be used in some studies and situations.

3.4.2 Integrating spectral imaging with applied N rates for enhanced prediction accuracy at V5 growth stage

The union of the two N sources did not bring a significant increase in the prediction of N rate to be applied at V5 in any of the VIs used, as well as in the relative VIs; therefore, the two N sources were tested separately. Among the fifteen indices evaluated in this study, three exhibited the highest performance: using urea as N source the highlighted VIs were GNDVI, GN, and TCARI/MSAVI, as for CAN the best VIs were GNDVI and GN. A gradual increase in GNDVI was associated with an increase in N rate applied. For GN and TCARI/MSAVI VIs, the opposite was observed. The narrow range of GNDVI (0.55–0.63) and GN (0.28–0.23) values for urea, GNDVI (0.55–0.62) and GN (0.28–0, 23) for CAN, which are responsive to the N rates applied, may be a concern, as even small variations in GNDVI and GN values can significantly change the predicted N rate in the model (Fig. 7). Sripada et al., (2005) also found a small variation in RGDVI values (0.95–1.02), not validating the model completely.

Sripada et al., (2006), trying to estimate N rate at V7, obtained weak linear and quadratic correlations of the VIs studied ($r^2 \leq 0.22$ with emphasis on R_Green, DVI, RDVI and R_GDVI). Scharf and Lory (2009) conducted similar work at V7 stage and observed a high linear model correlation for Green (R^2 = 0.70) and Blue (R^2 = 0.79). Sripada et al., (2005)

achieved an R^2 of 0.69 for the R_DVI, at a later stage (VT). In the present work, R_DVI and DVI had low correlation ($R^2 < 0.29$), thus not being ideal for recommending N rate.

Works such as those by Sripada et al., (2005), Scharf and Lory (2009), Maresma et al., (2016, 2018) also bring coefficients of determination of the NIR and G bands together that are higher than NIR and R together when defining the optimal N rate to apply. In fact, VIs that contain a green band have been found to be more useful for assessing leaf chlorophyll variability when the leaf area index is moderately high (Gitelson et al., 1996). These data show the reliability of the results obtained in this work to determine N rates to be applied at early corn growth stages.

Although Sripada et al., (2005) found a better estimate of N rate with relative VIs at VT stage than normal VIs, in this study we did not obtain a considerable improvement using relative VIs at V6 stage compared to normal VIs. Higher coefficients were obtained with the relative R_GDVI VI (linear-plateau model with $R^2 = 0.67$). Scharf and Lory (2009) also obtained better values with the relative VIs Rel_Blue-Green ($R^2 = 0.76$), Rel_RE ($R^2 = 0.74$), Rel_Green ($R^2 = 0.75$**) and Rel_Green /NIR ($R^2 = 0.65$) at V6 stage. Our work indicates that a reference area would not be necessary (plots receiving a higher N rate that did not limit corn growth; in this study the rate of 300 kg N ha^{-1}) to estimate N rate at V5.

3.4.3 Harnessing spectral imaging to optimize N management in corn at V5 growth stage based on LNC

The union of two N sources with LNC at V5 did not bring a significant increase in the prediction of N rate to be applied in any of the VIs used, as well as the relative VIs; thus, the two N sources were tested separately. These results bring reliability to estimate LNC in corn at V5 stage and define strategies regarding the N rates using VIs such as GNDVI, TCARI and GN. When Rel_VIs was used, there was no considerable improvement compared to VIs.

It is also possible to estimate the N rate to be applied at V5 using LNC as also stated by Gabriel et al., (2017) at R1 stage obtaining a saturation LNC of 34.32 g kg^{-1} at 118.6 kg N ha^{-1}. Our work indicates that it would not be necessary to use a reference area (plots receiving a higher rate of N that did not limit corn growth) in areas close to normal planting to estimate LNC at V5, which is a great advantage, according to Scharf and Lory (2009) and Sripada et al., (2005).

Gabriel et al., (2017) also found good correlations between LNC, TCARI ($R^2 = 0.75$) and TCARI/OSAVI ($R^2 = 0.89$). Leaf N concentration generated a linear-plateau regression with N rate applied, therefore, capable of detecting leaf N deficiency, leading to the identification of zones with greater nutrient demand. When using TCARI correlated with LNC, we were also able to estimate the N rate to be applied at V5, with a yield similar to the first experiment (Table 6). Indeed, TCARI is a vegetation index that measures chlorophyll (McMurtrey et al., 1994); when combining TCARI with OSAVI the correlation with LNC can be further increased, as OSAVI is considered a structural index, and in cases where the plant canopy has not yet covered the soil it can be an ally for TCARI to estimate LNC in corn. Our work also showed a good correlation between LNC, TCARI ($R^2 = 0.63$) and TCARI/OSAVI ($R^2 = 0.57$) (Table 5).

For indices such as NDVI, Rel_DVI and OSAVI, Gabriel et al., (2017) found a low correlation with LNC, not being indicated to predict LNC in corn plants at R1 stage. Our result also shows the same, bringing low correlation for NDVI ($R^2 < 0.30$), Rel_DVI, and OSAVI ($R^2 < 0.13$) at V5 stage.

3.4.4 Potential applications of this study and future work

Farmers and agricultural stakeholders have interest in evaluating and predicting the N status of crops and forecasting potential grain yield during the early stages of the season. This is important for several reasons, such as enhancing N management practices, scheduling harvest and tractor operations, anticipating milling and storage requirements, and guiding marketing strategies. Although there may be no advantages in applying N rate to reach higher yield due to the economic return, our experiment demonstrated the ability of VIs to estimate N rate, obtaining a grain yield like the best N rate used in the first experiment aiming high yield.

In Brazil, the stage at which most farmers apply N fertilizer to corn crops is typically during the V4 to V6 growth stages. This timing aligns with the period when corn plants have established a strong root system and are beginning rapid vegetative growth, allowing for efficient nutrient uptake and utilization. By applying N fertilizer during this stage, farmers aim to meet the crop's nutritional requirements and optimize grain yield potential.

To our knowledge, this is the first study to evaluate the comparative ability of predicting and evaluating the corn N recommendation at early stages using VIs, LNC, and N rate.

However, conducting experiments prior to utilizing vegetation indices and LNC for predicting N in corn crops is crucial because researchers can assess the performance of these indices and LNC measurements in relation to actual N requirements and crop response. In addition, these predictive models need to be validated under specific local conditions and corn variety to ensure their accuracy and reliability.

Other important aspects to take into consideration when estimating N rate are highlighted hereafter; even if the reflectance accurately estimates the N requirement at the time of the reflectance measurement, future conditions may change the N supply or demand. This would result in N deficiency with low detection by spectral reflectance. In fields with a history of organic residues or leguminous plants, mineralization at the beginning of planting may be slow, and the diagnosis may underestimate N availability. Lack of precipitation after N application could also reduce the effectiveness of this method. Despite the possible flaws, its application still proves to be quite viable, from both the economic and the operational perspective, due to the increasing availability of RGB and multispectral cameras embedded on UAVs with the possibility of local or regional calibration for corn and other crops.

The use of LNC can be advantageous over the N rate method once it required less N input applied at V5 corn stage in this study. Also, the linear-plateau and quadratic-plateau showed in the LNC method brings reliability in both N rate and yield estimation cases. The advantage of incorporating a linear-plateau relationship in this context is that it allows for a more realistic representation of the relationship between VIs and LNC. It accounts for the possibility that VIs may increase linearly with increasing LNC up to a certain threshold, beyond which further increases in LNC may not result in significant changes in the vegetation indices.

Continued advancements in UAV technology, remote sensing, and machine learning algorithms offer exciting prospects for further improving N management in precision agriculture. Future research should focus on considering other modeling approaches that combine multiple VIs, incorporating additional parameters such as weather data, soil characteristics, and crop genetics applying non-linear models or more complex machine learning techniques to enhance the accuracy and applicability of N rate recommendations.

3.5 Conclusion

The vegetation indices studied were useful to determine optimal grain yield and leaf N content for urea and CAN N sources. Regression models showed the best VIs based on the

wavelength of the green band (GNDVI and GN) to predict N rate. Some VIs related to the red band (Red) also predict N rate to be applied in V5, however, due to the low coefficient of determination of the regression models, its use is uncertain. The relative VIs did not significantly improve the prediction of N rate at V5, which brings a great benefit, as it does not need to use reference areas for decision-making in the management of nitrogen fertilization in corn.

In general VIs can contribute to improving the efficiency of N use by reducing N inputs while maintaining grain yield, improving the economic return and increasing or maintaining the maximum productivity of the area. Our reliance on these models to apply N at V5 is limited to the dataset obtained in geographic, edaphic and climatic conditions of this study. By integrating UAV data with variable-rate application systems on commercial tractors and implements, farmers can dynamically adjust N fertilizer rates based on real-time crop needs, leading to optimized resource utilization, reduced environmental impact, and improved profitability. Collaboration among researchers, technology developers, and farmers is essential for advancing the implementation, calibration, and validation of UAV-based sensing and VI analysis, paving the way for a more efficient and sustainable future of precision N management.

Author contributions All authors contributed to the study conception and design. Field management was performed by DCS, MCSC and BEM. Remote sensing data collection and analysis was performed by DCS, JVSC and MEF. Statistical analysis and modeling were performed by DCS, DCS provided significant contribution in leaf sampling. The first draft of the manuscript was written by DCS and all authors commented on previous versions of the manuscript. All authors read and approved the final manuscript.

Funding This work was supported by the Coordination of Superior Level Staff Improvement of Brasil (CAPES, Finance Code 001), by the Research Foundation of the State of Goiás (FAPEG) through the Emerging Nuclei Support Program (PRONEM, Grant nº 20170267000519), by the Brazilian Agricultural Research Corporation (Embrapa) and Yara (Cooperation Agreement n° 20200.21/0111-6), and by the Funding Authority for Studies and Projects (FINEP/CT – AGRO/FNDCT, Cooperation Agreement n° 01.22.0080.00, Ref. 1219/21). M.E.F. and B.E.M. have been continuously supported by the Productivity

Fellowship Grant of the National Council for Scientific and Technological Development (CNPq, Grant nº 315699/2020-5 and 307807/2022-3).

Data availability The datasets generated during and/or analyzed during the current study are available from the corresponding author on reasonable request.

Declarations

Conflict of interest The authors declare that they have no conflict of interest.

3.6 References

Argento, F., Anken, T., Abt, F., Vogelsanger, E., Walter, A., & Liebisch, F. (2020). Site-specific nitrogen management in winter wheat supported by low-altitude remote sensing and soil data. *Precision Agriculture*, 22(2), 364–386. https://doi.org/10.1007/s11119-020-09733-3

Arnhold, E. (2019). Performs analysis of regression in simple designs with quantitative treatments, including mixed models and nonlinear models. *R package version 4.0*. https://cran.r-project.org/package=easyreg

Bausch, W. C., & Duke, H. R. (1996). Remote sensing of plant nitrogen status in corn. *Transactions of the American Society of Agricultural Engineers*, 39(5), 1869–1875. https://doi.org/10.13031/2013.27665

Bausch, W. C., & Khosla, R. (2010). QuickBird satellite versus ground-based multi-spectral data for estimating nitrogen status of irrigated maize. *Precision Agriculture*, 11(3), 274–290. https://doi.org/10.1007/s11119-009-9133-1

Benincasa, P., Antognelli, S., Brunetti, L., Fabbri, C. A., Natale, A., Sartoretti, V., et al. (2017). Reliability of ndvi derived by high resolution satellite and uav compared to in-field methods for the evaluation of early crop n status and grain yield in Wheat. *Experimental Agriculture*, 54(4), 604–622. https://doi.org/10.1017/S0014479717000278

Blackmer, T. M., & Schepers, J. S. (1996). Aerial Photography to Detect Nitrogen Stress in Corn. *Journal of Plant Physiology*, 148(3–4), 440–444. https://doi.org/10.1016/S0176-1617(96)80277-X

Chancia, R., Bates, T., Heuvel, J. Vanden, & van Aardt, J. (2021). Assessing grapevine nutrient status from unmanned aerial system (UAS) hyperspectral imagery. *Remote Sensing*, 13(21). https://doi.org/10.3390/rs13214489

Chen, P., & Wang, F. (2022). Effect of crop spectra purification on plant nitrogen concentration estimations performed using high-spatial-resolution images obtained with unmanned aerial vehicles. *Field Crops Research*, 288(March), 108708. https://doi.org/10.1016/j.fcr.2022.108708

Cilia, C., Panigada, C., Rossini, M., Meroni, M., Busetto, L., Amaducci, S., et al. (2014). Nitrogen Status Assessment for Variable Rate Fertilization in Maize through Hyperspectral Imagery. *Remote Sensing*, 6(7), 6549–6565. https://doi.org/10.3390/rs6076549

Costa, L., Kunwar, S., Ampatzidis, Y., & Albrecht, U. (2021). Determining leaf nutrient concentrations in citrus trees using UAV imagery and machine learning. *Precision Agriculture*, 23(3), 854–875. https://doi.org/10.1007/s11119-021-09864-1

Daughtry, C. S. T., Walthall, C. L., Kim, M. S., Brown de Colstoun, E., & McMurtrey III, J. E. (2000). Estimating Corn Leaf Chlorophyll Concentration from Leaf and Canopy Reflectance. *Remote Sensing of Environment*, 74(2), 229–239. https://doi.org/10.1016/S0034-4257(00)00113-9

Deng, L., Mao, Z., Li, X., Hu, Z., Duan, F., & Yan, Y. (2018). UAV-based multispectral remote sensing for precision agriculture: A comparison between different cameras. *ISPRS Journal of Photogrammetry and Remote Sensing*, 146(September), 124–136. https://doi.org/10.1016/j.isprsjprs.2018.09.008

Fu, Z., Jiang, J., Gao, Y., Krienke, B., Wang, M., Zhong, K., et al. (2020). Wheat growth monitoring and yield estimation based on multi-rotor unmanned aerial vehicle. *Remote Sensing*, 12(3). https://doi.org/10.3390/rs12030508

Gabriel, J. L., Zarco-Tejada, P. J., López-Herrera, P. J., Pérez-Martín, E., Alonso-Ayuso, M., & Quemada, M. (2017). Airborne and ground level sensors for monitoring nitrogen status in a maize crop. *Biosystems Engineering*, 160, 124–133. https://doi.org/10.1016/j.biosystemseng.2017.06.003

García-Martínez, H., Flores-Magdaleno, H., Ascencio-Hernández, R., Khalil-Gardezi, A., Tijerina-Chávez, L., Mancilla-Villa, O. R., & Vázquez-Peña, M. A. (2020). Corn grain yield estimation from vegetation indices, canopy cover, plant density, and a neural network using multispectral and rgb images acquired with unmanned aerial vehicles. *Agriculture (Switzerland)*, 10(7), 1–24. https://doi.org/10.3390/agriculture10070277

Gitelson, A. A., Kaufman, Y. J., & Merzlyak, M. N. (1996). Use of a green channel in remote sensing of global vegetation from EOS-MODIS. *Remote Sensing of Environment*, 58(3), 289–298. https://doi.org/10.1016/S0034-4257(96)00072-7

Goel, P. K., Prasher, S. O., Landry, J. A., Patel, R. M., Bonnell, R. B., Viau, A. A., & Miller, J. R. (2003). Potential of airborne hyperspectral remote sensing to detect nitrogen deficiency and weed infestation in corn. *Computers and Electronics in Agriculture*, 38(2), 99–124. https://doi.org/10.1016/S0168-1699(02)00138-2

Haboudane, D., Miller, J. R., Tremblay, N., Zarco-Tejada, P. J., & Dextraze, L. (2002). Integrated narrow-band vegetation indices for prediction of crop chlorophyll content for application to precision agriculture. *Remote Sensing of Environment*, 81(2–3), 416–426. https://doi.org/10.1016/S0034-4257(02)00018-4

Han, S., Zhao, Y., Cheng, J., Zhao, F., Yang, H., Feng, H., et al. (2022). Monitoring Key Wheat Growth Variables by Integrating Phenology and UAV Multispectral Imagery Data into Random Forest Model. *Remote Sensing*, 14(15). https://doi.org/10.3390/rs14153723

Huete, A. (1988). A soil-adjusted vegetation index (SAVI). *Remote Sensing of Environment*, 25(3), 295–309. https://doi.org/10.1016/0034-4257(88)90106-X

Jakelaitis, A., Silva, A. A. da, & Ferreira, L. R. (2005). Efeitos do nitrogênio sobre o milho cultivado em consórcio com *Brachiaria brizantha* (Effects of nitrogen on corn grown in intercropping with *Brachiaria brizantha*). *Acta Scientiarum. Agronomy*, 27(1). https://doi.org/10.4025/actasciagron.v27i1.1916

Jiang, J., Zhang, Z., Cao, Q., Liang, Y., Krienke, B., Tian, Y., et al. (2020). Use of an active canopy sensor mounted on an unmanned aerial vehicle to monitor the growth and

nitrogen status of winter wheat. *Remote Sensing*, 12(22), 1–24. https://doi.org/10.3390/rs12223684

Jordan, C. F. (1969). Derivation of Leaf-Area Index from Quality of Light on the Forest Floor. *Ecology*, 50(4), 663–666. https://doi.org/10.2307/1936256

Keeney, D. R., & Bremner, J. M. (1967). Use of the Coleman model 29A analyzer for total nitrogen analysis of soils. *Soil Science*, (104(5)), 358–363.

Kyveryga, P. M., Blackmer, T. M., & Pearson, R. (2012). Normalization of uncalibrated late-season digital aerial imagery for evaluating corn nitrogen status. *Precision Agriculture*, 13(1), 2–16. https://doi.org/10.1007/s11119-011-9231-8

Li, M., Zhu, X., Li, W., Tang, X., Yu, X., & Jiang, Y. (2022). Retrieval of Nitrogen Content in Apple Canopy Based on Unmanned Aerial Vehicle Hyperspectral Images Using a Modified Correlation Coefficient Method. *Sustainability (Switzerland)*, 14(4). https://doi.org/10.3390/su14041992

Li, X., Ba, Y., Zhang, M., Nong, M., Yang, C., & Zhang, S. (2022). Sugarcane Nitrogen Concentration and Irrigation Level Prediction Based on UAV Multispectral Imagery. *Sensors*, 22(7). https://doi.org/10.3390/s22072711

Liu, H., Zhu, H., & Wang, P. (2016). Quantitative modelling for leaf nitrogen content of winter wheat using UAV-based hyperspectral data. *International Journal of Remote Sensing*, 38(8–10), 2117–2134. https://doi.org/10.1080/01431161.2016.1253899

Magdoff, F. (1991). Understanding the Pre-Sidedress Nitrate Test for Corn. *Journal of Production Agriculture*, 4(3), 297–305. https://doi.org/10.2134/jpa1991.0297

Malavolta, E., Vitti, G. C. e, & Oliveira, S. A. de. (1997). *Avaliação do estado nutricional das plantas: principios e aplicações* (Assessment of the nutritional status of plants: principles and applications) (2nd ed.). Associação Brasileira para Pesquisa da Potassa e do Fosfato.

Marang, I. J., Filippi, P., Weaver, T. B., Evans, B. J., Whelan, B. M., Bishop, T. F. A., et al. (2021). Machine learning optimised hyperspectral remote sensing retrieves cotton nitrogen status. *Remote Sensing*, 13(8). https://doi.org/10.3390/rs13081428

Maresma, Á., Ariza, M., Martínez, E., Lloveras, J., & Martínez-Casasnovas, J. (2016). Analysis of Vegetation Indices to Determine Nitrogen Application and Yield Prediction in Maize (Zea mays L.) from a Standard UAV Service. *Remote Sensing*, 8(12), 973. https://doi.org/10.3390/rs8120973

Maresma, Á., Lloveras, J., & Martínez-Casasnovas, J. A. (2018). Use of multispectral airborne images to improve in-season nitrogen management, predict grain yield and estimate economic return of maize in irrigated high yielding environments. *Remote Sensing*, 10(4), 1–19. https://doi.org/10.3390/rs10040543

McMurtrey, J., Chappelle, E., Kim, M., Meisinger, J., & Corp, L. (1994). Distinguishing nitrogen fertilization levels in field corn (Zea mays L.) with actively induced fluorescence and passive reflectance measurements. *Remote Sensing of Environment*, 47(1), 36–44. https://doi.org/10.1016/0034-4257(94)90125-2

Montgomery, K., Henry, J. B., Vann, M. C., Huseth, A. S., & Mitasova, H. (2020). Measures of canopy structure from low-cost uas for monitoring crop nutrient status. *Drones*, 4(3), 1–22. https://doi.org/10.3390/drones4030036

Osco, L. P., Junior, J. M., Ramos, A. P. M., Furuya, D. E. G., Santana, D. C., Teodoro, L. P. R., et al. (2020). Leaf nitrogen concentration and plant height prediction for maize using

UAV-based multispectral imagery and machine learning techniques. *Remote Sensing*, 12(19), 1–17. https://doi.org/10.3390/rs12193237

Peng, J., Manevski, K., Kørup, K., Larsen, R., & Andersen, M. N. (2021). Random forest regression results in accurate assessment of potato nitrogen status based on multispectral data from different platforms and the critical concentration approach. *Field Crops Research*, 268(April). https://doi.org/10.1016/j.fcr.2021.108158

Piikki, K., Söderström, M., Stadig, H., & Wolters, S. (2022). Remote sensing and on-farm experiments for determining in-season nitrogen rates in winter wheat – Options for implementation, model accuracy and remaining challenges. *Field Crops Research*, 289(March). https://doi.org/10.1016/j.fcr.2022.108742

Qi, J., Kerr, Y., & Chehbouni, A. (1994). External factor consideration in vegetation index development. In CNES, *Proceedings of 6th International Symposium on Physical Measurements and Signatures in Remote Sensing*.

Quemada, M., Baranski, M., Nobel-de Lange, M. N. J., Vallejo, A., & Cooper, J. M. (2013). Meta-analysis of strategies to control nitrate leaching in irrigated agricultural systems and their effects on crop yield. *Agriculture, Ecosystems & Environment*, 174, 1–10. https://doi.org/10.1016/j.agee.2013.04.018

Raij, B. V., Cantarella, H., Quaggio, J. A., & Furlani, A. M. C. (1996). *Fertilization and liming recommendations for the state of São Paulo* (2.ed.). Campinas: Campinas Agronomic Institute.

Rouse, J. W., Haas, R. H., Deering, D. W., Schell, J. A., & Harlan, J. C. (1974). *Monitoring the Vernal Advancement and Retrogradation (Green Wave Effect) of Natural Vegetation*. Greenbelt, MD, USA.

Santos, A. M., Pacheco, E. P., Vale, W. G., & Chaves, M. V. S. (2020). Approaching of GOPRO camera embedded on UAV to calculate NDVI for corn's crop. *Scientific Electronic Archives*, 13(8), 18. https://doi.org/10.36560/13820201015

Scharf, P. C., Brouder, S. M., & Hoeft, R. G. (2006). Chlorophyll meter readings can predict nitrogen need and yield response of corn in the north-central USA. *Agronomy Journal*, 98(3), 655–665. https://doi.org/10.2134/agronj2005.0070

Scharf, P. C., & Lory, J. A. (2009). Calibrating reflectance measurements to predict optimal sidedress nitrogen rate for corn. *Agronomy Journal*, 101(3), 615–625. https://doi.org/10.2134/agronj2008.0111

Schepers, J. S., Francis, D. D., Vigil, M., & Below, F. E. (1992). Comparison of corn leaf nitrogen concentration and chlorophyll meter readings. *Communications in Soil Science and Plant Analysis*, 23(17–20), 2173–2187. https://doi.org/10.1080/00103629209368733

Sharma, L. K., & Bali, S. K. (2018). A review of methods to improve nitrogen use efficiency in agriculture. *Sustainability* (Switzerland), 10(1), 1–23. https://doi.org/10.3390/su10010051

Silva, E. C. da, Buzetti, S., Guimarães, G. L., Lazarini, E., & Sá, M. E. de. (2005). Doses e épocas de aplicação de nitrogênio na cultura do milho em plantio direto sobre Latossolo Vermelho (Doses and times of nitrogen application in corn crops in no-till farming on Oxisol). *Revista Brasileira de Ciência do Solo*, 29(3), 353–362. https://doi.org/10.1590/S0100-06832005000300005

Snyder, C. S., Bruulsema, T. W., Jensen, T. L., & Fixen, P. E. (2009). Review of greenhouse gas emissions from crop production systems and fertilizer management effects.

Agriculture, Ecosystems & Environment, 133(3–4), 247–266. https://doi.org/10.1016/j.agee.2009.04.021

Sousa, D. M. G. de, & Lobato, E. (2004). *Cerrado: correção do solo e adubação* (Cerrado: soil correction and fertilization) (2nd ed.). Brasília, DF: Embrapa Technological Information; Planaltina, DF: Embrapa Cerrados. http://www.infoteca.cnptia.embrapa.br/infoteca/handle/doc/555355. Last accessed [December 6, 2023].

Sripada, R. P., Heiniger, R. W., White, J. G., & Meijer, A. D. (2006). Aerial Color Infrared Photography for Determining Early In-Season Nitrogen Requirements in Corn. *Agronomy Journal*, 98(4), 968–977. https://doi.org/10.2134/agronj2005.0200

Sripada, R. P., Heiniger, R. W., White, J. G., & Weisz, R. (2005). Aerial color infrared photography for determining late-season nitrogen requirements in corn. *Agronomy Journal*, 97(5), 1443–1451. https://doi.org/10.2134/agronj2004.0314

Thompson, L. J., & Puntel, L. A. (2020). Transforming unmanned aerial vehicle (UAV) and multispectral sensor into a practical decision support system for precision nitrogen management in corn. *Remote Sensing*, 12(10). https://doi.org/10.3390/rs12101597

Tucker, C. J. (1979). Red and photographic infrared linear combinations for monitoring vegetation. *Remote Sensing of Environment*, 8(2), 127–150. https://doi.org/10.1016/0034-4257(79)90013-0

Tyner, E. H., & Webb, J. R. (1946). The Relation of Corn Yields to Nutrient Balance as Revealed by Leaf Analysis 1. *Agronomy Journal*, 38(2), 173–185. https://doi.org/10.2134/agronj1946.00021962003800020008x

Varvel, G. E., Schepers, J. S., & Francis, D. D. (1997). Chlorophyll meter and stalk nitrate techniques as complementary indices for residual nitrogen. *Journal of Production Agriculture*, 10(1), 147–151. https://doi.org/10.2134/jpa1997.0147

Xu, X., Fan, L., Li, Z., Meng, Y., Feng, H., Yang, H., & Xu, B. (2021). Estimating leaf nitrogen content in corn based on information fusion of multiple-sensor imagery from uav. *Remote Sensing*, 13(3), 1–17. https://doi.org/10.3390/rs13030340

Yang, M., Xu, X., Li, Z., Meng, Y., Yang, X., Song, X., et al. (2022). Remote Sensing Prescription for Rice Nitrogen Fertilizer Recommendation Based on Improved NFOA Model. *Agronomy*, 12(8), 1–17. https://doi.org/10.3390/agronomy12081804

Zhang, J., Wang, W., Krienke, B., Cao, Q., Zhu, Y., Cao, W., & Liu, X. (2022). In-season variable rate nitrogen recommendation for wheat precision production supported by fixed-wing UAV imagery. *Precision Agriculture*, 23(3), 830–853. https://doi.org/10.1007/s11119-021-09863-2

Zheng, H., Li, W., Jiang, J., Liu, Y., Cheng, T., Tian, Y., et al. (2018). A comparative assessment of different modeling algorithms for estimating leaf nitrogen content in winter wheat using multispectral images from an unmanned aerial vehicle. *Remote Sensing*, 10(12). https://doi.org/10.3390/rs10122026

Zou, X., & Mõttus, M. (2017). Sensitivity of Common Vegetation Indices to the Canopy Structure of Field Crops. *Remote Sensing*, 9(10), 994. https://doi.org/10.3390/rs9100994

CAPÍTULO 3

OPTIMIZING NITROGEN ESTIMATES IN COMMON BEAN CANOPIES THROUGHOUT KEY GROWTH STAGES VIA FUSION OF SPECTRAL AND TEXTURAL DATA FROM UNMANNED AERIAL VEHICLE MULTISPECTRAL IMAGERY[1]

Diogo Castilho[2,3]; Beata Emoke Madari[2,3]; Maria da Conceição Santana Carvalho[3]; Manuel Eduardo Ferreira[4]

---

[1] Capítulo submetido como artigo ao periódico científico Computers and Electronics in Agriculture. Submetido em 15 nov. 2023.

[2] Programa de Pós-graduação em Agronomia (PPGA), Universidade Federal de Goiás (UFG), Goiânia, Goiás, Brasil.

[3] Embrapa Arroz e Feijão, Santo Antônio de Goiás, Goiás, Brazil.

[4] Laboratório de Processamento de Imagens e Geoprocessamento (LAPIG), IESA, UFG, Goiânia, Goiás, Brasil.

ABSTRACT

This study investigates the potential of utilizing multispectral imagery acquired from unmanned aerial vehicles (UAVs) to enhance the accuracy of leaf nitrogen content (LNC) estimation, a crucial parameter for assessing crop nitrogen status and guiding nitrogen management practices. We integrated selected vegetation indices (VIs) and texture data derived from UAV-based multispectral images to estimate LNC in common bean (*Phaseolus vulgaris* L.). The research spanned two consecutive years (2021–2022) and encompassed various nitrogen application rates. UAV flights coincided with critical growth stages (V4, R5, and R7) of common bean, where destructive leaf samplings were conducted. Following preprocessing of the UAV imagery, we computed VIs, texture metrics, and the normalized difference texture index (NDTI). Our findings revealed that the green normalized difference vegetation index (GNDVI) and the modified chlorophyll absorption in reflectance index (MCARI) delivered the most accurate LNC estimates at the V4 and R5 growth stages (R^2 of 0.53–0.57) among all the VI candidates. NDTIs incorporating correlation and homogeneity demonstrated the ability to explain 71% and 58% of LNC variability for the R7 growth stage and the entire growing season, respectively. Furthermore, we employed machine learning models, random forest (RF) and support vector machine (SVM), to combine VIs with gray level co-occurrence matrix (GLCM) texture features. These models significantly enhanced the accuracy of LNC estimation across all growth stages, as well as when examined separately. Therefore, the integration of band spectral indices with UAV-based textural information might be a promising technique in common bean growth monitoring.

Keywords: UAV, multispectral imagery, vegetation index, GLCM, LNC, common bean

4.1Introduction

The common bean (*Phaseolus vulgaris* L.) is a popular crop all around the world with more than 27 million tons produced in 2021, serving as a vital source of nutrition and sustenance for billions of people, offering a rich source of protein, fiber, and essential nutrients (FAOSTAT 2021). Proper rate and timing of nitrogen (N) is crucial factors for high yield and quality. A significant portion of N in the plant is directed towards the leaves (Ghanbari et al. 2013) thus the leaf nitrogen content (LNC) of a canopy has been widely used to characterize crop N status in field conditions (Fu et al. 2022). LNC is an important indicator used to measure the N status of beans. Plants that have nutritional deficiencies related to N show visual symptoms in their leaves, known as chlorosis (Xue et al. 2020). Monitoring crop N content is beneficial during the early growth stages for effective

fertilization planning (Maresma et al. 2018) and during maturing growth stages to assess yield (Luo et al. 2022). Therefore, the continuous monitoring of N is of great importance.

The efficiency of traditional methods of measuring LNC is low, time-consuming, laborious, and it does not meet the needs of rapid, real-time monitoring (Blackmer and Schepers 1996). Obtaining the LNC remotely, rapidly, efficiently and effectively has always been an urgent problem to be solved to either boost higher yield potential zones or reduce inputs to lower potential areas reducing environmental impact while increasing profit (Marang et al. 2021; Li et al. 2022).

In recent years, unmanned aerial vehicles (UAVs) have attracted significant scientific and public interest due to their flexibility, enabling rapid, non-destructive, and efficient operations (Jiang et al. 2020; Chen & Wang 2022). Their use in remote sensing offers the possibility of obtaining field data in an easy and profitable way, resulting in images with high spatial and temporal resolution (García-Martínez et al. 2020; Li et al. 2022). The major advantage of using UAV is that large populations of plants can be assessed quickly, while also reducing inaccuracies resulting from sampling a limited subset of plants (Costa et al. 2021). Several studies have shown the potential of UAV data for estimating LNC in several crops such as grape, cotton, corn, citrus trees, and rice (Osco et al. 2019; Wang et al. 2021; Xu et al. 2021; Peng et al. 2022). Though successful, these studies ignored more information stored in the high-resolution UAV images acquired at a low flight height, which contains not only spectral (vegetation indices – VIs or single bands) but also texture information related to crop N properties.

Gray level co-occurrence matrix (GLCM) based textures are derived from the gray tone spatial-dependance matrix and represent the heterogeneity in the tonal values of pixels within a region of interest (ROI) (Wood et al. 2012). Textural information can reflect the characteristics of objective surfaces once variations in N levels have an impact on both the size and color of crop leaves. Consequently, these variations result in disparities in how the canopy structure absorbs and reflects light, ultimately altering the textural characteristics at the pixel level (Fu et al. 2021). The incorporation of GLCM textures into this context remains relatively scarce. Liu et al. (2018) achieved great estimates of the nitrogen nutrition index in winter oilseed rape by combining VIs and GLCM textures, which were derived from VIs. The most valuable texture metrics identified were correlation and variance depending on the background removal or not within the ROI. Fu et al. (2020) used homogeneity, correlation

and contrast GLCM textures for all three bands (blue, green, and red) to improve estimates of plant N density and plant N concentration in winter wheat. Guo et al. (2022) highlighted important GLCM texture metrics such as contrast, homogeneity and mean for the winter wheat plant N content estimates with RF model achieving a coefficient of determination (R^2) of 0.92 and root mean square error (RMSE) of 3.17 g m^{-2}. Zheng et al. (2020) evaluated the potential of integrating texture and spectral information for improving the quantification of leaf and plant N concentration in rice crops, applying normalized difference texture index (NDTI) where it was based on the VIs and designed to emphasize differences between two spectral bands and directions. They indicated model VIs with a R^2 range of 0.00 – 0.20, texture features with a R^2 range of 0.00 – 0.35 and the combination of VIs and NDTI with a R^2 between of 0.68 and 0.70 for leaf N concentration and plant N concentration, respectively. The most important NDTIs were dissimilarity, correlation and mean using red edge and near infra-red bands.

Information of spatial heterogeneity provided by texture metrics may be complementary to the spectral characteristics. However, the selection of texture metrics to predict LNC in beans may be influenced by many factors, such as the genotypes, the light condition, and the image acquisition resolution (Barbier and Couteron 2015). Thus, the selected texture metrics in these studies may not be the best predictors for a different crop type or region.The findings underscored the promise of also utilizing image textures extracted from UAV imagery to estimate N levels in common bean. Additionally, it was observed that these image texture attributes, derived from high-resolution UAVs, frequently exhibit scale-dependent characteristics, potentially resulting in variations in model performance and transferability. Thus, the combination of machine learning (ML) methods and effective predictors (spectra, texture factors, etc.) would achieve good performance in solving the nonlinear problem of LNC estimation.

In recent years, with the advancement of data mining techniques, such as support vector machines (SVM), neural networks, artificial neural network (ANN), random forest (RF), and other methods have been increasingly applied to the prediction of crop N content, which outperform traditional models in terms of accuracy. For example, Wang et al. (2021) performed better LNC estimates of paddy rice using ANN, SVM and RF when single or multiple growth stages are involved. Peng et al. (2021) found that a combination of VIs using

RF provided better plant N concentration estimation with RMSE and relative root mean square error (RRMSE) of 0.19% and 10.11%, respectively for potato crop.

In addition, different ML methods differ in prediction accuracy. For example, Zha et al. (2020) used VIs with RF, ANN, and SVM models to perform estimates of plant N uptake and N nutrition index (NNI) in rice. The validation results indicated that the RF model performed the best among the tested methods with RMSE of 11.52 kg ha^{-1} and 0.09 for plant N uptake and NNI, respectively at stem elongation stage. Osco et al. (2020) evaluated the performance of nine supervised ML methods. The results indicated that the RF algorithm performed better, with R^2 and RMSE, respectively, of 0.91 and 1.9 g kg^{-1} for leaf N concentration, and 0.86 and 0.17 m for corn plant height estimates. They also demonstrated that VIs contributed more to the algorithm's performances than individual spectral bands.

To the best of our knowledge, research to the estimation of LNC for common bean using UAV-based sensors is relatively scarce. Most existing studies have focused on estimating yield, leaf area index, and dry matter content (Gutiérrez-Rodríguez et al. 2006; Köksal et al. 2008; Monteiro et al. 2013; Santana et al. 2016; Saravia et al. 2023). However, the importance of estimating LNC using RF and SVM, in conjunction with VIs and GLCM texture metrics, cannot be underestimated. Therefore, the objectives of this study were (i) to determine the optimal VIs and texture metrics from UAV multispectral imagery for estimating LNC, and (ii) to explore the capability of integrating spectral and textural information in the improvement of N status monitoring.

4.2 Materials and methods

The methodology consisted of three distinct phases: (a) conducting a field survey to gather relevant data, (b) performing chemical analysis on leaf tissue samples, and (c) utilizing digital image processing techniques for data analysis. Each phase comprised specific steps, which were visually represented in a workflow diagram (Fig. 1) and further elaborated upon below.

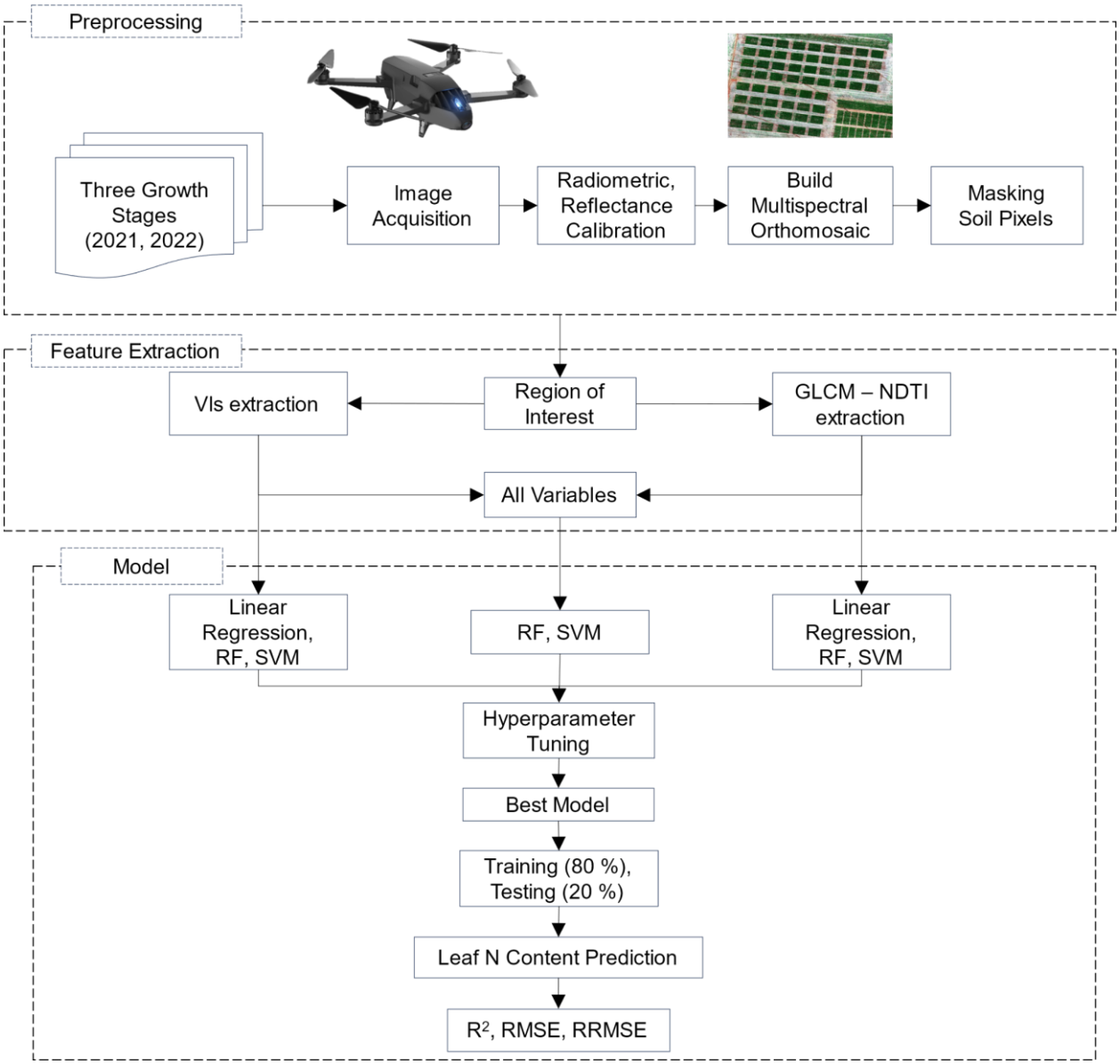

Fig. 1. Workflow diagram of the process performed in this study.

4.2.1 Study Area

The study area was located at Embrapa Rice and Beans field station at Santo Antônio de Goiás – Goiás State, Brazil (16°29'10.5"S, 49°17'53.7"W). The site area covers approximately 8600 m^2, located under a central pivot irrigation system used only when needed during summer season. Because it corresponds to a relatively small experimental area, the soil presents similar conditions. This area is constantly monitored, and soil corrections are conducted whenever necessary.

It should be noted that the plots were continuously used over the previous 5 years as an experimental field for studies related to the fertilization of corn and common bean with N. The same treatments were applied to each individual plot as in the previous years. As a result, it would be expected that the effect of different N treatments would be more evident. Three treatments were added in this experiment, in addition to those that had been used for 5 years (160 and 200 kg N ha^{-1} as urea and 200 kg N ha^{-1} as calcium ammonium nitrate – CAN source).

4.2.2 Experimental Design

The experimental field was divided into 50 plots, including 15 rows of common bean, which were planted at a row spacing of 45 cm, plot length was 10 m, and width was 7.2 m, with an alleyway in between each plot. The experimental design was a randomized complete block. Common bean (BRS FC402 cultivar) was planted on 26 May 2021, and 23 May 2022. There were ten treatments of N, including the control, 40, 80, 120, 160 and 200 kg ha^{-1} of urea and 40, 80, 120 and 200 kg ha^{-1} of CAN as N sources, applied randomly with five replicates (Fig. 2). All plots were fertilized based on soil test results and received uniform applications of Yara Basa fertilizer (6N-27P-6K plus sulfur, calcium and micronutrients) at a rate of 300 kg ha^{-1} at planting, and 170 kg ha^{-1} of KCl (60% K_2O) was hand-spread two days after planting. Thus, the 50 plots received 18 kg N ha^{-1} at planting, including the control treatment. The N application treatments were performed just after emergence in each year at V4 (4th trifoliolate unfolded at node 6 + branching).

Fig. 2. Location of the study area and detail of the experimental plots. The image was obtained using the parrot sequoia RGB camera on 16 July 2021, at R5 stage. The labels refer to N source: U – Urea (46% N) and CAN – Calcium Ammonium Nitrate (27% N). Numbers followed by U or CAN represent N rate applied at V4 stage (40, 80, 120, 160 and 200 kg N ha^{-1}). Zero represents the control (0 kg N ha^{-1}).

4.2.3 UAV Campaigns, Sensors and Data Collection

We used the Parrot® Sequoia™ multispectral imaging sensor (Parrot Drones S.A.S, Paris, France), which captures the reflected light at four spectral bands: green (G; 550 nm; 40 nm bandwidth), red (R; 660 nm; 40 nm bandwidth), red-edge (RE; 735 nm; 10 nm bandwidth), and near-infrared (NIR; 790 nm; 40 nm bandwidth) with 1.2 Mpx. The camera was mounted on a Bluegrass UAV from Sensefly (Fig. 3) and it was also equipped with an irradiance sensor for measuring incident light, in order to correct for variable lighting conditions during the flight. Prior to each flight, ground images from a calibration target (AIRINOV Aircalib; AIRINOV, Paris, France) were acquired, in order to derive accurate reflectance values. The latter was a polyvinyl chloride (PVC) board with a gray target area silkscreen printing and ArUco tags for the albedo measurements of each band, which have been measured specifically for the Sequoia sensor. The flight planning was generated using the Pix4D Capture software with a side and front overlap of 70%. The single images were subsequently combined to create an orthophotomosaic using the Pix4Dmapper Pro software (Pix4D SA, Lausanne, Switzerland), which employs an advanced Structure from Motion (SfM) workflow to generate precise orthophotomosaics with absolute reflectance values.

Pix4D accomplishes this by integrating calibration target images and irradiance sensor data into an automated process, eliminating the requirement for manual calibration or additional image processing by the user. This calibration procedure considered both the lighting circumstances during image capture and the specific attributes of the sensor. An overview of the acquisition procedures and processing of UAV imagery can be found in Aasen et al. (2018).

The flights were conducted under optimum weather condition at an altitude of 70 m above ground (Vega et al. 2015; Montgomery et al. 2020) with a spatial resolution of 6.6 cm pixel^{-1} during three growth stages: V4, R5 (One pod with fully developed seeds), and R7 (One pod at mature color – physiological maturity). The time of flight was less than 20 min between 10:00 and 12:00h a.m. on sunny days. UAV flight dates were adjusted to the field leaf sampling dates (Table 1).

Fig. 3. A: Calibration panel that accompanies the Parrot Sequoia camera for radiometric calibration of images; B: Parrot Sequoia multispectral camera. The central wavelengths of the bands are 550 nm (40 nm) green, 660 nm (40 nm) red, 735 nm (10 nm) red edge, and 790 nm (40 nm) NIR; C: Bluegrass UAV, from Sensefly company.

Table 1 Synthesis of field management and data acquisition calendar.

Year	Seedling	N Fertilizer	UAV Flight	Field Sampling	Growth Stage	Harvest Date
2021	26 May	21 June	30 June	30 June	V4	03 September
			16 July	16 July	R5	
			30 July	30 July	R7	
2022	23 May	20 June	28 June	28 June	V4	30 August
			14 July	14 July	R5	
			26 July	26 July	R7	

4.2.4 Masking Soil Pixels

To calculate the spatial mean of VIs for individual rows of common beans, it was crucial to eliminate bare soil pixels situated amidst the rows. The occurrence of such a phenomenon is noticed when plants are in the vegetative phenological stages. The background soil reflectance potentially decreases the effectiveness of the leaves in VI values (Barzin et al. 2020). The image processing pipeline aimed to segment vegetation areas within the acquired aerial imagery using the NDVI thresholding technique (Gallo et al. 2018). A defined threshold value of 0.7 was applied to the computed NDVI map. This threshold value was chosen to delineate the regions with healthy vegetation. A binary mask was generated by classifying NDVI values above the threshold as '1' (vegetation) and values below or equal to the threshold as '0' (non-vegetation). The binary mask was applied to the original image data using element-wise multiplication. This operation resulted in an image where non-vegetation areas were set to zero, effectively segmenting the vegetation regions from the background (Fig. 4).

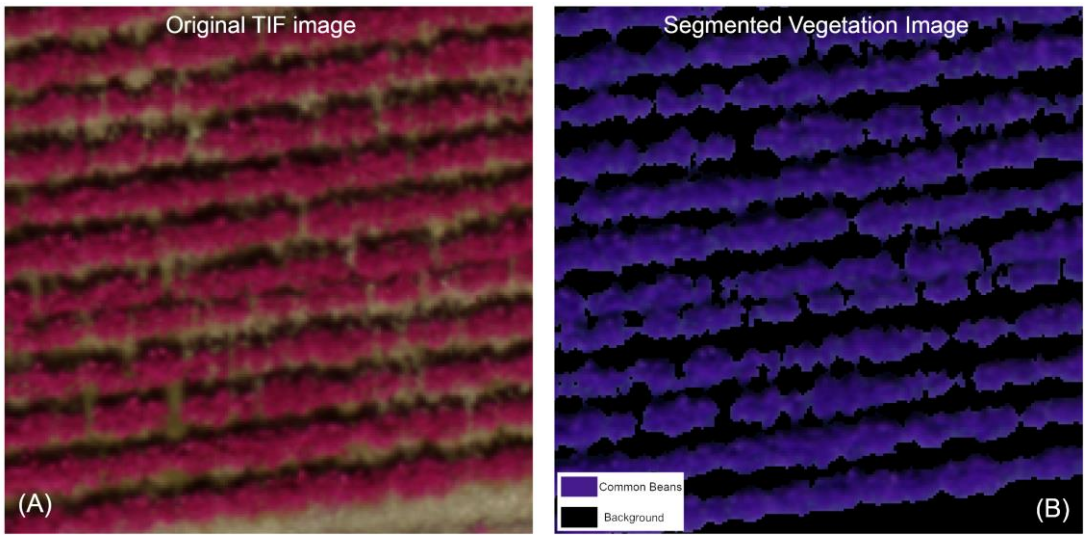

Fig. 4. Visual representation of the efficacy of the segmentation technique. The segmented vegetation image (B) was juxtaposed with the original TIF image (A). Both images were displayed side by side, with specific zoomed-in areas for detailed observation.

4.2.5 Calculation of Vegetation Indices and gray level co-occurrence matrix

The study utilized a high-resolution image captured by an aerial platform, serving as the source of spectral information. Additionally, a shapefile containing the delineated polygons (45 m^2) representing distinct plots was used to extract reflectance information. The image consisted of multiple spectral bands, each corresponding to a specific range of

wavelengths. The mean reflectance values of four bands (band 1: green, band 2: red, band 3: red edge, band 4: near-infrared) were calculated within each polygon using zonal statistics. To quantify various vegetation characteristics, seventeen widely used VIs reported in the literature, were calculated for each polygon using the extracted reflectance values (Table 2).

Table 2 Vegetation indices used.

Vegetation Index	Formula	Reference
Normalized Green-Red Difference Index (NGRDI)	$(Band1 - Band2) \div (Band1 + Band2)$	Zheng et al. 2018
Modified Triangular Vegetation Index (MTCI)	$(Band4 - Band3) \div (Band3 + Band2)$	Dash and Curran 2004
Chlorophyll Index Red Edge (CIRE)	$(Band4 \div Band3) - 1$	Gitelson et al. 2002
Normalized Difference Red Edge (NDRE)	$(Band4 - Band3) \div (Band4 + Band3)$	Perry et al. 2018
Normalized Difference Vegetation Index (NDVI)	$(Band4 - Band2) \div (Band4 + Band2)$	Rouse et al., 1974
Ratio Difference Vegetation Index (RDVI)	$(Band4 - Band2) \div (Band4 + Band2)^{0.5}$	Zheng et al. 2018
Optimized Soil-Adjusted Vegetation Index (OSAVI)	$1.16 \times (Band4 - Band2) \div (Band4 + Band2 + 0.16)$	Zou and Mõttus 2017
Modified Triangular Vegetation Index 2 (MTVI2)	$1.5 \times (1.2 \times (Band4 - Band1) - 2.5 \times (Band2 - Band1)) \div ((Band4 + 1)^2 - (2.4 \times Band4) - (1.8 \times Band2) + 0.5)$	Li et al. 2019
Green Normalized Difference Vegetation Index (GNDVI)	$(Band4 - Band1) \div (Band4 + Band1)$	Gitelson et al., 1996
Modified Soil-Adjusted Vegetation Index (MSAVI)	$(2 \times Band4 + 1 - ((2 \times Band4 + 1)^2 - 8 \times (Band4 - Band2))^{0.5} \div 2$	Qi et al., 1994
Green Soil-Adjusted Vegetation Index (GSAVI)	$1.16 \times (Band4 - Band1) \div (Band4 + Band1 + 0.16)$	Sripada et al., 2006
Modified Chlorophyll Absorption in Reflectance Index (MCARI)	$(1.5 \times (2.5 \times (Band4 - Band3) - 1.3 \times (Band4 - Band2))) \div ((2 \times Band4 + 1)^2 - (6 \times Band4 - 5 \times (Band3 - Band2)) - 0.5)$	Daughtry et al., 2000
Triangular Chlorophyll Absorption Ratio Index (TCARI)	$3 \times (Band3 - Band2) - 0.2 \times (Band3 - Band1) \times (Band3 / Band2)$	Haboudane et al., 2002
TCARI/OSAVI	$TCARI \div OSAVI$	Haboudane et al., 2002
TCARI/MSAVI	$TCARI \div MSAVI$	Haboudane et al., 2002
Ratio Vegetation Index (RVI)	$Band3 \div Band2$	Jordan 1969
Difference Vegetation Index (DVI)	$Band3 - Band2$	Tucker 1979

GLCM was employed in this study to evaluate the potential of texture analysis on reflectance images for improving beans N status monitoring. A shapefile containing geometries representing distinct regions of interest (ROIs) was employed. The 'id' column from this shapefile was extracted to establish correspondence between ROIs and identifiers. Furthermore, the orthomosaicked image comprising multiple spectral bands was read, considering the presence of bare soil and vegetation pixels. For each 'id' from the shapefile, the geometry bounds were derived to define the spatial extent of the ROI. Subsequently, the region of interest (ROI) was extracted from the image based on these bounds. The grayscale representation of the ROI was prepared to facilitate GLCM computation. GLCM was

computed for each band within the ROI. The analysis encompassed diverse directions, employing four fixed angles (D1 = 0°, D2 = 45°, D3 = 90° and D4 = 135°).

A set of eight texture metrics derived from GLCM analysis, encompassing mean (MEA), variance (VAR), homogeneity (HOM), contrast (CON), dissimilarity (DIS), entropy (ENT), second moment (ASM), and correlation (COR), were calculated. A detailed description of the eight-texture metrics can be found in Lu and Batistella (2005). Subsequently, the interrelationships among these diverse texture metrics were investigated to mitigate data dimensionality and heighten data processing efficiency. Upon this analysis, we selected a subset of four key texture metrics, namely HOM, CON, COR, and ASM, for the subsequent texture analysis. This focused analysis was performed across the five spectral bands and four distinct directions. The average value of each metric across different directions and bands was calculated for every plot. This step facilitated the generation of more comprehensive insights.

The extraction of the Normalized Difference Texture Index (NDTI) was also undertaken (Zheng et al. 2020; Zheng et al. 2018). These authors used NDTI because it has the capability to improve the performance of texture analysis and its wider variation than other texture metrics at high N levels at later growth stages. This allowed for better estimation of N nutrition parameters in rice crops using UAV-based multispectral imagery.

GLCM metrics (HOM, CON, COR, and ASM), four bands and four directions were performed using NDTI. The equation NDTI = (T1-T2)/(T1+T2) was proposed, where T1 and T2 are a random texture feature from the four bands in four directions. To identify a suitable texture pairing, an assessment of the correlation between LNC and NDTI was conducted, encompassing all feasible combinations of texture variations.

4.2.6 Harvest and Leaf N Content Process

Grain yield was measured in the three central rows (2.70 x 3.00 m) of each plot, which were manually harvested at the physiological maturity stage. Grain moisture was adjusted to 13% moisture content. The yield response to N rate was performed. Yield-normalization was accomplished by expressing relative grain yield values relative to the site-year maximum. The resulting relative yield values will typically range between 0 and 1, with higher values indicating higher grain yield.

Leaf sampling was collected at V4, R5 and R7 stages on the same UAV flight day for the determination of LNC (g kg^{-1}). These samples were obtained from 15 plants at random in each plot at three phenological stages. The leaf sample obtained was the last trifoliolate unfolded. The leaves were dried at 65 degrees Celsius until constant weight. Subsequently, the samples were ground for determining LNC, applying the Dumas combustion method – Rapid N cube by Elementary analyzer (Keeney & Bremner 1967).

Regression analysis was used to identify VIs, GLCM, and NDTI that were useful in predicting LNC. The linear model was used prior to the quadratic model only if its use resulted in a higher coefficient of determination.

4.2.7 Statistical Analysis

In this study, we employed Python programming language, utilizing Jupyter Lab as our development environment. The data analysis and manipulation were facilitated by leveraging the capabilities of Anaconda, a comprehensive platform that streamlines the management of packages and environments, ensuring reproducibility and consistency in our analyses.

The data collected from the two field experiments were pooled to explore the connections among agronomic variables, VIs, GLCM, and NDTI textures along with their composite interactions. This investigation was conducted employing simple regression, random forest (RF) and support vector machine (SVM) analyses.

To ensure the robustness of the models, the dataset was divided into training and testing sets using a test size of 20%. The input features were standardized to ensure that all features are on the same scale, preventing any one feature from disproportionately influencing the model's performance.

For both the SVM and RF models, hyperparameter tuning was conducted performing an exhaustive search over a specified hyperparameter grid. For SVM, the hyperparameters tuned were the kernel type ('linear', 'rbf', 'poly') and the regularization parameter 'C' (0.1, 1 or 10). For RF, hyperparameters included the number of estimators (100, 500 or 1000), maximum tree depth (none, 10 or 20), minimum samples required to split a node (2, 5 or 10), and minimum samples required to be at a leaf node (1, 2 or 4).

Following hyperparameter tuning, the best SVM and RF models were identified using the respective best hyperparameters for each growth stage and dataset (Table 3). These models were then trained on the scaled training data. Additionally, the importance of features in the RF model was determined. The top 10 most important features were selected based on their importance scores.

Table 3 Best hyperparameters for each model, growth stage, and dataset used.

Growth Stage	Dataset	All Features						Top 10 Features					
		Hyperparameters						Hyperparameters					
		RF				SVM		RF				SVM	
		n estimators	max depth	min samples split	min samples leaf	kernel	C	n estimators	max depth	min samples split	min samples leaf	kernel	C
V4	VIs	100	none	5	2	rbf	10	500	none	2	4	rbf	1
	GLCM + VIs	1000	none	5	1	linear	1	100	10	2	1	rbf	10
	NDTI + VIs	100	none	2	4	poly	1	1000	10	2	1	poly	1
R5	VIs	1000	none	5	1	linear	1	100	none	10	1	linear	0.1
	GLCM + VIs	1000	none	5	1	linear	1	1000	10	2	4	rbf	10
	NDTI + VIs	100	none	2	1	rbf	1	1000	none	10	2	linear	1
R7	VIs	1000	none	5	1	linear	1	1000	none	10	4	linear	10
	GLCM + VIs	100	none	2	1	linear	1	500	none	10	4	linear	10
	NDTI + VIs	1000	none	2	4	rbf	10	100	none	10	2	linear	10
Entire Season	VIs	1000	none	5	1	linear	1	1000	none	10	4	rbf	10
	GLCM + VIs	500	none	2	1	linear	10	100	none	10	1	rbf	10
	NDTI + VIs	500	10	2	1	linear	0.1	100	10	10	1	rbf	10

Furthermore, the SVM and RF models were re-trained using only the top 10 features. Like the initial model training, hyperparameter tuning, prediction, and metric calculation were performed for these models. To validate the models, a five-fold cross-validation procedure (k = 5) was applied to the merged dataset, and the evaluation was based on metrics such as root mean square error (RMSE) and relative RMSE (RRMSE).

4.3 Results

4.3.1 Variation of LNC and Yield Over the Three Growth Stages

Table 4 provides information on the LNC for different growth stages of two-year study, as well as the variability of the LNC at each N rate applied. The smallest LNC mean value for all growth stages was observed at an N rate of 0 kg ha^{-1}. The V4 growth stage exhibited the greatest mean LNC values compared to the other stages. As N application increased from 0 to 200 kg ha^{-1}, there was a corresponding increment in LNC. The mean LNC ranged from 56.59 to 64.37 g kg^{-1}, with a SD ranging from 2.73 to 3.50. The CV

indicated moderate to low relative variability, ranging from 4.35% to 6.56%. The observed minimum and maximum values were within a relatively narrow range, varying from 50.73 to 68.70. During the R5 growth stage, the LNC demonstrated a similar response pattern to varying N rates. Increasing N levels led to an augmentation in LNC, with mean values ranging from 49.28 to 56.53. The SD showed a slightly wider range, varying from 2.89 to 4.60, resulting in CV values of 5.13% to 9.08%. The LNC's range exhibited by the minimum and maximum values spanned from 43.89 to 62.74, indicating a broader spectrum of variability compared to the V4 stage. The R7 growth stage showcased distinct behavior in terms of LNC response to N rates. Like previous stages, an increase in N application led to an increase in LNC. The mean values ranged from 39.95 to 49.85, and the SD ranged from 4.74 to 7.03, yielding CV values of 10.50% to 16.09%. Notably, the R7 growth stage demonstrated the highest relative variability among the three growth stages, as indicated by the CV. The range between minimum and maximum values spanned from 29.72 to 57.91, suggesting considerable heterogeneity.

Table 4 Summary of descriptive statistics for LNC (g kg^{-1}) for each fertilization treatment (N rate) at V4, R5, and R7 growth stages. Average yield (t ha^{-1}) obtained at harvest is also shown. SD: standard deviation; CV: coefficient of variation.

Growth Stage	N rate (kg ha^{-1})	Mean	SD	CV	Min	Max	Yield (t ha^{-1})
V4	0	56.59	3.33	5.88	50.73	60.60	
	40	59.95	3.93	6.56	54.19	66.01	
	80	62.99	3.42	5.43	56.69	68.46	
	120	62.83	3.46	5.51	57.49	68.75	
	160	64.37	3.50	5.44	58.74	68.70	
	200	62.85	2.73	4.35	58.13	67.34	
R5	0	49.28	4.38	8.38	45.11	58.74	1.65
	40	50.67	4.60	9.08	43.89	56.98	2.36
	80	54.10	4.00	7.39	44.50	58.08	2.96
	120	54.01	3.13	5.80	50.14	61.99	3.40
	160	56.53	3.83	6.77	50.94	62.74	3.61
	200	56.41	2.89	5.13	52.47	61.04	3.36
R7	0	39.95	6.76	15.74	33.85	52.26	
	40	41.22	6.60	16.01	29.72	53.96	
	80	43.67	7.03	16.09	31.92	54.65	
	120	45.75	6.20	13.56	36.30	56.35	
	160	45.16	4.74	10.50	40.27	53.14	
	200	49.85	6.33	12.70	38.64	57.91	

Grain yield was lowest in the 0N treatment, ranging from 1.47 up to 1.92 t ha^{-1} with a mean of 1.65 t ha^{-1}. Across all years, yields increased with increasing N rate up to a maximum and either plateaued or decreased at the highest N rates. Maximum yields ranged from 3.56 to 3.98 t ha^{-1}. Based on the linear-plateau regression model, maximum yields were achieved with an average N fertilizer rate of 91 kg N ha^{-1} (Fig. 5).

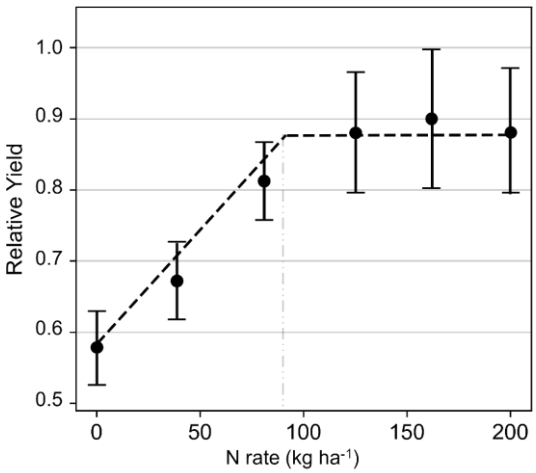

Fig. 5. The relationship between N rate and relative grain yield as described by a linear-plateau regression model. The mean and standard deviation relative yield for each N rate (0, 40, 80, 120, 160, and 200 kg N ha^{-1}) are presented. The vertical dashed line at 91 kg N ha^{-1} represents the N fertilizer value where the relationship reaches a plateau.

4.3.2 Performance of Spectral Vegetation Indices, Gray Level Co-occurrence Matrix, and Normalized Difference Texture Indices

From a pool of 21 VIs, the top 10 VIs were selected based on their performance in estimating LNC at various growth stages. Similarly, the analysis encompassed a vast spectrum of 64 GLCM texture features. The most informative texture features were identified, with the top 10 GLCM features emerging as consistent indicators of spatial variations in LNC. Additionally, an extensive set of 4032 NDTI combinations were assessed. From this extensive array, the top 5 NDTI combinations stood out as reliable tools for assessing LNC across diverse growth stages.

VIs, GLCM and NDTI across various growth stages and the entire growing season provided valuable insights into their capacity to predict LNC (Table 5). At the V4 growth stage, the GNDVI demonstrated the highest R^2 value of 0.571. Likewise, GSAVI and the GVI showed notable R^2 values of 0.567 and 0.537, respectively. GLCM features such as COR_{B4_D4} and HOM_{B1_D4} demonstrated promising R^2 values of 0.486 and 0.483,

respectively. NDTI involving (HOM_{B1_D3}, HOM_{B4_D2}) or (HOM_{B4_D2}, HOM_{B1_D3}) displayed high R^2 values of 0.551, indicating their potential for assessing LNC at this early stage.

Transitioning to the R5 stage, the MCARI emerged as the top-performing VI with an R^2 value of 0.539. Additionally, the Green and Red Edge reflectance displayed substantial correlations with R^2 values of 0.513 and 0.490, respectively. GLCM COR_{B2_D3} and COR_{B2_D2} exhibited R^2 values of 0.398 and 0.397, respectively, indicating their potential in distinguishing LNC at this intermediate growth stage. HOM_{B1_D4} also exhibited significant performance with an R^2 value of 0.393. NDTI like (HOM_{B1_D4}, ASM_{B4_D3}) or (HOM_{B1_D4}, ASM_{B4_D4}) displayed R^2 values of 0.465.

Moving to the R7 stage, the DVI took the lead with an R^2 of 0.452, while the Red Edge and the NGRDI exhibited significant R^2 values of 0.431 and 0.403, respectively. The RVI also proved its suitability for this growth stage with R^2 of 0.390. GLCM features derived from COR_{B2} (COR_{B2_D4}, COR_{B2_D3}, COR_{B2_D2}, COR_{B2_D1}) demonstrated high R^2 values, with COR_{B2_D4} leading the pack with R^2 of 0.696. These features underscored their effectiveness in capturing textural information relevant to LNC as the crop developed. NDTI like (COR_{B1_D3}, COR_{B4_D1}) achieved a remarkable R^2 value of 0.714, indicating their strong correlation with LNC. (COR_{B2_D3}, COR_{B4_D3}) also exhibited high R^2 values of 0.708.

Throughout the entire growing season, while several VIs, GLCM and NDTI showed strong performance at specific growth stages, it appears that they might not maintain the same level of performance when applied across the entire growing season. This could be due to variations in crop conditions, environmental factors, or the specific characteristics of the metrics themselves. NDTI achieved the highest R^2 values compared to Vis and GLCM. NDTI like (CON_{B2_D2}, CON_{B2_D4}) or (CON_{B1_D2}, CON_{B1_D3}) maintained R^2 values of 0.570 and 0.568, respectively, indicating their consistency in assessing LNC across different growth stages.

Table 5 Simple linear relationship between LNC, vegetation indices, GLCM and NDTI (R^2) at different growth stages.

V4		R5		R7		Entire Season	
Vegetation Index							
	R^2		R^2		R^2		R^2
GNDVI	**0.571**	**MCARI**	**0.539**	DVI	0.452	MTCI	0.311
GSAVI	0.567	Green	0.513	Red Edge	0.431	CIRE	0.297
Green	0.537	Red Edge	0.490	NGRDI	0.403	RVI	0.287
CIRE	0.530	DVI	0.479	RVI	0.390	GSAVI	0.245

MCARI	0.528	CIRE'	0.436	MTVI2	0.306	MSAVI	0.243
MTCI	0.526	TCARI	0.431	MSAVI	0.290	RDVI	0.232
NDRE	0.521	NDRE	0.431	RDVI	0.281	NIR	0.222
TCARI/MSAVI	0.514	MTCI	0.400	OSAVI	0.280	MCARI	0.222
TCARI/OSAVI	0.511	TCARI/OSAVI	0.393	NIR	0.277	NGRDI	0.220
Red Edge	0.504	GNDVI	0.389	NDVI	0.258	NDRE	0.215
			GLCM				
COR_{B4_D4}	0.486	COR_{B2_D3}	0.398	COR_{B2_D4}	0.696	ASM_{B1_D3}	0.205
HOM_{B1_D4}	0.483	COR_{B2_D2}	0.397	COR_{B2_D3}	0.686	ASM_{B1_D2}	0.205
COR_{B4_D3}	0.482	HOM_{B1_D4}	0.393	COR_{B1_D4}	0.684	ASM_{B1_D4}	0.205
ASM_{B1_D1}	0.480	COR_{B4_D4}	0.391	COR_{B1_D3}	0.678	ASM_{B1_D1}	0.205
HOM_{B1_D2}	0.479	COR_{B1_D3}	0.387	COR_{B2_D2}	0.667	ASM_{B4_D2}	0.205
ASM_{B1_D3}	0.479	COR_{B4_D3}	0.384	COR_{B1_D2}	0.648	ASM_{B4_D4}	0.205
ASM_{B1_D4}	0.479	HOM_{B1_D3}	0.384	COR_{B2_D1}	0.643	ASM_{B4_D3}	0.205
ASM_{B1_D2}	0.479	COR_{B1_D2}	0.383	COR_{B3_D4}	0.628	ASM_{B4_D1}	0.201
HOM_{B1_D3}	0.479	COR_{B2_D1}	0.381	COR_{B3_D3}	0.618	ASM_{B3_D3}	0.193
COR_{B3_D4}	0.474	COR_{B4_D2}	0.381	COR_{B1_D1}	0.599	ASM_{B3_D2}	0.193
			NDTI				
HOM_{B1_D3}, HOM_{B4_D2}	0.551	HOM_{B1_D4}, ASM_{B4_D3}	0.465	**COR_{B1_D3}, COR_{B4_D1}**	**0.714**	**HOM_{B2_D2}, HOM_{B2_D4}**	**0.588**
HOM_{B4_D2}, HOM_{B1_D3}	0.551	HOM_{B1_D4}, ASM_{B4_D4}	0.465	COR_{B2_D3}, COR_{B4_D3}	0.708	CON_{B2_D2}, CON_{B2_D4}	0.570
HOM_{B1_D3}, HOM_{B4_D4}	0.548	HOM_{B1_D4}, ASM_{B4_D2}	0.465	COR_{B1_D4}, COR_{B4_D1}	0.706	CON_{B1_D2}, CON_{B1_D3}	0.568
HOM_{B4_D4}, HOM_{B1_D3}	0.548	HOM_{B1_D4}, ASM_{B4_D1}	0.464	COR_{B2_D3}, COR_{B4_D1}	0.703	HOM_{B2_D2}, HOM_{B2_D3}	0.533
HOM_{B4_D2}, HOM_{B1_D4}	0.547	HOM_{B1_D3}, ASM_{B4_D3}	0.462	COR_{B2_D3}, COR_{B4_D2}	0.700	CON_{B1_D2}, CON_{B1_D4}	0.503

All regressions are statistically significant at $p < 0.001$. ASM, Second Moment; CON, Contrast; COR, Correlation; HOM, Homogeneity. The acronyms represent the texture parameter from corresponding band and direction. For example, COR_{B4_D4} represents the mean texture parameter from NIR band reflectance at 135º direction. The most significant feature for each growth stage is highlighted.

4.3.3 Performance of VIs, GLCM and NDTI Combinations

Table 6 shows the testing performance of the combination of VIs and texture indices in the estimation of LNC with linear regression, RF and SVM models for different growth stages. Three different datasets were compared: "VIs", "GLCM + VIs" (Texture Features + VIs), and "NDTI + VIs" (Normalized Difference Texture Index + VIs). Additionally, all available features and the top 10 features for modeling were experimented. The RF and SVM outperformed the best linear regressions (VIs and NDTIs) for V4, R5 and R7 growth stages. The best linear regression was achieved with GNDVI at V4 stage with RMSE of 1.79 g kg^{-1} and RRMSE of 14.17%. Among the models, the top 10 features generated the lowest RMSE and RRMSE compared to all features for each phenological stage, regardless of the machine

learning model used. Generally, RF and SVM models showed competitive performance across various datasets and growth stages.

At the V4 growth stage, for the "VIs" dataset, the "Top 10 Features" SVM model had the lowest RMSE of 1.80 and RRMSE of 2.93%. At the R5 growth stage, also using "VIs" dataset, the RF model with the top 10 features had the lowest RMSE of 2.79 and RRMSE of 5.20. However, the R7 and entire season the best dataset was the "GLCM + VIs", using RF model and the top 10 features with RMSE of 3.42 and 3.96, and RRMSE of 7.39 and 7.32, respectively.

Table 6 Accuracy assessment with RMSE and RRMSE values for the estimation of LNC with different datasets and models across growth stages.

Growth Stage	Dataset	All Features				Top 10 Features				Best Linear Regression		
		RF		SVM		RF		SVM				
		RMSE	RRMSE	RMSE	RRMSE	RMSE	RRMSE	RMSE	RRMSE	Dataset	RMSE	RRMSE
V4	VIs	1.92	3.13	2.05	3.34	1.92	3.13	**1.80**	**2.93**	GNDVI	1.79	14.17
	GLCM + VIs	3.36	5.93	4.73	8.34	3.01	5.30	5.10	8.99			
	NDTI + VIs	1.99	3.23	2.35	3.82	1.87	3.05	2.14	3.47			
R5	VIs	2.80	5.25	3.90	5.77	**2.79**	**5.20**	3.15	5.89	MCARI	3.07	16.68
	GLCM + VIs	3.28	6.04	4.92	9.08	4.06	7.49	5.91	10.90			
	NDTI + VIs	3.02	5.64	3.42	6.40	3.10	5.79	2.95	5.52			
R7	VIs	6.38	13.80	6.29	13.60	6.27	13.56	6.30	13.63	COR_{B1_D3}, COR_{B4_D1}	4.59	18.82
	GLCM + VIs	3.50	7.85	3.60	7.78	**3.42**	**7.39**	3.67	7.95			
	NDTI + VIs	4.00	8.66	3.73	8.07	4.17	9.00	4.51	9.75			
Entire Season	VIs	4.86	9.00	6.01	11.12	4.93	9.12	5.92	10.96	HOM_{B2_D2}, HOM_{B2_D4}	5.60	16.22
	GLCM + VIs	4.04	7.54	4.19	7.75	**3.96**	**7.32**	5.37	9.93			
	NDTI + VIs	4.28	7.93	4.33	8.01	4.98	9.22	4.93	9.13			

COR_{B1_D3}, COR_{B4_D1} and HOM_{B2_D2}, HOM_{B2_D4} represents the correlation and homogeneity GLCM from green, NIR and red band reflectance at 90º, 0º, 45º and 135º direction, respectively. The most significant dataset for each growth stage is highlighted.

The data presented in Fig. 6 comprise the feature importance of the top 10 features (representing the contribution of each feature to the model's predictive performance) and the scatter plots of measured LNC values versus estimated ones derived from the optimal non-parametric algorithm in each growth stage. At V4 stage, the SVM model outperformed the RF model with GSAVI, MCARI, DVI, and green reflectance as the most important VIs used in the model reaching RMSE and RRMSE values of 1.80 and 2.93, respectively (Fig. 6a,b). The R5 stage also showed MCARI, DVI and green reflectance as the most important VIs for the RF model, including TCARI/OSAVI reaching RMSE and RRMSE values of 2.79 and 5.20, respectively (Fig. 6c,d). As for the last growth stage studied, the GLCM + VIs was the

best dataset to estimate LNC at the R7 stage. Interestingly, among the four GLCM textures analyzed, only the COR was present as the most important features for the RF model. Furthermore, the green and red bands at three directions (45º, 90º and 135º) composed the COR texture in the prediction of LNC, reaching RMSE and RRMSE values of 3.42 and 7.40, respectively (Fig. 6e,f). Throughout the entire growing season, the GLCM COR with NIR band at the 135º direction, TCARI/OSAVI, MTCI and MCARI VIs were the most important features using RF model, reaching RMSE and RRMSE values of 3.96 and 7.33, respectively (Fig. 6g,h).

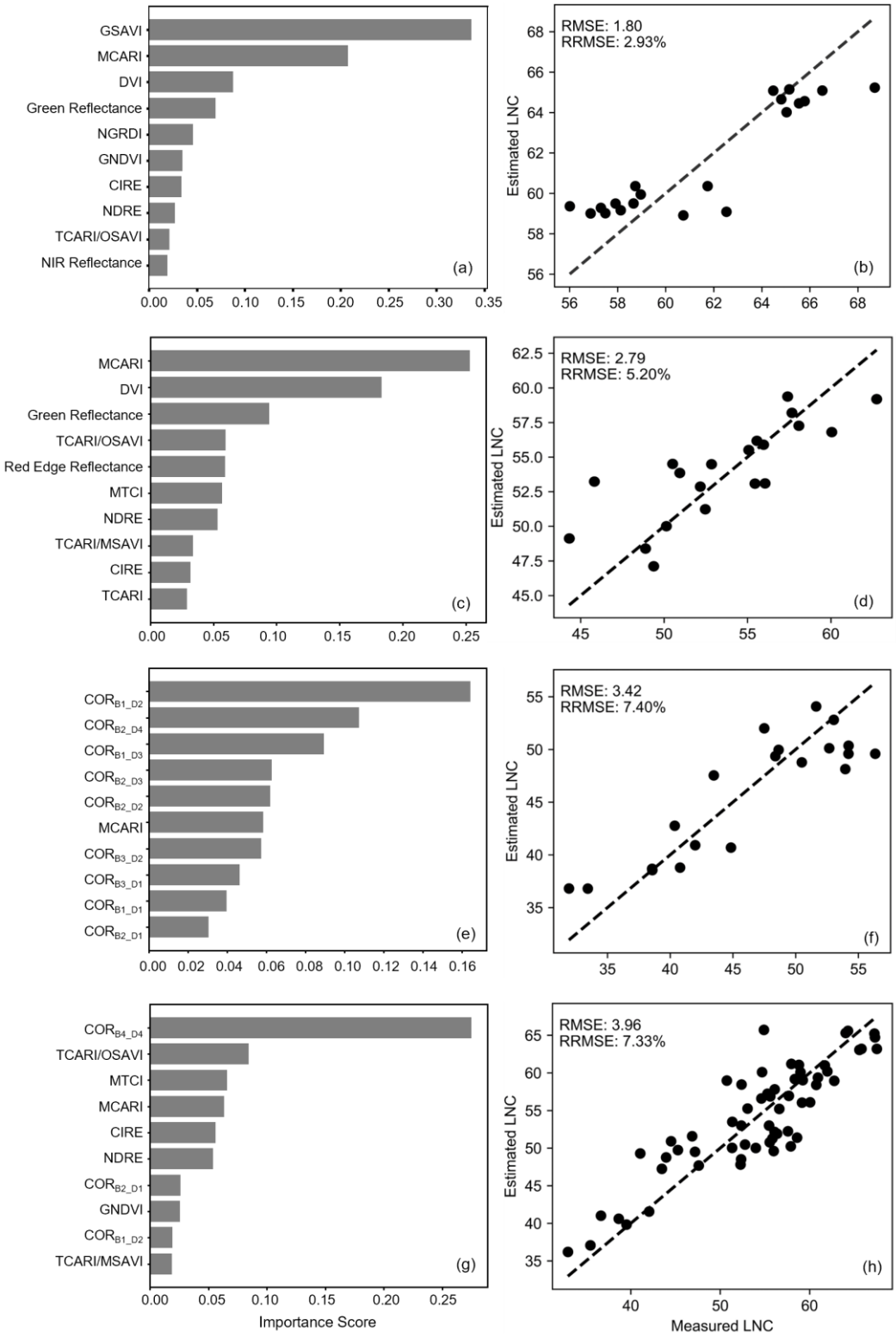

Fig. 6. Top ten features importance and the relationship between the LNC (g kg^{-1}) estimated vs. the LNC measured by VIs and texture metrics using (a, b) SVM model at V4; (c, d) RF model at R5; (e, f) RF model at R7 growth stage; and (g, h) RF model over the three stages (entire season). The dashed lines indicate 1:1.

To highlight the viability of the proposal, a map was generated using the SVM model at V4 stage, incorporating VIs as input parameters, to predict values for LNC (Fig. 7). This map offers a qualitative insight into the outcomes. After training, a machine learning model can analyze image data and produce a visual representation of the area.

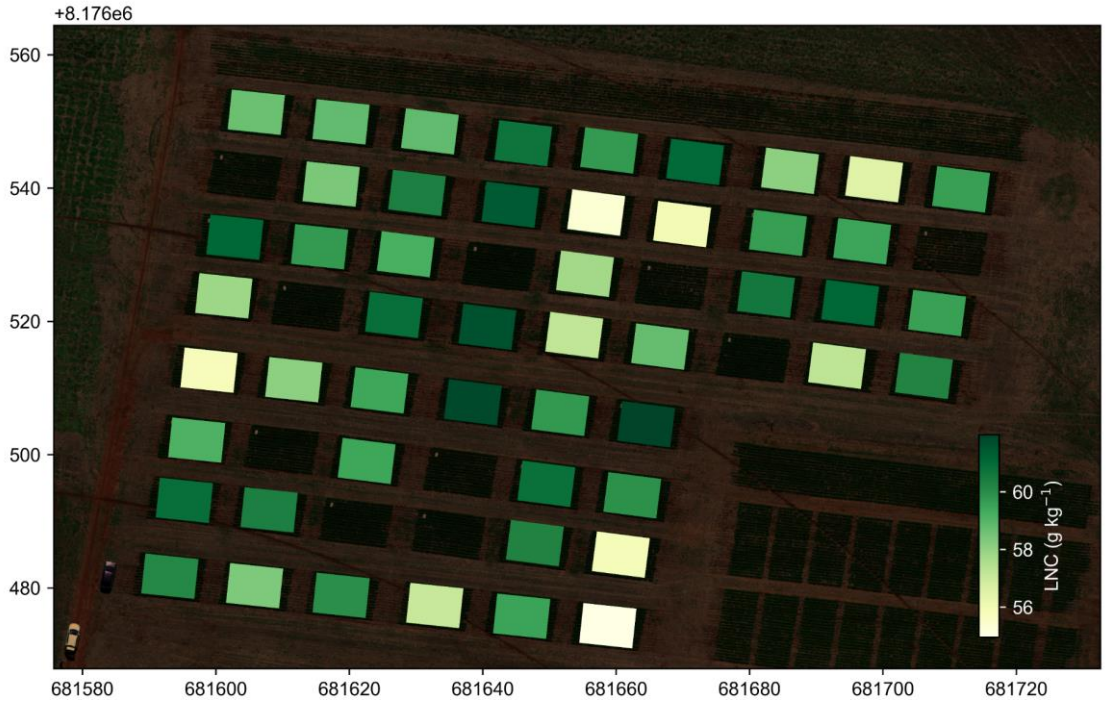

Fig. 7. Prediction map over the 2021/2022 crop season indicating the LNC related to every plot in the UAV-based image for the V4 common bean growth stage. The model used for inference was the SVM and only the top 10 features VIs were used as input data to calculate the predicted LNC.

4.4 Discussion

4.4.1 Different Performances of Individual VIs and Textures

The estimation accuracy for LNC was significantly higher using VIs at V4 and R5 growth stages. The optimal VIs at V4 (GNDVI, GSAVI) could explain 57% of the variability in LNC, respectively. On the other hand, the optimal VIs at R5 (MCARI, Green Reflectance) could explain 54% and 51% of the variability in LNC, respectively. The LNC varied in a broad range across the growing season and N rate applied. It increased from the beginning, leveled off in the middle and then decreased until physiological maturity (Ghanbari et al. 2013).

The best-performing VIs were GNDVI and GSAVI at V4 stage, which was expected and in agreement with the findings (Li et al. 2020; Marin et al. 2021; Osco et al. 2019; Wright et al. 2004). Texture indices showed a better performance when compared to VIs at R7 and entire growth stage which is in agreement to the performance of texture ratios in rice plant N accumulation estimation (Zheng et al. 2020). For the R7 stage, all the 10 best GLCM and NDTI indices textures were related to the COR texture reaching R^2 between 0.60 and 0.71 with green, red and NIR bands at 90 (D3) and 135º (D4) directions. Correlation measures how correlated or linearly related the pixel intensities are in different directions within the image. It quantifies how similar the grayscale values of pairs of pixels are when they are separated by a specific distance and orientation. Fu et al. (2020), Fu et al. (2021), Guo et al. (2022) and Li et al. (2022) also found COR as one of the best GLCM texture features to estimate LNC, plant N density and content using green and red bands for winter wheat and tea plants.

The entire growth stage was best correlated with LNC using NDTI indices such as HOM and CON metrics accompanied by green and red bands reaching R^2 between 0.50 and 0.59. HOM performed well at late growth stages and most texture features at 720 nm were superior to other texture features for the entire season for estimating plant N concentration in rice (Zheng et al. 2018), which is in contrast to this study where we found green and red bands better correlated to LNC for the entire growth season. That might be because the reflectance at red edge and NIR bands had a broader variation through the growing season and the texture features from these bands could explain more variation in plant N concentration than LNC.

Texture indices (NDTI) performed significantly better than individual texture (GLCM) measurements, which might be similar to advantages of VIs that could reduce the influence of canopy geometry (Huete 1988; Zheng et al. 2018). Given different growth stage, the optimal NDTI was different, because canopy structure varies as common bean plants grow, and leaves dominate the canopy before reproductive stage. Interestingly, the optimal NDTIs across all growth stages consisted of texture parameters from green and red bands (Table 4). Since they are good indicators of canopy chlorophyll, LAI, biomass, amount of supplied N, and grain yield (Gitelson et al. 2003; Maresma et al. 2016, 2018), the NDTIs from those bands performed well in LNC estimation.

Specifically, NDTI (HOM red, HOM red) and NDTI (CON red, CON red) were the optimal texture indices across the entire growing season in linear regression for LNC estimation. Zheng et al. (2020) found NDTI (MEA nir, MEA red edge) and NDTI (MEA nir, MEA green) the optimal texture indices across the whole growing season using exponential regression for leaf N accumulation and plant N accumulation estimates in rice.

The texture analysis was always performed with a pattern direction (45º) (Jin et al. 2015; Yue et al. 2019; Guo et al. 2022). The direction as stated by Zheng et al. (2020) was rarely studied to verify the best one to estimate plant variables. They found the 45º and 90º direction the most important ones to estimate LNC, leaf N accumulation and plant N accumulation using red edge band. However, Fu et al. (2020) did not find significant difference between the four orientations studied for plant N concentration estimates in winter wheat. In this study, texture metrics using the 90º (D3) and 135º (D4) constructed the optimal GLCM and NDTI for LNC estimation, which might be explained by the strong capability of across-row texture metrics in differentiating the tonal variations caused by N status. That is because common bean is grown in rows, and the local window sliding along the row orientation contains more homogeneous vegetation than from other directions. Furthermore, the bean plants in the same row grow more homogenously than those in different rows, resulting in lower contrast.

4.4.2 The Benefits of Combined Information for Enhancing Leaf N Content

Machine learning methods are increasingly used to estimate parameters to monitor crop growth. The results of this study show that machine-learning estimates of N content based on multispectral UAV imagery or texture metrics are more accurate than single-index estimates, which is also in agreement to Feng et al. (2022). The testing set estimation using the SVM or RF models are also better than all single VIs or texture metrics (Table 6) which may be related to the number of features importance involved in the construction of these models. Han et al. (2022) compared linear regression with RF built from single bands and VIs. Their results of the saturation problem showed by individual VIs can be alleviated in RF model which accuracy is significantly improved.

The combination of spectral data and texture measurements has been proposed to improve plant N concentration (Zheng et al. 2018; Fu et al. 2020; Guo et al. 2022), leaf area index (Li et al. 2022), grain protein content (Fu et al. 2021), residue cover (Jin et al. 2015), leaf N concentration (Zheng et al. 2020) and biomass (Yue et al. 2019). In this study, the combination of VIs and GLCM textures significantly improved the estimation of LNC at R7 and for the entire season as compared to using VIs alone, with an increase of more than 45% in RMSE using RF regression (Table 6). This finding agrees well with the results of Fu et al. (2021) which reported that the combination of texture indices and VIs improved the estimation of LNC significantly in wheat. Furthermore, a universal model suitable for the entire season could not only be used to guide N fertilization applications (Maresma et al. 2016; Zhang et al. 2022) but also to predict grain yield before harvest (Luo et al. 2022; Tian et al. 2022; Walsh et al. 2022).

The combination of VIs to estimate LNC at V4 and R5 growth stages was significantly better than combining texture and VIs. Interestingly, using the top 10 features improved the LNC estimation as compared to all features for across all phenological stages assessed. GSAVI, MCARI, DVI and green reflectance composed the most important indices to estimate LNC using SVM and RF models (Fig. 6). The highest correlation between N rates, plant N uptake, grain yield and GSAVI were also found (Barzin et al. 2020; Maresma et al. 2018; Zha et al. 2020). Li et al. (2020) also estimated yield using RF model with MCARI and plant height derived from crop surface models. Han et al. (2022) found DVI as one of the most important VIs features to perform plant N accumulation and N nutrition index estimation using RF model.

For R7 and entire season stages the use of VIs and GLCM textures significantly improved LNC predictions. Most top 10 best features were related to the COR GLCM metric. TCARI/OSAVI, MTCI and MCARI also were considered important VIs features for the entire season for LNC estimation. López-Calderón et al. (2020) also found TCARI/OSAVI as the most important multispectral VI to estimate N content in forage maize using RF. Berni et al. (2009) also highlighted the efficacy of the TCARI/OSAVI index in mitigating the influence of bare soil and fluctuations in leaf area when assessing olive trees. Chen and Wang (2022) showed that MTCI was the best index for estimating plant N concentration in cotton with RRMSE of 9.31%. These indices offer a valuable tool for

establishing predictive models to estimate chlorophyll concentration through multispectral imaging.

With spectral information alone, VIs often exhibit weak capabilities of detecting N status at late growth stages due to the fact of crop senescence. Textural information could capture the variation of leaf color within and between plots, especially at later stages when leaf color changes dramatically. However, our results demonstrated that the fusion of spectral and textural information could improve N status monitoring efficient. Therefore, UAV multispectral imagery could be used to estimate common bean LNC with independent models for different growth stages.

4.4.3 Common bean plant variables estimation

This study was one of the first to study the use of UAV-based sensors to perform common bean LNC estimates. Saravia et al. (2023) predicted yield using multispectral camera with multiple linear regression highlighting DVI, EVI and TVI as the best VIs for that purpose when bean plants reached maximum canopy cover. Other studies used handheld canopy reflectance spectroradiometer sensor taken at 0.5 – 1.5 m above the canopy to estimate yield at 80 days after sowing using NDVI, GNDVI and SAVI (Gutiérrez-Rodríguez et al. 2006; Köksal et al. 2008). Monteiro et al. (2013) and Santana et al. (2016) also estimated yield, leaf area index and dry matter using NDVI, SAVI and EVI at R6 stage with a coefficient of determination above 0.84.

In this research, we performed multispectral data, VIs, and textural metrics through UAV remote sensing. Utilizing predictive models based on RF or SVM, we generated distribution maps depicting the LNC of beans at various growth stages. Specifically, the LNC map during the V4 stage offers valuable guidance to farmers for applying N fertilizers at adaptable rates once this stage is where most producers broadcast N rates. The LNC response to N rate applied at V4 stage also showed the capacity of N rates estimates at that stage (Fig. 8). LNC is the major index for representing the plant's leaf N nutrition, and through monitoring the LNC, proper fertilizer-N measures can be enacted (Liu et al. 2016). By putting together fig. 5 and 8, it is possible to transform these multispectral sensor readings into a practical N recommendation system to be applied in farming operations as stated in

References (Sripada et al. 2005; Gabriel et al. 2017; Maresma et al. 2016, 2018). Employing UAV proves highly effective in addressing the limitations associated with satellite remote sensing and proximal crop canopy sensing. It establishes a dependable data source for diagnosing the nutritional status of beans in terms of N and for making in-season variable rate recommendations. The applicability of these models still needs to be improved through further testing with more datasets from different geographic sites.

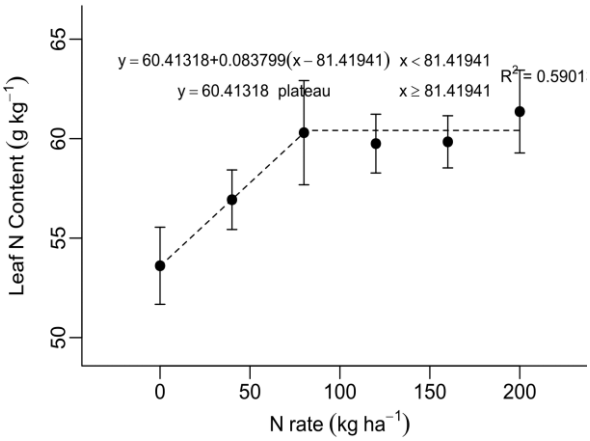

Fig. 8. Linear plateau model of LNC response to N rate applied at V4 growth stage. Each circle is the average of 5 replications. Error bars represent standard deviation at $p < 0.01$.

4.5 Conclusions

We explored the feasibility of multispectral imagery from unmanned aerial vehicles as a means of monitoring nitrogen status. Our investigation encompassed vegetation indices, texture metrics, texture directions, and texture indices. When it came to estimating leaf nitrogen content, the testing accuracy of predictions was notably low when relying solely on vegetation indices, individual texture metrics, or texture indices. Nevertheless, substantial enhancements in accuracy were realized when VIs and texture metrics were combined. The highest accuracy for LNC (RMSE = 1.80 g kg^{-1} and RRMSE = 2.93%) was obtained using SVM model at V4 growth stage with VIs combination. For the R5 stage the VIs combination also showed the greatest accuracy (RMSE = 2.79 g kg^{-1} and RRMSE = 5.20%). The R7 and entire growth stages better predicted LNC using the combination of VIs and texture metrics showing RMSE values of 3.42 and 3.96 g kg^{-1}, RRMSE values of 7.40 and 7.33%, respectively.

In the computation of texture metrics, it's advisable to employ the across-row directions (D3 and D4) when dealing with row-planted crops, rather than the default diagonal direction (D2), as they deliver superior performance. These discoveries can be valuable as guidelines for formulating suitable texture indices using multispectral UAV imagery for monitoring N nutrition. This research offers fresh perspectives on amplifying the N-related signals extracted from common beans canopies by incorporating textural data alongside conventional vegetation indices. This approach exhibits significant potential for accurately assessing and developing more effective strategies for advanced crop nutrient in-season management.

CRediT authorship contribution statement

Diogo Castilho Silva: Conceptualization, Visualization, Methodology, Writing – Original Draft, Data Curation, Investigation, Formal analysis, Software. **Beata Emoke Madari**: Writing - Review & Editing, Resources, Supervision. **Maria da Conceição Santana Carvalho**: Writing - Review & Editing, Supervision, Project administration. **Manuel Eduardo Ferreira**: Writing - Review & Editing, Resources, Software.

Declaration of Competing Interest

The authors declare that they have no known competing financial interests or personal relationships that could have appeared to influence the work reported in this paper.

Acknowledgements

The authors thank the Embrapa Arroz e Feijão team for providing field support and the Federal University of Goiás/LAPIG/Pro-Vant for providing the aerial platforms and multispectral sensors.

Funding

This study was financed by the Coordination of Superior Level Staff Improvement of Brasil (CAPES, Finance Code 001), by the Research Foundation of the State of Goiás

(FAPEG) through the Emerging Nuclei Support Program (PRONEM, Grant nº 20170267000519), by the Brazilian Agricultural Research Corporation (Embrapa) and Yara (Cooperation Agreement n° 20200.21/0111-6), and by the Funding Authority for Studies and Projects (FINEP/CT – AGRO/FNDCT, Cooperation Agreement n° 01.22.0080.00, Ref. 1219/21). M.E.F. and B.E.M. have been continuously supported by the Productivity Fellowship Grant of the National Council for Scientific and Technological Development (CNPq, Grant nº 315699/2020-5 and 307807/2022-3).

Data Availability

Related files and summary of the data are available at Mendeley Data repository (Castilho et al., 2023): https://data.mendeley.com/datasets/fyct5d7sz7/1.

4.6 References

Aasen, H.; Honkavaara, E.; Lucieer, A.; Zarco-Tejada, P.; Aasen, H.; Honkavaara, E.; Lucieer, A.; Zarco-Tejada, P.J. (2018). Quantitative Remote Sensing at Ultra-High Resolution with UAV Spectroscopy: A Review of Sensor Technology, Measurement Procedures, and Data Correction Workflows. *Remote Sens*., 10, 1091.

Barbier, N., & Couteron, P. (2015). Attenuating the bidirectional texture variation of satellite images of tropical forest canopies. *Remote Sensing of Environment*, *171*, 245–260. https://doi.org/10.1016/j.rse.2015.10.007

Barzin, R., Pathak, R., Lotfi, H., Varco, J., & Bora, G. C. (2020). Use of UAS multispectral imagery at different physiological stages for yield prediction and input resource optimization in corn. *Remote Sensing*, *12*(15). https://doi.org/10.3390/RS12152392

Berni, J., Zarco-Tejada, P. J., Suarez, L., & Fereres, E. (2009). Thermal and Narrowband Multispectral Remote Sensing for Vegetation Monitoring From an Unmanned Aerial Vehicle. *IEEE Transactions on Geoscience and Remote Sensing*, *47*(3), 722–738. https://doi.org/10.1109/TGRS.2008.2010457

Blackmer, T. M., & Schepers, J. S. (1996). Aerial Photography to Detect Nitrogen Stress in Corn. *Journal of Plant Physiology*, *148*(3–4), 440–444. https://doi.org/10.1016/S0176-1617(96)80277-X

Blackmer, T. M., Schepers, J. S., Varvel, G. E., & Meyer, G. E. (1996). Analysis of Aerial Photography for Nitrogen Stress within Corn Fields. *Agronomy Journal*, *88*(5), 729–733. https://doi.org/10.2134/agronj1996.00021962008800050008x

[dataset] Castilho Silva, Diogo; Emoke Madari, Beata; Santana Carvalho, Maria da Conceição; Eduardo Ferreira, Manuel (2023), "Optimizing nitrogen estimates in common bean canopies throughout key growth stages via fusion of spectral and textural data from unmanned aerial vehicle (UAV) multispectral imagery", Mendeley Data, V1, doi: 10.17632/fyct5d7sz7.1

Chen, P., & Wang, F. (2022). Effect of crop spectra purification on plant nitrogen concentration estimations performed using high-spatial-resolution images obtained with unmanned aerial vehicles. *Field Crops Research*, *288*(March), 108708. https://doi.org/10.1016/j.fcr.2022.108708

Costa, L., Kunwar, S., Ampatzidis, Y., & Albrecht, U. (2021). Determining leaf nutrient concentrations in citrus trees using UAV imagery and machine learning. *Precision Agriculture*, *23*(3), 854–875. https://doi.org/10.1007/s11119-021-09864-1

Dash, J., & Curran, P. J. (2004). The MERIS terrestrial chlorophyll index. *International Journal of Remote Sensing*, *25*(23), 5403–5413. https://doi.org/10.1080/0143116042000274015

Daughtry, C. S. T., Walthall, C. L., Kim, M. S., Brown de Colstoun, E., & McMurtrey III, J. E. (2000). Estimating Corn Leaf Chlorophyll Concentration from Leaf and Canopy Reflectance. *Remote Sensing of Environment*, *74*(2), 229–239. https://doi.org/10.1016/S0034-4257(00)00113-9

FAOSTAT. (2021). Food and Agriculture Organization of the United Nations Database of Agricultural Production. https://www.fao.org/faostat/en/#data/QCL/visualize

Feng, H., Tao, H., Li, Z., Yang, G., & Zhao, C. (2022). Comparison of UAV RGB Imagery and Hyperspectral Remote-Sensing Data for Monitoring Winter Wheat Growth. *Remote Sensing*, *14*(15). https://doi.org/10.3390/rs14153811

Fu, Y., Yang, G., Li, Z., Song, X., Li, Z., Xu, X., et al. (2020). Winter wheat nitrogen status estimation using uav-based rgb imagery and gaussian processes regression. *Remote Sensing*, *12*(22), 1–27. https://doi.org/10.3390/rs12223778

Fu, Z., Yu, S., Zhang, J., Xi, H., Gao, Y., Lu, R., et al. (2021). Combining UAV multispectral imagery and ecological factors to estimate leaf nitrogen and grain protein content of wheat. *European Journal of Agronomy*, *132*(October 2021), 126405. https://doi.org/10.1016/j.eja.2021.126405

Fu, Z., Yu, S., Zhang, J., Xi, H., Gao, Y., Lu, R., et al. (2022). Combining UAV multispectral imagery and ecological factors to estimate leaf nitrogen and grain protein content of wheat. European Journal of Agronomy, 132(September 2021), 126405. https://doi.org/10.1016/j.eja.2021.126405

Gabriel, J. L., Zarco-Tejada, P. J., López-Herrera, P. J., Pérez-Martín, E., Alonso-Ayuso, M., & Quemada, M. (2017). Airborne and ground level sensors for monitoring nitrogen status in a maize crop. *Biosystems Engineering*, *160*, 124–133.

https://doi.org/10.1016/j.biosystemseng.2017.06.003

Gallo, B., Demattê, J., Rizzo, R., Safanelli, J., Mendes, W., Lepsch, I., et al. (2018). Multi-Temporal Satellite Images on Topsoil Attribute Quantification and the Relationship with Soil Classes and Geology. *Remote Sensing*, *10*(10), 1571. https://doi.org/10.3390/rs10101571

García-Martínez, H., Flores-Magdaleno, H., Ascencio-Hernández, R., Khalil-Gardezi, A., Tijerina-Chávez, L., Mancilla-Villa, O. R., & Vázquez-Peña, M. A. (2020). Corn grain yield estimation from vegetation indices, canopy cover, plant density, and a neural network using multispectral and rgb images acquired with unmanned aerial vehicles. *Agriculture (Switzerland)*, *10*(7), 1–24. https://doi.org/10.3390/agriculture10070277

Ghanbari, A. A., Mousa, S. H. V. I., Mousapour Gori, A., & Rao, I. (2013). Effects of water stress on leaves and seeds of bean (Phaseolus vulgaris L.). *Turkish Journal of Field Crops*, *18*(1), 73–77.

Gitelson, A. A., Gritz, Y., & Merzlyak, M. N. (2003). Relationships between leaf chlorophyll content and spectral reflectance and algorithms for non-destructive chlorophyll assessment in higher plant leaves. *Journal of Plant Physiology*, *160*(3), 271–282. https://doi.org/10.1078/0176-1617-00887

Gitelson, A. A., Kaufman, Y. J., & Merzlyak, M. N. (1996). Use of a green channel in remote sensing of global vegetation from EOS-MODIS. *Remote Sensing of Environment*, *58*(3), 289–298. https://doi.org/10.1016/S0034-4257(96)00072-7

Gitelson, A. A., Zur, Y., Chivkunova, O. B., & Merzlyak, M. N. (2002). Assessing Carotenoid Content in Plant Leaves with Reflectance Spectroscopy¶. *Photochemistry and Photobiology*, *75*(3), 272. https://doi.org/10.1562/0031-8655(2002)075<0272:ACCIPL>2.0.CO;2

Guo, Y., He, J., Huang, J., Jing, Y., Xu, S., Wang, L., et al. (2022). Effects of the Spatial Resolution of UAV Images on the Prediction and Transferability of Nitrogen Content Model for Winter Wheat. *Drones*, *6*(10), 1–21. https://doi.org/10.3390/drones6100299

Gutiérrez-Rodríguez, M., Escalante-Estrada, J. A., Rodriguez Gonzalez, M. T., & Reynolds, M. P. (2006). Canopy reflectance indices and its relationship with yield in common bean plants (*Phaseolus vulgaris* L.) with phosphorous supply. *International Journal of Agriculture and Biology*, *8*(2), 203–207. http://www.fspublishers.org/

Haboudane, D., Miller, J. R., Tremblay, N., Zarco-Tejada, P. J., & Dextraze, L. (2002). Integrated narrow-band vegetation indices for prediction of crop chlorophyll content for application to precision agriculture. *Remote Sensing of Environment*, *81*(2–3), 416–426. https://doi.org/10.1016/S0034-4257(02)00018-4

Han, S., Zhao, Y., Cheng, J., Zhao, F., Yang, H., Feng, H., et al. (2022). Monitoring Key Wheat Growth Variables by Integrating Phenology and UAV Multispectral Imagery Data into Random Forest Model. *Remote Sensing*, *14*(15).

https://doi.org/10.3390/rs14153723

Huete, A. . (1988). A soil-adjusted vegetation index (SAVI). *Remote Sensing of Environment*, *25*(3), 295–309. https://doi.org/10.1016/0034-4257(88)90106-X

Jiang, J., Zhang, Z., Cao, Q., Liang, Y., Krienke, B., Tian, Y., et al. (2020). Use of an active canopy sensor mounted on an unmanned aerial vehicle to monitor the growth and nitrogen status of winter wheat. *Remote Sensing*, *12*(22), 1–24. https://doi.org/10.3390/rs12223684

Jin, X., Ma, J., Wen, Z., & Song, K. (2015). Estimation of Maize Residue Cover Using Landsat-8 OLI Image Spectral Information and Textural Features. *Remote Sensing*, *7*(11), 14559–14575. https://doi.org/10.3390/rs71114559

Jordan, C. F. (1969). Derivation of Leaf-Area Index from Quality of Light on the Forest Floor. *Ecology*, *50*(4), 663–666. https://doi.org/10.2307/1936256

KEENEY, D. R., & BREMNER, J. M. (1967). Use of the Coleman model 29A analyzer for total nitrogen analysis of soils. *Soil Science*, (104(5)), 358–363.

Kim, D. W., Silva, R. R., Kim, J. S., Kim, Y., Kim, H. J., & Chung, Y. S. (2020). Comparison of Various Kinds of Vegetative Indices for Chlorophyll Contents Using Low-Resolution Camera. *Journal of Crop Science and Biotechnology*, *23*(1), 73–79. https://doi.org/10.1007/s12892-019-0347-0

Köksal, E. S., Kara, T., Apan, M., Üstün, H., & Ilbeyi, A. (2008). Estimation of green bean yield, water deficiency and productivity using spectral indexes during the growing season. *Irrigation and Drainage Systems*, *22*(3–4), 209–223. https://doi.org/10.1007/s10795-008-9052-8

Li, B., Xu, X., Zhang, L., Han, J., Bian, C., Li, G., et al. (2020). Above-ground biomass estimation and yield prediction in potato by using UAV-based RGB and hyperspectral imaging. *ISPRS Journal of Photogrammetry and Remote Sensing*, *162*(December 2019), 161–172. https://doi.org/10.1016/j.isprsjprs.2020.02.013

Li, He, Wang, Y., Fan, K., Mao, Y., Shen, Y., & Ding, Z. (2022). Evaluation of important phenotypic parameters of tea plantations using multi-source remote sensing data. *Frontiers in Plant Science*, *13*. https://doi.org/10.3389/fpls.2022.898962

Li, Hongjun, Zhang, Y., Lei, Y., Antoniuk, V., & Hu, C. (2020). Evaluating different non-destructive estimation methods for winter wheat (Triticum aestivum L.) nitrogen status based on canopy spectrum. *Remote Sensing*, *12*(1), 1–16. https://doi.org/10.3390/RS12010095

Li, M., Zhu, X., Li, W., Tang, X., Yu, X., & Jiang, Y. (2022). Retrieval of Nitrogen Content in Apple Canopy Based on Unmanned Aerial Vehicle Hyperspectral Images Using a Modified Correlation Coefficient Method. *Sustainability (Switzerland)*, *14*(4). https://doi.org/10.3390/su14041992

Li, X., Ba, Y., Zhang, M., Nong, M., Yang, C., & Zhang, S. (2022). Sugarcane Nitrogen Concentration and Irrigation Level Prediction Based on UAV Multispectral Imagery. *Sensors*, *22*(7). https://doi.org/10.3390/s22072711

Li, Z., Li, Z., Fairbairn, D., Li, N., Xu, B., Feng, H., & Yang, G. (2019). Multi-LUTs method for canopy nitrogen density estimation in winter wheat by field and UAV hyperspectral. *Computers and Electronics in Agriculture*, *162*(June 2018), 174–182. https://doi.org/10.1016/j.compag.2019.04.005

Liu, H., Zhu, H., & Wang, P. (2016). Quantitative modelling for leaf nitrogen content of winter wheat using UAV-based hyperspectral data. *International Journal of Remote Sensing*, *38*(8–10), 2117–2134. https://doi.org/10.1080/01431161.2016.1253899

Liu, S., Li, L., Gao, W., Zhang, Y., Liu, Y., Wang, S., & Lu, J. (2018). Diagnosis of nitrogen status in winter oilseed rape (Brassica napus L.) using in-situ hyperspectral data and unmanned aerial vehicle (UAV) multispectral images. *Computers and Electronics in Agriculture*, *151*, 185–195. https://doi.org/10.1016/j.compag.2018.05.026

López-Calderón, M. J., Estrada-ávalos, J., Rodríguez-Moreno, V. M., Mauricio-Ruvalcaba, J. E., Martínez-Sifuentes, A. R., Delgado-Ramírez, G., & Miguel-Valle, E. (2020). Estimation of total nitrogen content in forage maize (Zea mays l.) using spectral indices: Analysis by random forest. *Agriculture (Switzerland)*, *10*(10), 1–15. https://doi.org/10.3390/agriculture10100451

Lu, D., & Batistella, M. (2005). Exploring TM image texture and its relationships with biomass estimation in Rondônia, Brazilian Amazon. Acta Amaz., 35, 249–257. https://doi.org/10.1590/S0044-59672005000200015

Luo, S., Jiang, X., Jiao, W., Yang, K., Li, Y., & Fang, S. (2022). Remotely Sensed Prediction of Rice Yield at Different Growth Durations Using UAV Multispectral Imagery. *Agriculture*, *12*(9), 1447. https://doi.org/10.3390/agriculture12091447

Marang, I. J., Filippi, P., Weaver, T. B., Evans, B. J., Whelan, B. M., Bishop, T. F. A., et al. (2021). Machine learning optimised hyperspectral remote sensing retrieves cotton nitrogen status. *Remote Sensing*, *13*(8). https://doi.org/10.3390/rs13081428

Maresma, Á., Ariza, M., Martínez, E., Lloveras, J., & Martínez-Casasnovas, J. (2016). Analysis of Vegetation Indices to Determine Nitrogen Application and Yield Prediction in Maize (Zea mays L.) from a Standard UAV Service. *Remote Sensing*, *8*(12), 973. https://doi.org/10.3390/rs8120973

Maresma, Á., Lloveras, J., & Martínez-Casasnovas, J. A. (2018). Use of multispectral airborne images to improve in-season nitrogen management, predict grain yield and estimate economic return of maize in irrigated high yielding environments. *Remote Sensing*, *10*(4), 1–19. https://doi.org/10.3390/rs10040543

Marin, D. B., Ferraz, G. A. e. S., Guimarães, P. H. S., Schwerz, F., Santana, L. S., Barbosa, B. D. S., et al. (2021). Remotely piloted aircraft and random forest in the evaluation of

the spatial variability of foliar nitrogen in coffee crop. *Remote Sensing*, *13*(8), 1–15. https://doi.org/10.3390/rs13081471

Monteiro, P. F. C., Filho, R. A., Xavier, A. C., & Monteiro, R. O. C. (2013). Índices De Vegetação Simulados De Diferentes Sensores Na Estimativa Das Variáveis Biofísicas Do Feijoeiro. *Pesquisa Agropecuaria Brasileira*, *48*(4), 433–441. https://doi.org/10.1590/S0100-204X2013000400012

Montgomery, K., Henry, J. B., Vann, M. C., Huseth, A. S., & Mitasova, H. (2020). Measures of canopy structure from low-cost uas for monitoring crop nutrient status. Drones, 4(3), 1–22. https://doi.org/10.3390/drones4030036

Osco, L. P., Junior, J. M., Ramos, A. P. M., Furuya, D. E. G., Santana, D. C., Teodoro, L. P. R., et al. (2020). Leaf nitrogen concentration and plant height prediction for maize using UAV-based multispectral imagery and machine learning techniques. *Remote Sensing*, *12*(19), 1–17. https://doi.org/10.3390/rs12193237

Osco, L. P., Ramos, A. P. M., Pereira, D. R., Moriya, érika A. S., Imai, N. N., Matsubara, E. T., et al. (2019). Predicting canopy nitrogen content in citrus-trees using random forest algorithm associated to spectral vegetation indices from UAV-imagery. *Remote Sensing*, *11*(24), 1–17. https://doi.org/10.3390/rs11242925

Peng, J., Manevski, K., Kørup, K., Larsen, R., & Andersen, M. N. (2021). Random forest regression results in accurate assessment of potato nitrogen status based on multispectral data from different platforms and the critical concentration approach. *Field Crops Research*, *268*(April). https://doi.org/10.1016/j.fcr.2021.108158

Peng, X., Chen, D., Zhou, Z., Zhang, Z., Xu, C., Zha, Q., et al. (2022). Prediction of the Nitrogen, Phosphorus and Potassium Contents in Grape Leaves at Different Growth Stages Based on UAV Multispectral Remote Sensing. *Remote Sensing*, *14*(11). https://doi.org/10.3390/rs14112659

Perry, E. M., Goodwin, I., & Cornwall, D. (2018). Remote sensing using canopy and leaf reflectance for estimating nitrogen status in red-blush pears. *HortScience*, *53*(1), 78–83. https://doi.org/10.21273/HORTSCI12391-17

Qi, J., Kerr, Y., & Chehbouni, A. (1994). External factor consideration in vegetation index development. In *CNES, Proceedings of 6th International Symposium on Physical Measurements and Signatures in Remote Sensing*.

Rouse, J. W., Haas, R. H., Deering, D. W., Schell, J. A., & Harlan, J. C. (1974). *Monitoring the Vernal Advancement and Retrogradation (Green Wave Effect) of Natural Vegetation*. Greenbelt, MD, USA.

Santana, A. V. de, Heinemann, A., Stone, L. F., & Nascente, A. S. (2016). Índice De Refletância Na Estimativa Da Área Foliar E Biomassa Das Folhas Em Feijão-Comum. *Colloquium Agrariae*, *12*, 07–19. https://doi.org/10.5747/ca.2016.v12.n1.a128

Saravia, D., Valqui-Valqui, L., Salazar, W., Quille-Mamani, J., Barboza, E., Porras-Jorge, R., et al. (2023). Yield Prediction of Four Bean (Phaseolus vulgaris) Cultivars Using Vegetation Indices Based on Multispectral Images from UAV in an Arid Zone of Peru. *Drones*, *7*(5), 325. https://doi.org/10.3390/drones7050325

Sripada, R. P., Heiniger, R. W., White, J. G., & Meijer, A. D. (2006). Aerial Color Infrared Photography for Determining Early In-Season Nitrogen Requirements in Corn. *Agronomy Journal*, *98*(4), 968–977. https://doi.org/10.2134/agronj2005.0200

Sripada, R. P., Heiniger, R. W., White, J. G., & Weisz, R. (2005). Aerial color infrared photography for determining late-season nitrogen requirements in corn. *Agronomy Journal*, *97*(5), 1443–1451. https://doi.org/10.2134/agronj2004.0314

Tian, Z., Zhang, Y., Liu, K., Li, Z., Li, M., Zhang, H., & Wu, J. (2022). UAV Remote Sensing Prediction Method of Winter Wheat Yield Based on the Fused Features of Crop and Soil. *Remote Sensing*, *14*(19), 1–18. https://doi.org/10.3390/rs14195054

Tucker, C. J. (1979). Red and photographic infrared linear combinations for monitoring vegetation. *Remote Sensing of Environment*, *8*(2), 127–150. https://doi.org/10.1016/0034-4257(79)90013-0

Vega, F. A., Ramírez, F. C., Saiz, M. P., & Rosúa, F. O. (2015). Multi-temporal imaging using an unmanned aerial vehicle for monitoring a sunflower crop. Biosystems Engineering, 132, 19–27. https://doi.org/10.1016/j.biosystemseng.2015.01.008

Walsh, O. S., Marshall, J., Jackson, C., Nambi, E., Shafian, S., Jayawardena, D. M., et al. (2022). Wheat yield and protein estimation with handheld- and UAV-based reflectance measurements. *Agrosystems, Geosciences and Environment*, *5*(4), 1–14. https://doi.org/10.1002/agg2.20309

Wang, L., Chen, S., Li, D., Wang, C., Jiang, H., Zheng, Q., & Peng, Z. (2021). Estimation of paddy rice nitrogen content and accumulation both at leaf and plant levels from uav hyperspectral imagery. *Remote Sensing*, *13*(15), 1–21. https://doi.org/10.3390/rs13152956

Wood, E. M., Pidgeon, A. M., Radeloff, V. C., & Keuler, N. S. (2012). Image texture as a remotely sensed measure of vegetation structure. *Remote Sensing of Environment*, *121*, 516–526. https://doi.org/10.1016/j.rse.2012.01.003

Wright, D. L., Rasmussen, V. P., Ramsey, R. D., Baker, D. J., & Ellsworth, J. W. (2004). Canopy Reflectance Estimation of Wheat Nitrogen Content for Grain Protein Management. *GIScience & Remote Sensing*, *41*(4), 287–300. https://doi.org/10.2747/1548-1603.41.4.287

Xu, X., Fan, L., Li, Z., Meng, Y., Feng, H., Yang, H., & Xu, B. (2021). Estimating leaf nitrogen content in corn based on information fusion of multiple-sensor imagery from uav. *Remote Sensing*, *13*(3), 1–17. https://doi.org/10.3390/rs13030340

Xue, J.; Gao, S.; Fan, Y.; Li, L.; Ming, B.; Wang, K.; Xie, R.; Hou, P.; Li, S (2020). Traits of plant morphology, stalkmechanical strength, and biomass accumulation in the selection of lodging-resistant maize cultivars. Eur. J.Agron., 117, 126073. https://doi.org/10.1016/j.eja.2020.126073

Yue, J., Yang, G., Tian, Q., Feng, H., Xu, K., & Zhou, C. (2019). Estimate of winter-wheat above-ground biomass based on UAV ultrahigh-ground-resolution image textures and vegetation indices. *ISPRS Journal of Photogrammetry and Remote Sensing*, *150*, 226–244. https://doi.org/10.1016/j.isprsjprs.2019.02.022

Zha, H., Miao, Y., Wang, T., Li, Y., Zhang, J., & Sun, W. (2020). Sensing-based rice nitrogen nutrition index prediction with machine learning. *Remote Sensing*, *12*(215), 1–22.

Zhang, J., Wang, W., Krienke, B., Cao, Q., Zhu, Y., Cao, W., & Liu, X. (2022). In-season variable rate nitrogen recommendation for wheat precision production supported by fixed-wing UAV imagery. *Precision Agriculture*, *23*(3), 830–853. https://doi.org/10.1007/s11119-021-09863-2

Zheng, H., Cheng, T., Li, D., Yao, X., Tian, Y., Cao, W., & Zhu, Y. (2018). Combining unmanned aerial vehicle (UAV)-based multispectral imagery and ground-based hyperspectral data for plant nitrogen concentration estimation in rice. *Frontiers in Plant Science*, *9*(July), 1–13. https://doi.org/10.3389/fpls.2018.00936

Zheng, H., Cheng, T., Li, D., Zhou, X., Yao, X., Tian, Y., et al. (2018). Evaluation of RGB, color-infrared and multispectral images acquired from unmanned aerial systems for the estimation of nitrogen accumulation in rice. *Remote Sensing*, *10*(6). https://doi.org/10.3390/rs10060824

Zheng, H., Li, W., Jiang, J., Liu, Y., Cheng, T., Tian, Y., et al. (2018). A comparative assessment of different modeling algorithms for estimating leaf nitrogen content in winter wheat using multispectral images from an unmanned aerial vehicle. *Remote Sensing*, *10*(12). https://doi.org/10.3390/rs10122026

Zheng, H., Ma, J., Zhou, M., Li, D., Yao, X., Cao, W., et al. (2020). Enhancing the nitrogen signals of rice canopies across critical growth stages through the integration of textural and spectral information from unmanned aerial vehicle (UAV) multispectral imagery. *Remote Sensing*, *12*(6). https://doi.org/10.3390/rs12060957

Zou, X., & Mõttus, M. (2017). Sensitivity of Common Vegetation Indices to the Canopy Structure of Field Crops. *Remote Sensing*, *9*(10), 994. https://doi.org/10.3390/rs9100994

5 CONSIDERAÇÕES FINAIS

O primeiro capítulo desta tese traz resultados importantes quanto à quantidade de pesquisas que vem sendo feitas com RPAS no monitoramento em tempo real do nitrogênio (N) nas principais culturas agrícolas. Apesar do progresso considerável, ainda existem muitas lacunas no uso de RPAS/drones em culturas agrícolas. Muitos estudos não utilizam os mesmos índices de vegetação (IVs) para analisar uma característica específica da planta e/ou estágio fenológico. Além disso, numerosos estudos forneceram métricas (R^2 e/ou RMSE) da relação entre característica da planta e índice de vegetação, mas muitas vezes omitiram os dados correspondentes, restringindo o uso futuro desses estudos. Estágio fenológico diferente apresentará condições variadas, o que indica a necessidade de relatar adequadamente a fenologia da cultura e as condições ambientais (sequeiro vs. irrigado) ao correlacionar uma variável de planta (produtividade, conteúdo de nitrogênio foliar etc.) com quaisquer IV.

Atualizações futuras do conjunto de dados do capítulo 1 poderão incluir estudos recentemente publicados e dados anteriormente indisponíveis (com potencial para mais contribuições de diferentes autores). O objetivo é expandir continuamente o conjunto de dados para incentivar a colaboração, a ciência aberta e a inclusão de mais dados para estimativas mais abrangentes das características das culturas e possível utilização dos dados para tomada de decisão em qualquer lugar do mundo.

O capítulo 2 mostrou que os IVs baseados no comprimento de onda da banda verde (GNDVI e GN, por exemplo) foram os melhores para prever a dose de N no milho. Os IVs relativos não melhoraram significativamente a predição da dose de N em V5, o que traz um grande benefício, pois não necessita utilizar áreas de referência para tomada de decisão no manejo da adubação nitrogenada no milho.

O uso do conteúdo de N foliar é mais vantajoso em relação ao método da dose de N, uma vez que exigiu menor aporte de N aplicado no estádio V5 do milho neste estudo.

Além disso, usar modelos de platô linear e platô quadrático mostrados no método de conteúdo de N foliar trazem confiabilidade tanto nos casos de estimativa de dose de N quanto de produtividade. A vantagem de incorporar uma relação platô linear neste contexto é que ela permite uma representação mais realista da relação entre IVs e conteúdo de N foliar. Mesmo que a refletância estime com precisão a necessidade de N no momento da medição da refletância, as condições futuras poderão alterar a oferta ou demanda de N.

Conduzir experimentos antes de utilizar índices de vegetação para prever N no milho é crucial porque os pesquisadores/consultores podem avaliar o desempenho desses índices em relação às necessidades reais de N e à resposta da cultura. Além disso, esses modelos preditivos precisam ser validados sob condições locais e variedades de milho específicas para garantir sua precisão e confiabilidade.

O capítulo 3 descobriu que utilizando modelos preditivos baseados em Random Forest (RF) ou Support Vector Machine (SVM) combinando IVs e métricas de textura, geraram-se mapas de distribuição representando o conteúdo de N foliar do feijão no estágio V4, oferecendo orientação valiosa aos agricultores para a aplicação de N em taxa variável, uma vez que esta fase é onde a maioria dos produtores aplicam N em cobertura. Índices como GSAVI, MCARI, DVI e refletância do comprimento do verde compuseram os índices mais importantes para estimar conteúdo de N foliar usando modelos SVM e RF.

No cálculo de métricas de textura, é aconselhável empregar as direções transversais (90º e 135º) às fileiras ao lidar com culturas plantadas em linha, em vez da direção diagonal padrão (45º), pois elas proporcionam desempenho superior.

Integrando dados de RPAS com sistemas de aplicação de taxa variável em tratores e implementos comerciais, os agricultores podem ajustar dinamicamente as taxas de fertilizantes com base nas necessidades das culturas em tempo real, levando a uma otimização de recursos, redução do impacto ambiental e maior rentabilidade. A colaboração entre pesquisadores, desenvolvedores de tecnologia e agricultores é essencial para avançar na implementação, calibração e validação de detecção baseada em RPAS, abrindo caminho para um futuro mais eficiente e sustentável de gerenciamento de precisão do N.